U.S. Department of Transportation

Federal Railroad Administration

Ground Penetrating Radar (GPR) Technology Evaluation and Implementation

Office of Research,
Development
and Technology
Washington, DC 20590

DOT/FRA/ORD-20/18

Final Report
May 2020

NOTICE

This document is disseminated under the sponsorship of the Department of Transportation in the interest of information exchange. The United States Government assumes no liability for its contents or use thereof. Any opinions, findings and conclusions, or recommendations expressed in this material do not necessarily reflect the views or policies of the United States Government, nor does mention of trade names, commercial products, or organizations imply endorsement by the United States Government. The United States Government assumes no liability for the content or use of the material contained in this document.

NOTICE

The United States Government does not endorse products or manufacturers. Trade or manufacturers' names appear herein solely because they are considered essential to the objective of this report.

REPORT DOCUMENTATION PAGE

Form Approved
OMB No. 0704-0188

1. AGENCY USE ONLY (Leave blank)	2. REPORT DATE	3. REPORT TYPE AND DATES COVERED
	May 2020	Technical Report June 2015 to January 2018

4. TITLE AND SUBTITLE
Ground Penetrating Radar (GPR) Technology Evaluation and Implementation

5. FUNDING NUMBERS
DTFR53-11-D-00008
Task Order 357

6. AUTHOR(S)
Colin Basye, Stephen Wilk, and Yin Gao

7. PERFORMING ORGANIZATION NAME(S) AND ADDRESS(ES)
Transportation Technology Center, Inc.
55500 DOT Road
Pueblo, CO 81001

8. PERFORMING ORGANIZATION REPORT NUMBER

9. SPONSORING/MONITORING AGENCY NAME(S) AND ADDRESS(ES)
U.S. Department of Transportation
Federal Railroad Administration
Office of Railroad Policy and Development
Office of Research, Development and Technology
Washington, DC 20590

10. SPONSORING/MONITORING AGENCY REPORT NUMBER
DOT/FRA/ORD-20/18

11. SUPPLEMENTARY NOTES
COR: Hugh Thompson

12a. DISTRIBUTION/AVAILABILITY STATEMENT
This document is available to the public through the FRA website.

12b. DISTRIBUTION CODE

13. ABSTRACT (Maximum 200 words)
From June 2015 to January 2018, the Federal Railroad Administration (FRA) contracted Transportation Technology Center, Inc. (TTCI) to perform a 3-year study to develop guidelines for the implementation of Ground Penetrating Radar (GPR) technology by North American railroads. To achieve this goal, current background information was collected to establish the status of the technology, and a short history was compiled of the development of GPR technology in a railway environment. An assessment was completed of existing GPR performance criteria, data collection and processing procedures, and reporting standards. Basic requirements were described regarding the necessity of system hardware.

This document describes the development and implementation of GPR on a railbound research car, which included evaluation of the relationship between the GPR-based substructure parameters and the track condition in terms of stiffness and track geometry. An assessment was also conducted for the track substructure degradation conditions identified by GPR parameters, and recommendations were developed for use of these parameters.

14. SUBJECT TERMS
Ground Penetrating Radar, GPR, substructure parameters, track condition, track substructure degradation, track

15. NUMBER OF PAGES
99

16. PRICE CODE

17. SECURITY CLASSIFICATION OF REPORT	18. SECURITY CLASSIFICATION OF THIS PAGE	19. SECURITY CLASSIFICATION OF ABSTRACT	20. LIMITATION OF ABSTRACT
Unclassified	Unclassified	Unclassified	

METRIC/ENGLISH CONVERSION FACTORS

ENGLISH TO METRIC	METRIC TO ENGLISH
LENGTH (APPROXIMATE)	**LENGTH (APPROXIMATE)**
1 inch (in) = 2.5 centimeters (cm)	1 millimeter (mm) = 0.04 inch (in)
1 foot (ft) = 30 centimeters (cm)	1 centimeter (cm) = 0.4 inch (in)
1 yard (yd) = 0.9 meter (m)	1 meter (m) = 3.3 feet (ft)
1 mile (mi) = 1.6 kilometers (km)	1 meter (m) = 1.1 yards (yd)
	1 kilometer (km) = 0.6 mile (mi)
AREA (APPROXIMATE)	**AREA (APPROXIMATE)**
1 square inch (sq in, in^2) = 6.5 square centimeters (cm^2)	1 square centimeter (cm^2) = 0.16 square inch (sq in, in^2)
1 square foot (sq ft, ft^2) = 0.09 square meter (m^2)	1 square meter (m^2) = 1.2 square yards (sq yd, yd^2)
1 square yard (sq yd, yd^2) = 0.8 square meter (m^2)	1 square kilometer (km^2) = 0.4 square mile (sq mi, mi^2)
1 square mile (sq mi, mi^2) = 2.6 square kilometers (km^2)	10,000 square meters (m^2) = 1 hectare (ha) = 2.5 acres
1 acre = 0.4 hectare (he) = 4,000 square meters (m^2)	
MASS - WEIGHT (APPROXIMATE)	**MASS - WEIGHT (APPROXIMATE)**
1 ounce (oz) = 28 grams (gm)	1 gram (gm) = 0.036 ounce (oz)
1 pound (lb) = 0.45 kilogram (kg)	1 kilogram (kg) = 2.2 pounds (lb)
1 short ton = 2,000 pounds (lb) = 0.9 tonne (t)	1 tonne (t) = 1,000 kilograms (kg)
	= 1.1 short tons
VOLUME (APPROXIMATE)	**VOLUME (APPROXIMATE)**
1 teaspoon (tsp) = 5 milliliters (ml)	1 milliliter (ml) = 0.03 fluid ounce (fl oz)
1 tablespoon (tbsp) = 15 milliliters (ml)	1 liter (l) = 2.1 pints (pt)
1 fluid ounce (fl oz) = 30 milliliters (ml)	1 liter (l) = 1.06 quarts (qt)
1 cup (c) = 0.24 liter (l)	1 liter (l) = 0.26 gallon (gal)
1 pint (pt) = 0.47 liter (l)	
1 quart (qt) = 0.96 liter (l)	
1 gallon (gal) = 3.8 liters (l)	
1 cubic foot (cu ft, ft^3) = 0.03 cubic meter (m^3)	1 cubic meter (m^3) = 36 cubic feet (cu ft, ft^3)
1 cubic yard (cu yd, yd^3) = 0.76 cubic meter (m^3)	1 cubic meter (m^3) = 1.3 cubic yards (cu yd, yd^3)
TEMPERATURE (EXACT)	**TEMPERATURE (EXACT)**
[(x-32)(5/9)] °F = y °C	[(9/5) y + 32] °C = x °F

QUICK INCH - CENTIMETER LENGTH CONVERSION

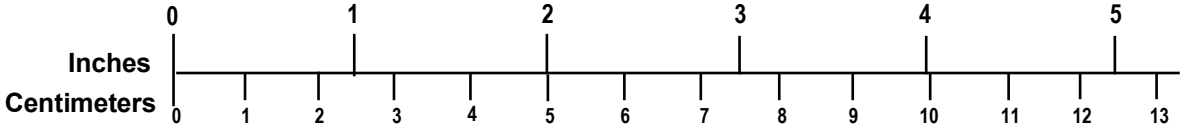

QUICK FAHRENHEIT - CELSIUS TEMPERATURE CONVERSIO

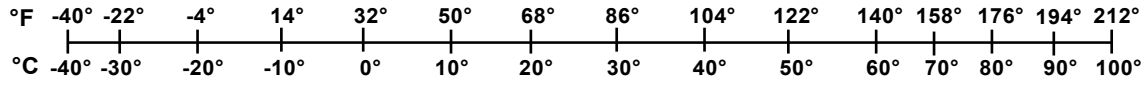

For more exact and or other conversion factors, see NIST Miscellaneous Publication 286, Units of Weights and Measures. Price $2.50 SD Catalog No. C13 10286

Updated 6/17/98

Acknowledgements

Transportation Technology Center, Inc. (TTCI) would like to acknowledge the following participants and railways in making this project a success:

Federal Railroad Administration:

- Hugh Thompson
- Ted Sussman

Balfour Beatty Rail:

- Steve Atherton
- Peter Goff

BNSF Railway:

- Adam Bankston

CSX Transportation (railroad research team)

Sol Solution SAS

- Younes Haddini
- Fabien Ranvier

Zetica Rail

- Asger Eriksen
- Jon Gascoyne

Contents

Illustrations

Tables

Executive Summary

The Federal Railroad Administration (FRA) contracted Transportation Technology Center, Inc. (TTCI) to perform a study from June 2015 to January 2018 to develop guidelines for the implementation of ground-penetrating radar (GPR) technology by North American railroads. To achieve this, background information was collected to establish the current status of the technology, and a short history was compiled of the development of GPR technology in a railway environment. Ultimately, an assessment of existing GPR performance criteria was developed; basic requirements were described regarding system hardware needed, the data collection and processing procedures, and reporting standards were assessed.

A physical GPR system was installed on the FRA DOTX220 ("T-20") railbound research car, and the system underwent several rounds of initial testing, calibration, and refinement to prepare it for field testing, including an evaluation of the relationship between the GPR-based substructure parameters and the track condition in terms of stiffness and track geometry. Three rounds of field tests of the GPR system were conducted, which consisted of a 30-mile run on the Peninsula Subdivision with CSX Transportation (CSX) in Virginia, a 19-mile test/calibration run on the High Tonnage Loop (HTL) at the Facility for Accelerated Service Testing (FAST) at the Transportation Technology Center (TTC) near Pueblo, CO, and 30 miles of field testing and calibration on Burlington Northern Santa Fe (BNSF) Railway's Ravenna line in Nebraska. Many significant improvements were made during this period. Improvements are still ongoing, with work in progress to improve the signal quality of the shoulder antennas. An assessment was also conducted for the track substructure degradation conditions identified by GPR parameters, along with development of recommendations for use of these parameters.

Results include estimates of the Ballast Fouling Index (BFI), which is a measure of the percentage of fine material that is trapped in the ballast and sub-ballast layers to a modelled average depth, and the Fouling Depth Layer (FDL), which is a measure of the thickness of clean ballast. These were validated using a combination of laboratory analysis of ballast samples, visual inspection of the depth to fouled layers, and a handheld cone penetrometer device. Trackbed Inspection Reports (TBIR) were also produced and designed to provide an assessment of overall track bed condition based on track geometry, GPR-derived track bed condition metrics, and aerial photos.

Recommendations are presented at the end of the report, along with potential topics for further research.

1. Introduction

From June 2015 to January 2018, the Federal Railroad Administration (FRA) provided funding to Transportation Technology Center, Inc., to increase the applications of Ground Penetrating Radar (GPR) inspection technology for railroads through the development of improved guidelines supporting implementation of GPR.

In recent years, GPR has become an increasingly useful tool for track substructure inspection. GPR can be performed at track speeds, and many miles of track can be surveyed in a cost-effective and short time duration. GPR can also be performed under inclement weather conditions, and is a well-established inspection technique used to characterize subsurface conditions from the signal response of radio waves that are transmitted into the ground. Like all inspection technologies, GPR has its limitations and drawbacks, and a discussion of the effectiveness of the various parameters is included in this report.

1.1 Background

As railway traffic volume and overall importance of the railway industry to the transportation sector has increased in recent years, factors influencing rail safety and dependability have also become paramount in maintaining a viable public service.

The track and the track substructure support system must remain in a stable and serviceable condition under repeated, heavy or high-speed loading and unloading cycles, even as uncontrollable factors, such as ballast and sub-ballast moisture and progressive fines degradation, constantly change. Track stability may be influenced by the amount and type of fine material that is retained in the ballast and sub-ballast layer, particularly when significant moisture is also present in the fine material. The fines may consist of ballast wear particles, materials pumped from below up through the ballast layer, windblown fines from neighboring fields, or car lading materials. The dynamic stability of the ballast mass can be influenced by the various fines material properties, since clay, silt, coal fines, and fine sand exhibit varying frictional, lubricating, porosity, and hydraulic permeability properties. Moisture can have varying effects on the stability of some materials over others, and the ballast particles can actually "float" in a matrix supported ballast mass, as opposed to an "interlocked" ballast mass that is clean and well-drained.

Various methods have been utilized to help determine when ballast becomes worn or infiltrated with fines to the point where it becomes degraded and needs to be cleaned or replaced, including visual inspection, track geometry data analysis, dynamic deflectometer analysis, and other methods, but each inspection and analysis method has its own limitations and application parameters. In addition, laboratory testing has demonstrated that high fines content alone in the ballast and sub-ballast layer does not produce unstable track.

1.2 Objectives and Overall Approach

The fundamental goal and result of this research project is to develop guidelines for the implementation of GPR inspection technology by North American railroads. To achieve this goal, several specific topics were investigated, including:

- A means to validate the GPR parameters
- Development of recommendations for use of GPR-based track substructure parameters

- Evaluation of the relationship between the GPR-based substructure parameters and the track condition in terms of stiffness and track geometry
- An assessment of the track substructure degradation conditions identified by GPR

1.3 Organization of the Report

This report is comprised of the following five sections, as well as appendices that are separate from the report:

Section 1 provides an introduction of the work performed.

Section 2 offers a breakdown of background information with information to display the importance of the work.

Section 3 provides the data gathered during the second 19-mile run on the High Tonnage Loop (HTL) at the Facility for Accelerated Service Testing (FAST).

Section 4 outlines the third 30-mile data gathering and processing field trip at the Ravenna Subdivision in Nebraska.

Section 5 provides concluding information and recommendations for future work.

Appendices A through F was published separately from the report on FRA's eLibrary.

2. Background and GPR Deployment on a Research Car

The historical background for railway application of GPR is focused on three areas: a literature search to identify and briefly describe the historical use of GPR in a railway environment; an assessment of existing GPR performance criteria; and, finally, recommendations for the use of GPR data..

2.1 Work Breakdown

The project consisted of two phases [6] [7]. The first phase was the development of guidelines for GPR data analysis and procurement. This involved a literature review of the existing capabilities and performance criteria of GPR. Additionally, TTCI provided planning and management assistance to FRA for the installation of a GPR system on one of its railbound track inspection vehicles so it could be used in revenue service.

The second phase was field testing for ballast and subgrade assessment. This research involved installing a new GPR system on the FRA T-20 research car and performing calibration/testing of the system to assess track at three locations: (1) 30 miles of CSX track, (2) 19 miles of the HTL at the Transportation Technology Center's (TTC) FAST, (3) 30 miles of BNSF Ravenna Subdivision track. For the FAST and BNSF testing, TTCI performed physical sampling for ground truth of the GPR results. The results from Phase II is presented in Sections 3 to 5.

The following is a list of tasks for each phase:

Phase 1: Development of guidelines for GPR data analysis and procurement

- Task 1: Literature search/review
- Task 2: Assess existing GPR performance criteria
- Task 3: Develop recommendations for use of GPR data
- Task 4: GPR system procurement and initial testing
- Task 5: GPR data processing

Phase 2: Field testing for ballast and subgrade assessment

- Task 6: Test plan
- Task 7: Field testing
- Task 8: Data analysis
- Task 9: Final report
- Task 10: Research results and social media posting

2.2 Literature Search

The literature search establishes the technical background for the project with a search and summarization of published material related to the types of track degradation and potential failures related to the conditions detected using GPR for railway track inspection [1] [2] [3] [4] [5] [6] [7] [8] [9] [10].

Li, Hyslip, Sussmann, and Chrismer (2016) published a book that includes a discussion of GPR use in railway applications [1]. GPR topics include the fundamentals of how and why GPR works in an environment of dry to moist soils; how antenna frequencies correlate with resolution and survey depth; interaction of different GPR wavelengths with subgrade materials, moisture, and properties; and a discussion on data interpretation and results.

Eriksen et al. (2010) shared four examples of GPR that was used by various globally spaced passenger and freight railroads for their differing needs [2]. Network Rail utilized GPR to map the ballast in its system to reduce the number of trial holes required to analyze the state of its ballast. Irish Rail used various GPR measurements—ballast depth, layer roughness, and drainage quality—in a single index to help plan maintenance activities. A freight railroad in the United States compared GPR results against field sampling and found a reassuring correlation. An Australian railroad used GPR to map the level of ballast fouling within its system and found general agreement. This research shows the versatility of GPR and its ability to be used in different stages of ballast maintenance planning.

Milsom and Eriksen (2011) included a chapter on GPR fundamentals in a field geophysics book, which consisted of a basic description of the utility of GPR, radio wave permittivity and attenuation in different materials, how to set up a GPR survey, and instrumentation, and data processing and presentation [5]. The chapter includes numerous diagrams and images for illustrative purposes. Although the book is not specific to railroad investigations, it presents an overview of different geophysical methods in subsurface environments so the application and correlations are useful.

Hyslip et al. (2005) were involved in a multiple-year study to determine the feasibility and benefits of GPR [3]. It involved testing different configurations and resulted in the currently used three-antenna configuration on both shoulders and the center of the track. The study also summarized over 200 miles of track and gave examples of typical substructure issues and how GPR can be used to identify these conditions. Multiple indices and presentation methods were also tested and recommendations were listed on how to improve GPR in the future.

Selig and Cantrell (2001) listed multiple substructure component issues and discussed the causes, problems, and potential maintenance of each component [4]. The paper emphasized that substructure maintenance is difficult, provided an understanding of the root cause of the problem required before an effective remedy can be implemented, and found that drainage is another important factor.

Early work was also done at TTCI to test GPR technology on various platforms and environments [6] [7]. GPR was found to be useful in identifying and remedial targeting of subsurface features and defects such as ballast pockets and high moisture zones, particularly when used with other methods such as cone penetrometer rigs.

2.2.1 Assessment of Existing GPR Performance Criteria

Table 1 summarizes a list of track substructure problems detectable with GPR, types of track damage associated with the problems, and rankings in terms of risk of occurrence and damage potential. Table 2 provides the performance criteria after an understanding of the problems and potential for damage is established.

Table 1. Substructure Problem, Likelihood of Occurrence and Damage Potential

Problem	Associated Track Damage	Damage Potential	Likelihood of Occurrence
Inadequate ballast drainage	Low track strength • Ballast deformation • Accelerated track geometry degradation • Excessive track deflection • Uneven track settlement Subgrade deformation • Softening of the subgrade surface • Overstressing of the subgrade through reduction of the load distribution capacity of the ballast layer	Damage potential related to moisture and subgrade strength. Potential increases with: • Wet ballast • Moderate to highly plastic clay soil • Heavy-axle-load and high-density traffic environment	High likelihood that some moisture is retained in the ballast fines Likelihood of fully saturated ballast conditions having the highest damage potential depends on the permeability of the subgrade, the slope of the subgrade surface and the amount of ballast fouling
Subgrade deformation	Continual squeezing of the subgrade surface from under the ties toward the tie ends (progressive shear or shoulder heaving) Formation of large-scale ballast pockets in embankments (excessive plastic deformation). Accelerated track geometry degradation and uneven settlement. Inadequate ballast drainage. Embankment instability.	Damage potential is highest for: • Clay subgrades with higher than optimal moisture content • Water trapped in ballast pockets • Heavy-axle loads	High likelihood for clay soils with high moisture content Low likelihood for coarse grained subgrade soils
Ballast fouling	Inadequate ballast drainage	Damage potential is related to the ballast moisture content. Highly fouled ballast that is dry has low damage potential. Damage potential increases with increasing moisture content.	Some amount of fouling is common Likelihood of severe fouling is dependent on the traffic environment, infiltration of fouling material from outside the track, and maintenance frequency.
Track transitions	Accelerated track geometry degradation Excessive track deflection Uneven track settlement	Damage potential is related to the differences in track stiffness and rates of settlement between the at-grade and structure tracks	Likelihood exists at all track transitions.
Subgrade attrition	Ballast fouling from upward pumping of subgrade soil	Damage potential is similar to ballast fouling	Likelihood depends on a thin ballast layer, moderate to complete ballast saturation and fine-grained subgrade soil
Soil swelling and shrinkage	Accelerated track geometry degradation and uneven track settlement	Damage is related to changing moisture content	Likelihood depends on the existence of expansive clay soils in the subgrade

2.2.2 Assess Existing GPR Performance Criteria

Table 2 shows a performance-based specification for GPR procurement and describes what GPR system data and quality is required to successfully diagnose track support problems related to fouled ballast and subgrade issues.

Table 2. GPR Inspection Specifications

Inspection Parameter	GPR Method	Required Output	Reporting Requirements	Problem Diagnosis
Ballast fouling	Analysis of 2 GHz signal-scattering data to model the reduction of ballast inter-particle void spaces due to fouling	One-dimensional BFI that is the average of fouling data over a depth of 16 to 18 inches (406 to 457 mm) from top of tie and a linear distance of track that will be specified Two-dimensional BFI that is the fouling data used to calculate the average is plotted as a function of depth	Distance history plots of color coded BFI categorized as clean, fouled, and highly fouled, which are based on existing or new calibrations to field samples. Fouling data color coded and plotted to show vertical distribution of fouling within the layer	Ballast fouling Subgrade attrition
Granular layer thickness interpretation	Depths of primary and secondary ballast layer interfaces determined from 400 MHz and 2 GHz signal velocities and travel times Velocities are calculated from dielectric values that are based on established values for similar types of ballast material or newly measured values	Depth in inches from the top of tie to the layer interface	Distance histories of primary and secondary layer depths Ballast depth index (BDI) identifying locations where the primary layer thickness is less than a defined minimum Layer roughness index (LRI) identifying variations in primary layer depth over a specified distance	Subgrade deformation Track transitions Subgrade attrition Subgrade swelling and shrinkage
Moisture detection	Analysis of 2 GHz signal reflection amplitude at layer interfaces Increasing amplitude indicates increasing contrast in the dielectric properties of materials at the interface, likely due to moisture	Magnitude of the reflection amplitude	Reflection amplitude, or layer amplitude exceedance (LAE) categorized as low (low moisture), moderate, or high (high moisture)	Inadequate drainage Subgrade deformation Track transitions Subgrade attrition
Subsurface features	Signal anomalies caused by buried features such as	Identification of features by location, depth, and description	Location of structures shown on the layer depth distance history plots	Track geometry anomalies

Inspection Parameter	GPR Method	Required Output	Reporting Requirements	Problem Diagnosis
	culverts, cables, or derailment debris		Summary listing of features	

The basic GPR system performance requirements are as follows:

- System hardware and deployment (the number and orientation may be different on truck hi-rail systems versus the rail-mounted system):
  - Three 2 GHz center frequency air-coupled time domain pulsed radar horn antennas
  - Three 400 MHz center frequency ground-coupled time domain pulsed radar bow-tie antennas
  - Appropriate control and digital GPR acquisitions units
  - GPR system installed on the FRA DOTX220 track inspection vehicle
  - An antenna of each frequency to be positioned at the track center and 6 inches (152 mm) or less beyond the ends of ties on both shoulders
  - GPR distance data to be collected with an existing encoder onboard the T-20 car
- Data collection and processing:
  - Maximum GPR survey capability of 80 mph
  - Processing of the GPR data to be performed with software developed to handle large volumes of data and having automated processing and analysis capabilities for rapid reporting
  - GPR data to be integrated with the track geometry and gage restraint measurement system (GRMS) data generated by the T-20 car
- Data reporting:
  - Standard reporting to include CSV with milepost; elapsed distance; latitude; longitude; ballast fouling values and categories for the left shoulder, center, and right shoulder; and the thickness of clean ballast as values and categories for the left shoulder, center, and right shoulder
  - Track charts with milepost (MP) and asset labels showing ballast fouling and ballast depth categories for the left shoulder, center, and right shoulder
  - On request for specified track sections, CSV files and track charts for ballast pockets, layer roughness representing potential subgrade erosion and wet beds
  - If requested, detailed track bed inspection reports on a per 1/2-mile basis to investigate the potential cause of track geometry faults
- System commissioning:
  - The commissioning of the GPR system on the DOTX220 car on the HTL at the TTC
- GPR data analysis requirements are as follows:
  - Ballast fouling requirements

  - The BFI is calibrated against Selig's Fouling Index (FI), which is defined as the sum of the percentages passing the No. 4 and No. 200 sieves. The BFI has a value between 0 and 200.
  - Existing data correlating GPR BFI to sieve analysis of field samples of typical mainline track ballast is adequate unless questions arise
  - The one-dimensional BFI data is calculated to a depth of 16 inches (406 mm) below top of tie and over 15 feet (4.6 m).
- Layer interpretation requirements
  - Layer depths to be estimated using an assumed dielectric value of 4.5 for basic reporting (48-hour turnaround). The assumed value may be increased if extremely wet and fouled ballast conditions are known to exist.
  - The dielectric value may be further refined if needed in the enhanced report (2-week turnaround) by incorporating the one-dimensional fouling data.
  - BDI to be calculated as the average depth of the primary layer over 15 feet (5 m)
  - Primary LRI to be calculated as the difference in the maximum and minimum primary layer depth over 66 feet (20 m)
- Moisture detection
  - The likelihood of trapped moisture (moisture likelihood index [MLI]) to be derived from the normalized amplitude of the signal reflection at the interface between the primary and secondary layers. The higher the amplitude, the higher the probable moisture content.
  - MLI categories: relatively dry, moist, and wet

BFI, BDI, LRI, and MLI categories are defined in Table 3.

Table 3. GPR Indices

Index	Category	Definition
Modeled ballast fouling (Selig) BFI	5 4 3 2 1	clean <1% fines moderately clean 1 – <10% fines moderately fouled 10-<20% fines fouled 20 - <40% fines highly fouled >40% fines
Ballast depth index BDI	3 2 1	> 20 inches 15 to 20 inches < 15 inches
Layer roughness index LRI	3 2 1	< 1 inches 1 to 2 inches > 2 inches
Moisture detection MLI	3 2 1	relatively dry moist relatively wet

2.2.3 Develop Recommendations for Use of GPR Data

Recommendations for use of GPR output parameters based on the analysis completed in Task 1 and the GPR capability analysis for available commercial GPR systems completed in Task 2 are as follows:

- Basic use of GPR data
  - Ballast maintenance planning, which tends to focus on the fouling parameter output over relatively long distances
  - Site-specific substructure problem solving, in which the GPR output parameters coupled with track geometry data are evaluated
  - Advancing the use of GPR for problem solving is an objective of this research and the primary application of GPR inspection technology by FRA
- Development of a track substructure quality index (TSQI) based on GPR data
  - The various GPR output parameters should be viewed in terms of their combined effect on substructure performance.
  - Adding the indices in Table 3 into a single TSQI that reflects their net influence enhances the usefulness of GPR data
  - Development of the TSQI requires careful consideration of the influence and, therefore, the weighting of individual GPR parameters
  - Consideration should also be given as to how the track center and shoulder datasets should be treated in the overall TSQI
  - Additional indices may be developed that account for differences between the center and shoulder data
- Finalize the TSQI development with a matrix that pairs the GPR-derived TSQI category with a vertical track roughness data
  - Track roughness that is calculated as the standard deviation over a defined distance of the track surface data can be categorized as low, moderate, and high roughness, on the basis of threshold exceedances. Low roughness has the highest category.
  - A TSQI matrix with track roughness is shown as an example only in Table 4. Note: the TSQI values in Table 4 are simply the individual GPR categories from Table 3 added together with no weighting.
- Investigating localized track faults
  - Problem locations are flagged by track geometry data exceptions
  - GPR parameters are evaluated on a case-by-case basis to determine the substructure conditions that are likely causing or contributing to the problem.

Table 4. Example of a TSQI Matrix

		GPR TSQI		
		12 to 10	9 to 7	6 to 4
Track Roughness Categories	3 – low track roughness	High TSQI	Moderately high TSQI	Moderately low TSQI
	2 – moderate track roughness	Moderately high TSQI	Moderately high TSQI	Moderately low TSQI
	1 – high track roughness	Moderately low TSQI	Moderately low TSQI	Poor TSQI

2.3 Instrumentation, Mounting, and Testing on the T-20 Car

2.3.1 Car Selection and Antenna Positioning

Initially, the FRA DOTX218 research car was preferred and considered for mounting the GPR system onto. It has many other instrumentation systems and capabilities already in use, but it was found that the car did not have enough room beneath it to accommodate the antennas needed, or other support instrumentation and systems on the car (see Appendix A). Consequently, the T-20 car was selected for mounting the GPR system onto. A careful examination and measurement of the T-20 car revealed adequate space for instrumentation (Figure 1).

Figure 1. T-20 Car Storage Compartment with Plywood Mockup of 2 GHz Antenna

Plate A and C clearances, as well as physical mounting and space parameters, were important factors in antenna placement and fitment; ENSCO and Balfour Beatty Rail, Inc. (BBRI) worked together to accomplish this task. Figure 2 shows a unidimensional image of the Amtrak

Clearance Code A as well as Plate C clearance envelope with the instrumentation bin fitted within that envelope.

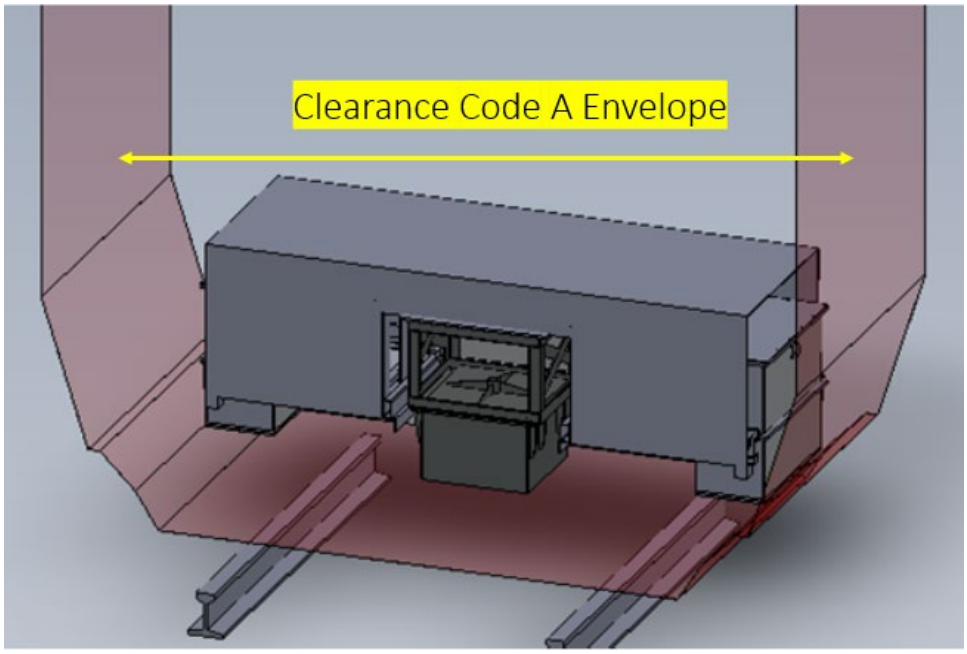

Figure 2. Conceptual Positioning of Antennas within Amtrak Clearance Code A and Plate C

The GPR system was assembled and bench tested on March 1–4, 2016, at the BBRI facility in Jacksonville, FL, and it consisted of:

- 3 x 2 GHz GSSI horn antennas
- 1 x 400 MHz GSSI
- 1 x SIR 30 4 channel MF-30 mainframe unit
- 1 x RASC DC system (also see comments below)
- 4 x customized GPR antenna control cables designed for the T-20 vehicle

The final orientation of the antennas is shown in Figure 3 which shows the right antenna in a retracted position and the left antenna deployed.

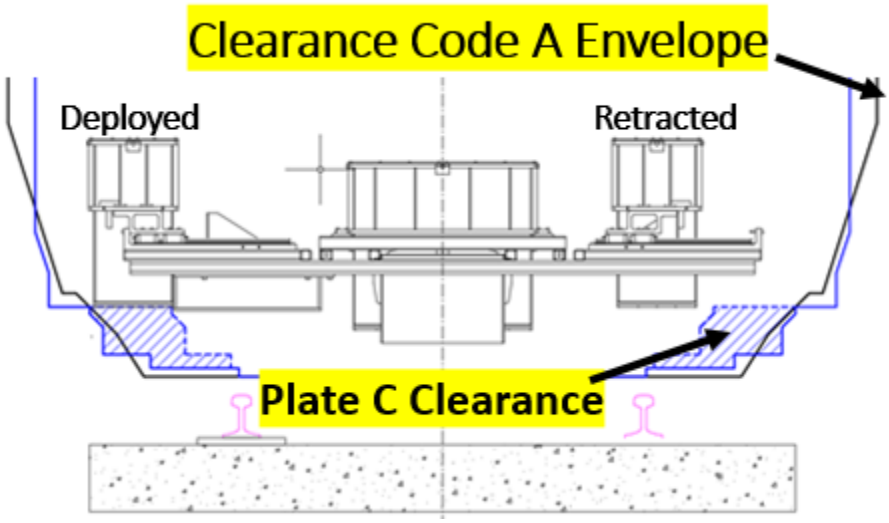

Figure 3. Antenna Configuration Within Plate A and C Constraints, Showing Retracted (right) and Deployed (left) Positioning

After the initial testing, it was proposed that a fourth 2 GHz antenna be mounted in the center along with the 400 MHz antenna already in position.

The final configuration on the DOTX220 car includes three 2 GHz antennas (two mounted on the shoulders and one above and between the rails) and a single 400 MHz antenna mounted above and between the rails.

The onboard signal acquisition, processing, and storage communication system allows remote telemetry of the data for storage, image processing, and reporting from a home location to FRA. Figure 4 summarizes the conceptual information flow.

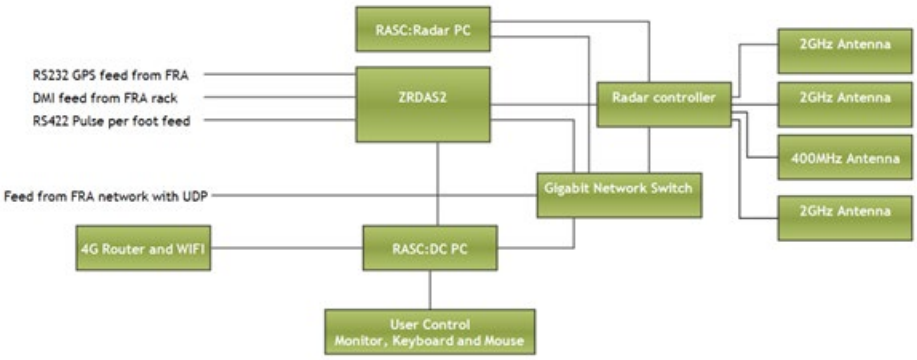

Figure 4. Onboard Signal Preprocessing and Transmittal System

2.3.2 2 GHz Antenna Rail Offset Testing

Rail offset testing was performed on the deployed shoulder antennas to understand how the Plate A and C requirements, as well as deployed antenna dimensions, would be expected to affect signal metrics. Offsets were measured from the outer edge of the rail to the inner edge of the antenna (Figure 5).

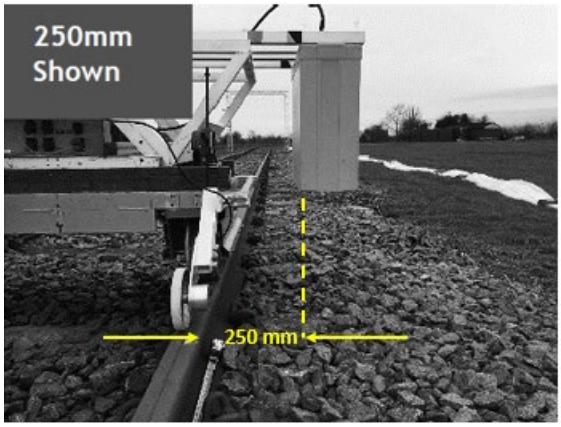

Figure 5. Antenna Offset Testing
(A final offset of 10.5 inches [267 mm] was chosen)

After several trials and calibrations, an offset of ~10.5 inches (267 mm) was chosen for the antenna offset. The final configuration of the T-20 shoulder antennas is shown in Figure 6 where a comparison is made between positioning on BBRI hi-rail trucks and the T-20 car. The results and comparison of the modeled signals from each are discussed in Section 4. In addition to these lateral differences, the center 400 MHz antenna on the T-20 car is 15 inches (381 mm) above the top of tie compared to 11 inches (279 mm) on the hi-rail GPR truck.

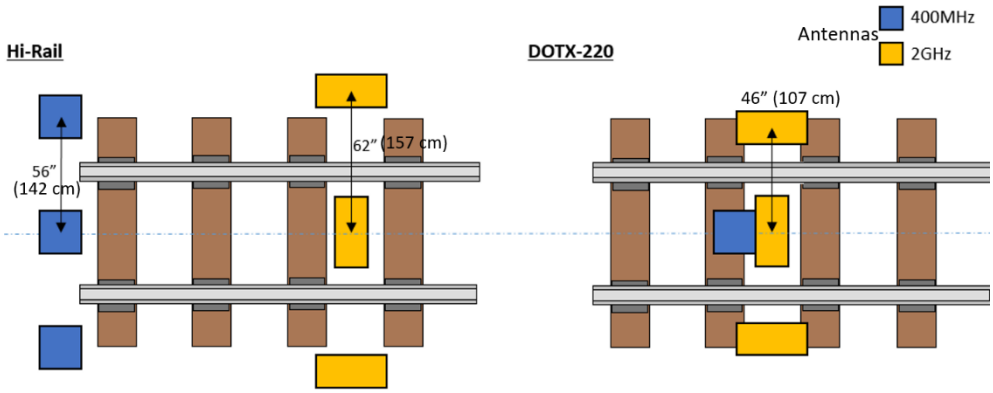

Figure 6. Antenna Configuration for the Standard BBRI Hi-Rail Vehicle vs. FRA's T-20 Car

2.3.3 Antenna Plate Calibration

Plate calibrations are performed weekly on hi-rail truck antennas to measure the signal and reflected response on a standard metal plate at a known vertical offset, which must be parallel to the antenna bottom face. The vertical offset is 11 inches (279 mm) on the standard hi-rail trucks.

During testing, it was found that inconsistent plate calibration data was generated for the T-20 antennas because the T-20 car was not generally on a consistent, flat, stable surface on a weekly basis (as the hi-rail trucks are). Instead, the T-20 car is usually on a nonparallel, nonplanar ballast surface. This condition resulted in a variation in rail height and plate positioning and leveling, which produced inconsistent calibration data, as shown in Figure 7.

To address this problem, BBRI designed plate tests for calibration, which had the following

characteristics: (a) lightweight, (b) small footprint for stowage, (c) perfectly flat reflecting surface, (d) adjustability for uneven surfaces, and (e) visible level indicators to ensure surface is level with respect to top of rail, and thus, with sensors (Figure 8).

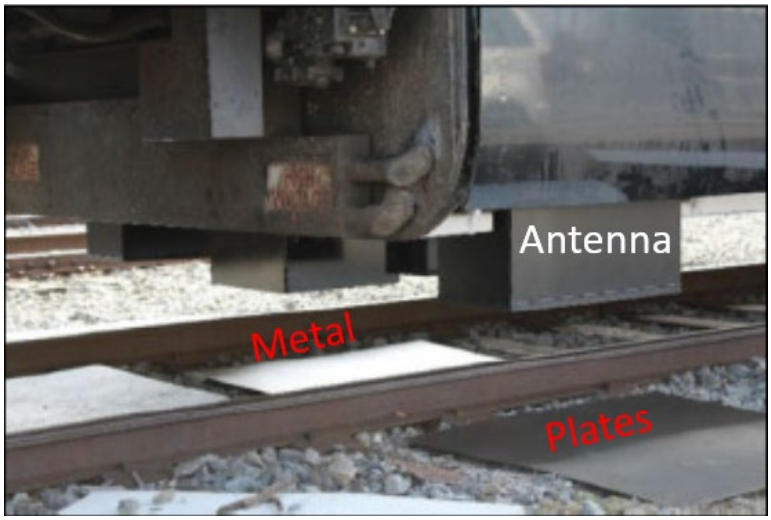

Figure 7. An Example of the Calibration Test

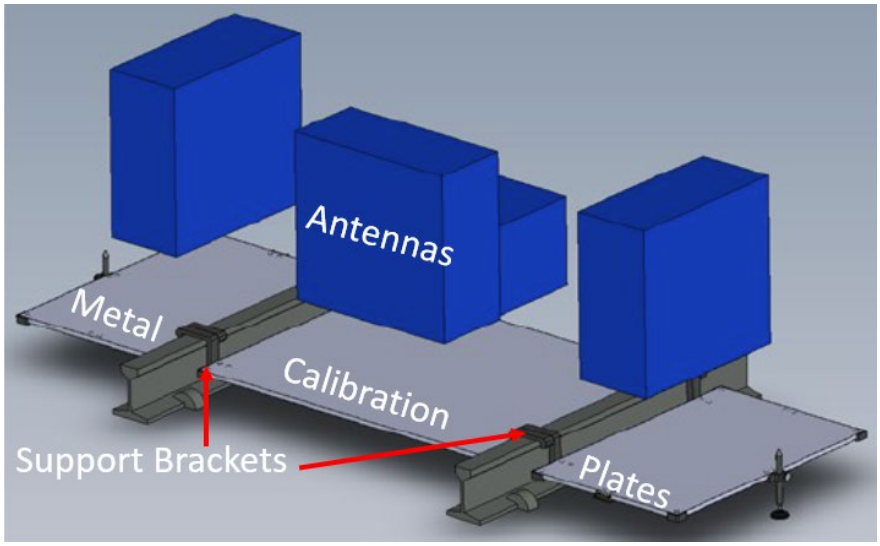

Figure 8. Conceptual Model of New Plate Test Rig and Support Brackets

The instrumentation and data acquisition system was tested in Chambersburg, PA, after fitment onto the T-20 car, after which it was ready for field testing in revenue service. The first 30-mile test run was on the Peninsula Subdivision in Virginia.

2.4 Phase II: Field Testing

Phase II of the project tested the FRA GPR system at three locations: (1) 30 miles of CSX track on the Peninsula Subdivision, (2) 19 miles of HTL track at the TTC, and (3) 30 miles of BNSF track on the Ravenna Subdivision. For the HTL and BNSF testing, TTCI performed physical sampling to ground truth the GPR results.

Phase II used the data gathered from the field tests to determine the strengths of the FRA GPR system and areas in which it required further improvement.

2.4.1 First 30-Mile Data Gathering and Processing Field Trip—Peninsula Subdivision, May 4, 2016

BBRI provided a data gathering run using the T-20 car on the Peninsula Subdivision MP 39.84 to MP 70, between Newport News and Richmond, VA, on May 4, 2016, shown in Figure 9.

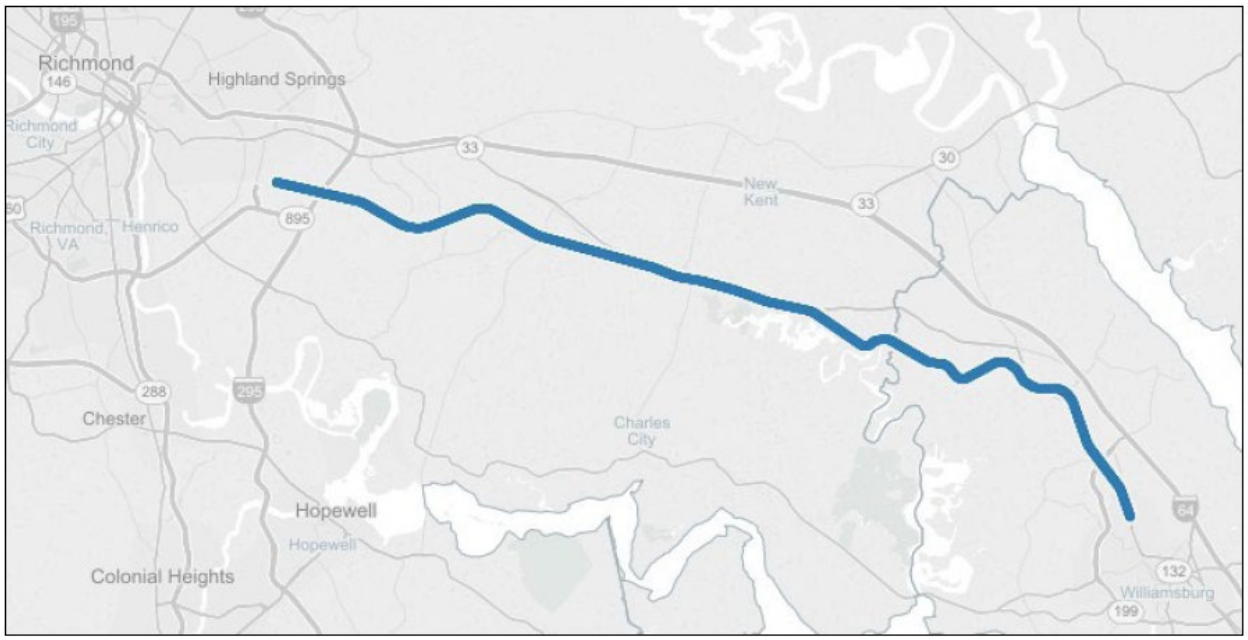

Figure 9. Route for the 30-Mile Data Collection on the CSX Peninsula Subdivision MP 39.8 to MP 78.0

Procedure and Result

The right shoulder antenna was not functioning during the test run, and due to this the data was not usable during this run. (Although, it was repaired for subsequent testing.) However, crib and left shoulder antennas and systems functioned properly, so an analysis and modeling was completed on the available data.

Figure 10 shows a Google Earth overview snapshot of the Peninsula Subdivision route MP 70–70.1 tested by the T-20 car. The data is densely packed in this figure but, using Google Earth, the user can zoom in and turn on/off the different layers to examine specific areas of interest for the different parameters presented. The detail area from MP 70.02 to MP 70.04 below is described in Figure 12.

Figure 10. Google Image Overview of the Tested Zone of the CSX Peninsula Line Detail Area shown in Figure 12

2.4.2 Ballast Fouling Index

When a user zooms in on Google Earth and turns on/off various layers, a detail of the track is viewable for left, center, and right shoulders (right shoulder data was unavailable at this time but was available after a follow-up run when the antenna had been repaired), on an approximately measured 18.2-foot (5.5 m) minimum averaged interval. The BFI is also represented by colors, as shown in Figure 11.

Ballast Fouling Index (BFI)

BFI Category	Description	Modelled Fouling Index (Selig)
5	Clean	0 to <5
4	Moderately Clean	5 to <10
3	Moderately Fouled	10 to <25
2	Fouled	25 to <30
1	Highly Fouled	>30
0	Unavailable	n/a

Figure 11. Various Color Categories and Descriptions for BFI

The BFI is calibrated against Selig's fouling index, which is defined as the sum of the percentages passing the No. 4 and No. 200 sieves [1]. Accordingly, the BFI has a value between 0 and 200, and counts the No. 200 fines percentage twice, as this helps to account for the large

influence the fines have on track stability. This recognizes the large influence that the fines have on track substructure behavior and moisture retention.

Figure 12 shows a closer view of the detail area as a red circle, and Figure 10, i.e., MP 70.02 to MP 70.04, shows the BFI detail.

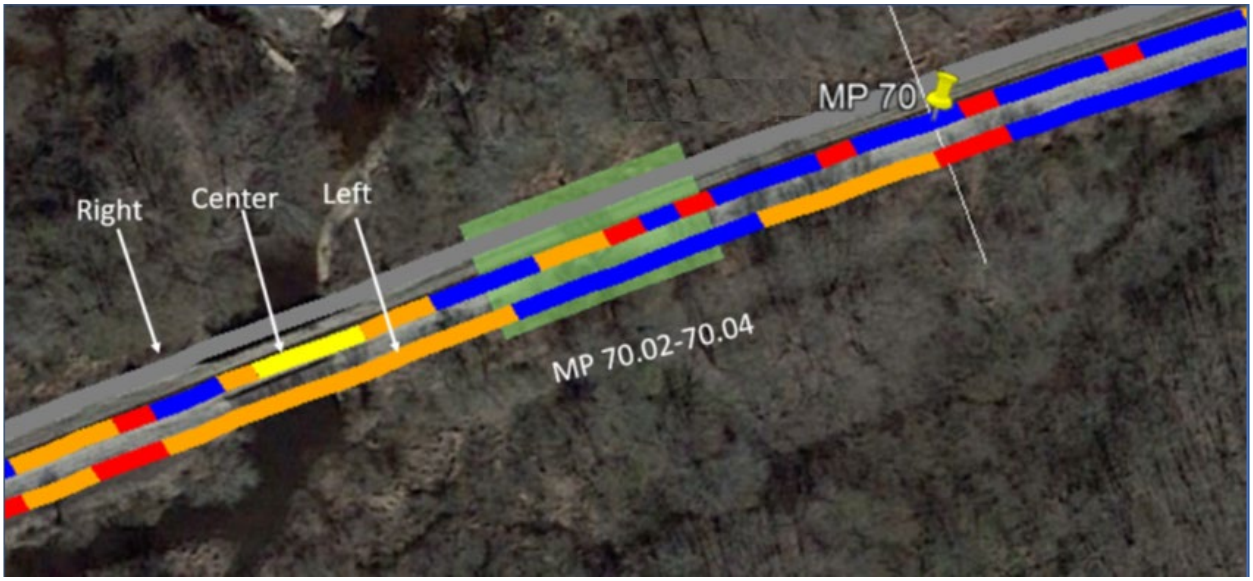

Figure 12. MP 70.02 to MP 70.04 Showing BFI Detail

A GPR modeled longitudinal cross-sectional area from MP 70.02 to MP 70.04 (see the green shaded area in Figure 12) is illustrated in Figure 13. Figure 12 shows mud spots in the track detail (with the layers turned off), and they are evident in the mounded areas in the GPR modeled cross-sectional area in Figure 13.

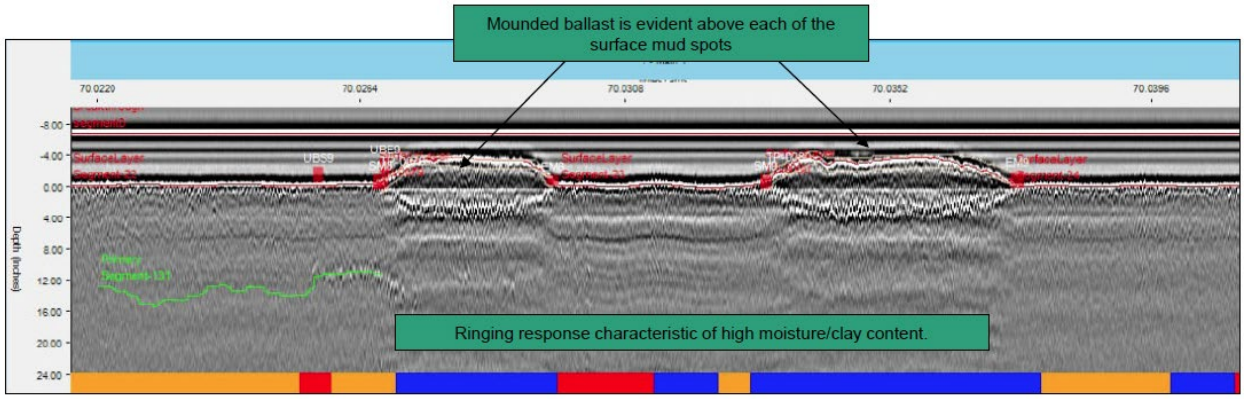

Figure 13. BFI Cross Section of MP 70.02 to MP 70.04 of BFI and Modeled Presence of Excessive Fine-Grained Matrix Material

It may be noted that as the user begins to zoom in to the various segments of the test section, it begins to become apparent what sections have significant levels of fines in the ballast, and possibly where shoulder cleaning equipment has recently serviced the shoulders. For example, potential issues that may need to be examined include road crossings (Figure 14) or areas where ballast cleaning services may have been terminated (Figure 15).

Figure 14. GPR System on the T-20 Car Identifying Areas that Have Crossing Issues or Where Cleaning Equipment Has Terminated (Figure 15)

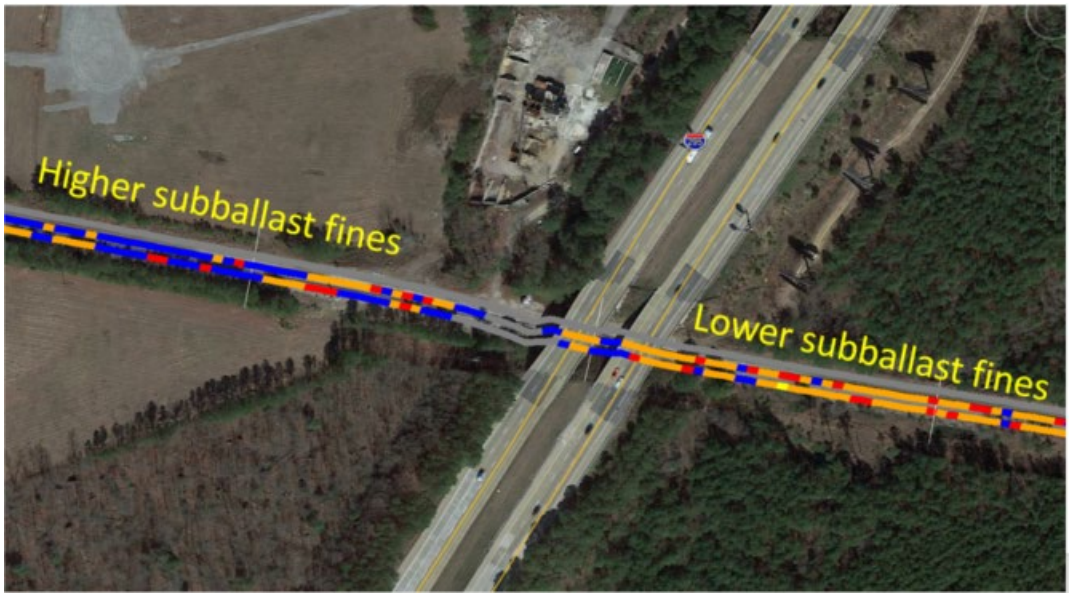

Figure 15. Example of Railroad Bridge Crossing Highway

Larger areas may also be examined to see the relative BFI condition of curves (Figure 16), lowland areas, or other general geographic influences.

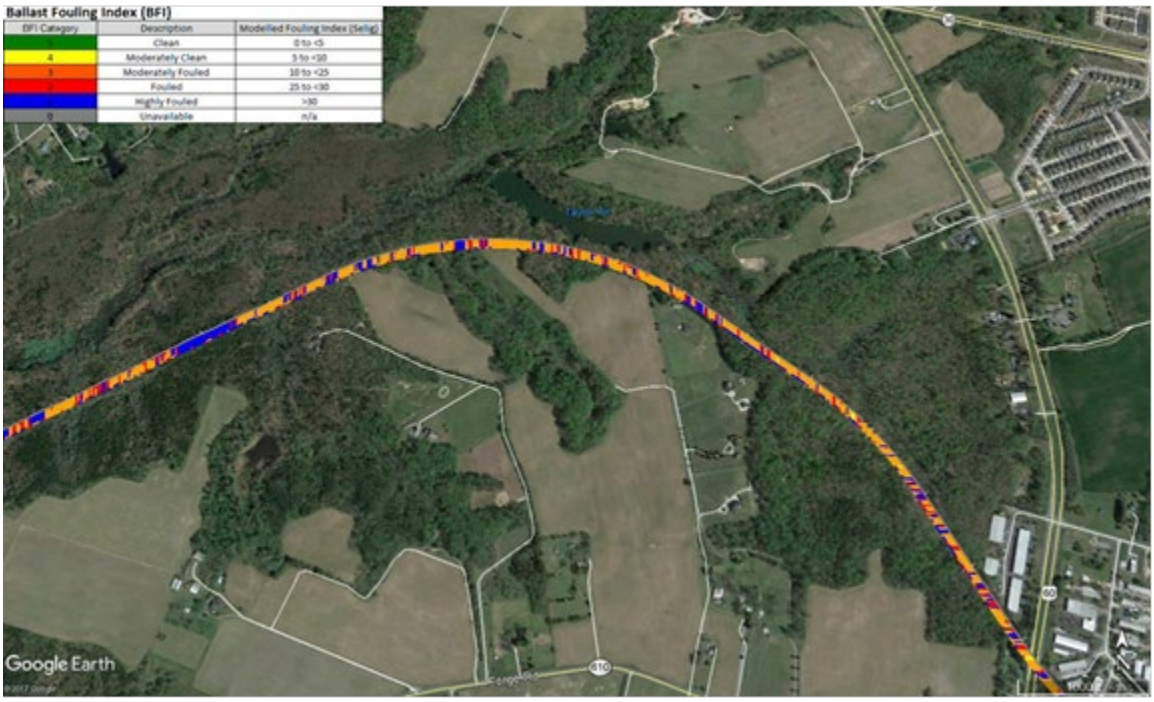

Figure 16. Example of BFI Results on Peninsula Subdivision

2.4.3 The Layer Roughness Index

The LRI indicates the variance in vertical track surface over a 62-foot (19-m) chord. The FRA Safety Standards of vertical surface are listed in Table 5 [11].

Table 5. FRA Track Safety Standards for Vertical Surface for a 62-foot Chord

Class	Maximum Operating Speed (mph)	Maximum Deviation (inches)
1	10	3
2	25	2¾
3	40	2¼
4	60	2
5	80	1¼

The categories of LRI for the Peninsula Subdivision are listed in Table 6, and an example of the LRI visual results is shown in Figure 17.

Table 6. Description of LRI Categories for Peninsula Subdivision

LRI Category	LRI Color	Description	Variance (inches)
3	Green	Good	<2
2	Yellow	Poor	2 to 4
1	Red	Very Poor	>4
0	Unavailable	N/A	

Figure 17. Example of LRI Results on Peninsula Subdivision

2.4.4 The Ballast Thickness Index (BTI)

BTI indicates the thickness of the ballast layer. A typical ballast thickness is 12 inches (305 mm), and ballast thickness layers less than 12 inches (305 mm) are considered suboptimal. The categories of BTI for the Peninsula Subdivision are listed in Table 7, and an example of the BTI visual results is shown in Figure 18.

Table 7. Description of BTI Categories for Peninsula Subdivision

BTI Category	BTI Color	Description	Thickness (inches)
5	Purple	Positive Exceedance Level 2	>23
4	Blue	Positive Exceedance Level 1	17 to 23
3	Green	No Exceedance	11 to 17
2	Yellow	Negative Exceedance Level 1	5 to 11
1	Red	Negative Exceedance Level 2	<5

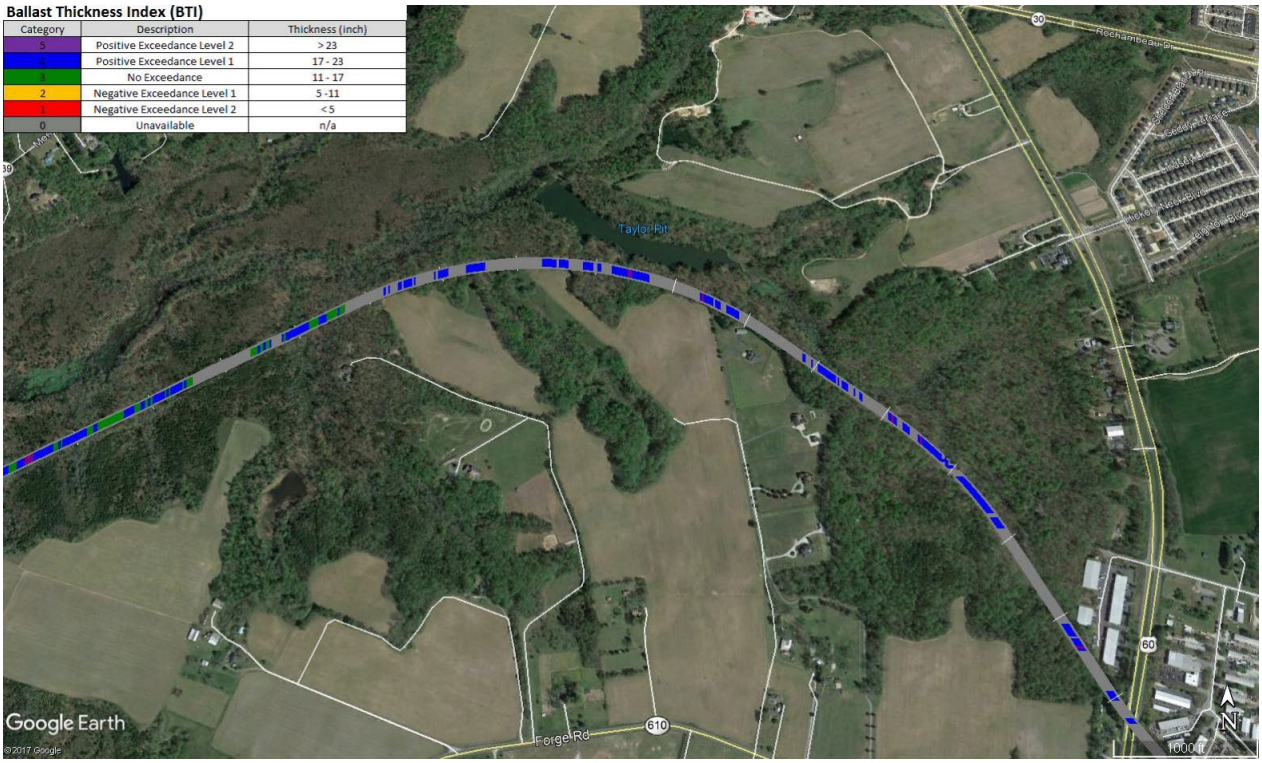

Figure 18. Example of BTI Results on Peninsula Subdivision

2.4.5 The Fouling Depth Layer (FDL)

The FDL (also known as the free-draining layer) is another assessed metric that is modeled using GPR, and it provides an indication of the depth of the relatively clean ballast layer, including the approximately 7-inch-thick (178-mm) ballast section in the upper crib area. The categories of FDL for the Peninsula Subdivision are listed in Table 8 and an example of the FDL visual results is shown in Figure 19.

Table 8. Description of FDL Categories for Peninsula Subdivision

FDL Category	FDL Color	Description	Variance (inches)
3	Green	Good	>12
2	Yellow	Poor	12 to <6
1	Red	Very Poor	<6

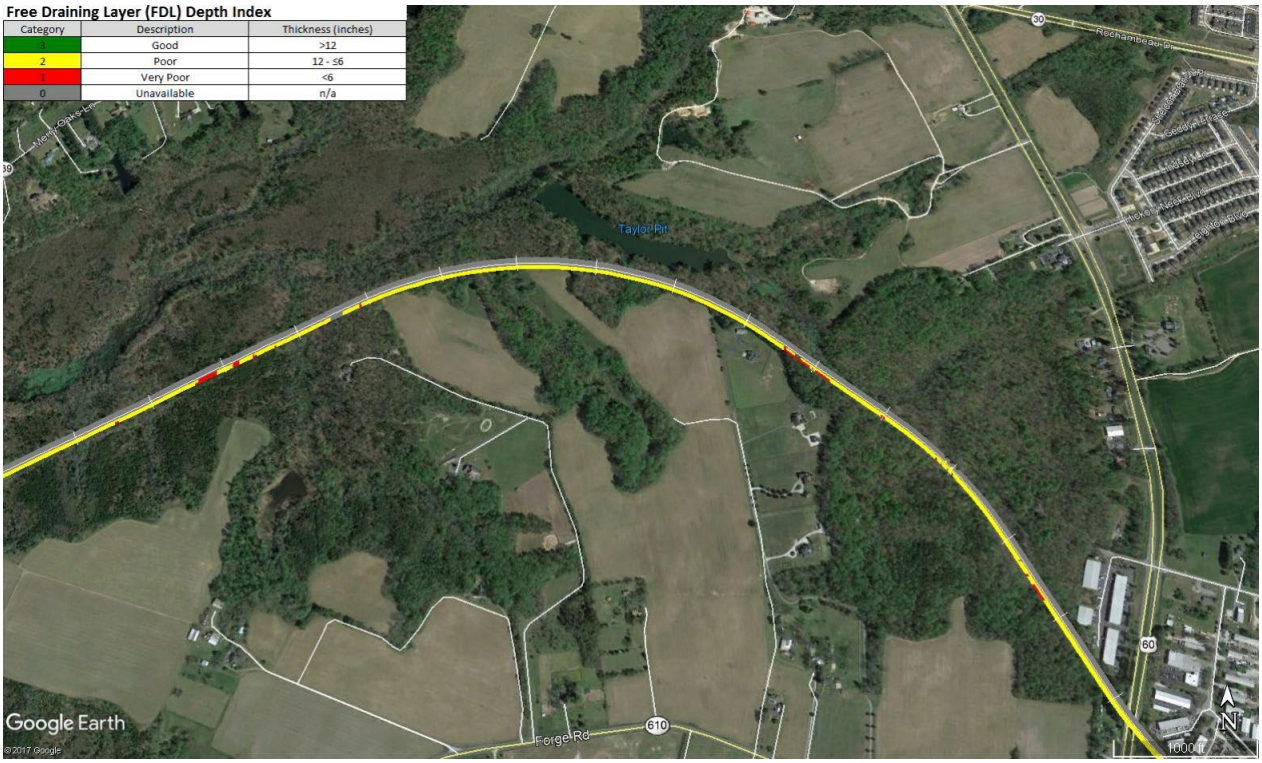

Figure 19. Example of FDL Results on Peninsula Subdivision

2.4.6 Peninsula Subdivision GPR Results and Conclusions

The primary objective of the first test run was to test the equipment on revenue track to ensure that it worked and provided reasonable results.

The 2 GHz right shoulder data was unavailable due to poor antenna matching results. The track had relatively high levels of ballast fines in some areas, but identification should be confirmed when the right shoulder antenna is repaired; the one-dimensional BFI shows ballast to have high fines content in the track center in many areas.

An overview of the BFI, LRI, BTI, and FDL results over the measured 30-mile section is as follows:

- The BFI results showed high levels of ballast fouling, with most of the BFI ranging from moderately fouled to highly fouled. Approximately 48 percent of the track center was categorized as fouled or highly fouled (FI > 25). This is displayed in Figure 20.
- The LRI results showed a high level of track surface variance, with 44 percent of LRI showing over 4 inches (102 mm) of variance and 54 percent showing between 2 to 4 inches (51 to 102 mm) of variance. This is displayed in Figure 21.
- The BTI results showed variable ballast thickness, with the majority ranging from 5 to 17 inches (127 to 432 mm). This is displayed in Figure 22.
- The FDL results showed free draining layers ranging from approximately 6 to 12 inches (152 to 305 mm) in depth. This is displayed in Figure 23.

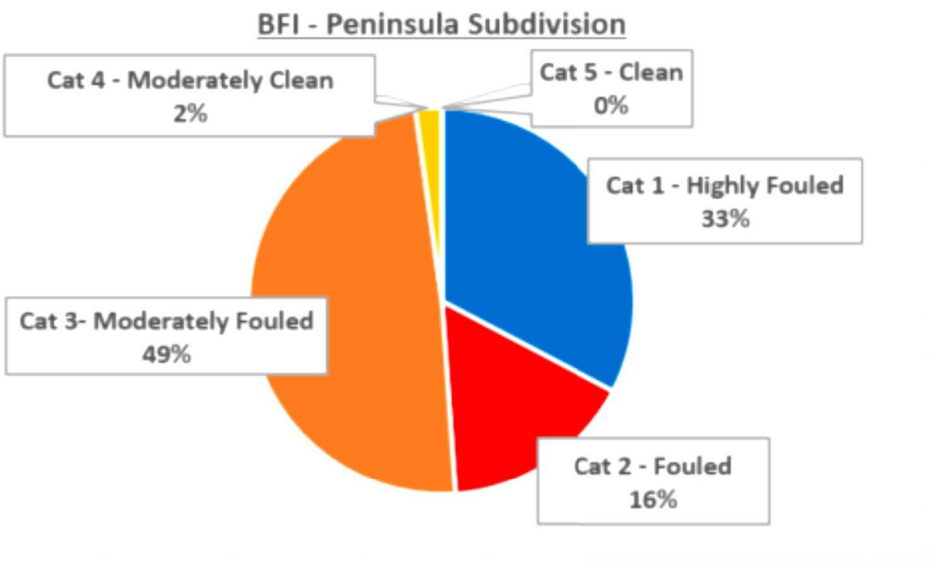

Figure 20. Peninsula Subdivision Surveyed Moderately to Highly Fouled Ballast from Surface Depth of Approximately 16 Inches (406 mm) Below Top of Ballast

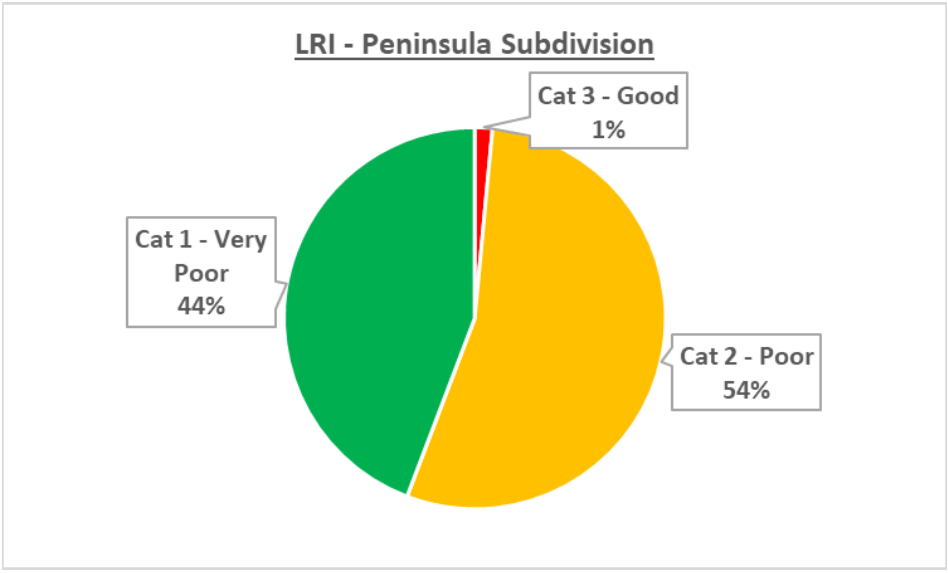

Figure 21. Percentage of LRI Categories on the Center Track of the Peninsula Subdivision

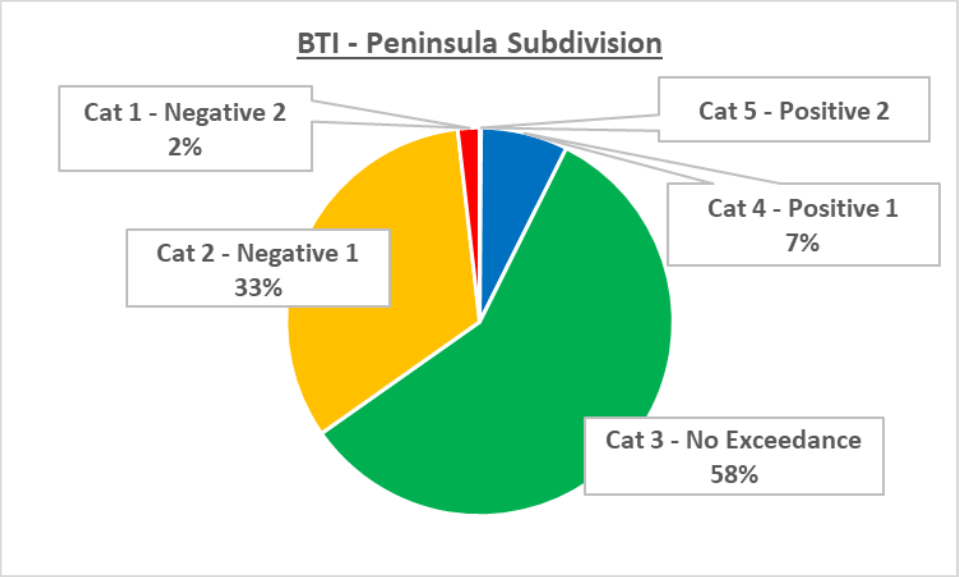

Figure 22. Percentage of BTI Categories on the Center Track of the Peninsula Subdivision

The FDL indicates the thickness of the ballast layer. As mentioned previously, a greater FDL depth will result in better drainage and is desired. The pie chart in Figure 23 indicates that the FDL for the Peninsula Subdivision is classified as poor for the majority (75%) of the tested track.

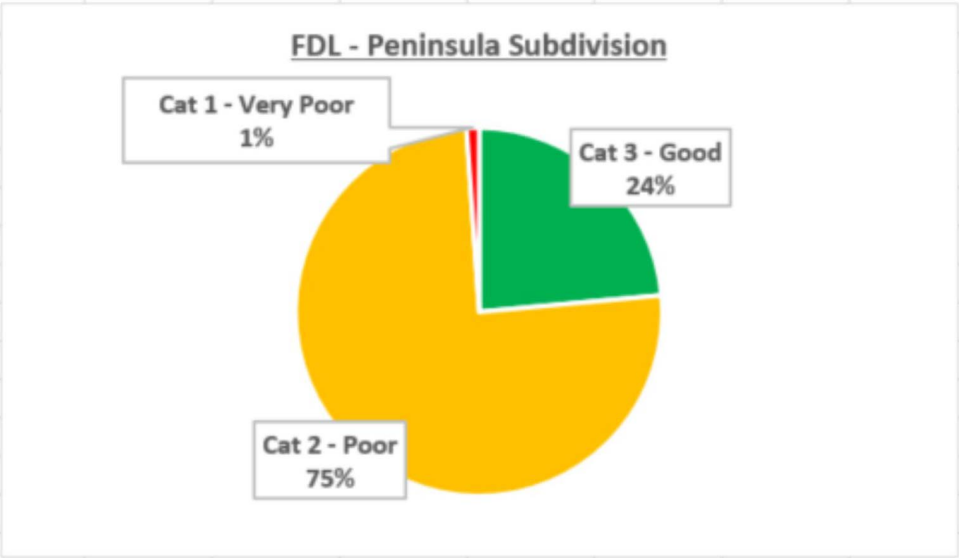

Figure 23. FDL Average for the Peninsula Subdivision

Other track geometry indices may be found in Appendix C.

3. Second 30-Mile Data Gathering and Processing Field Trip

This section outlines the second 19-mile data gathering and processing field trip on the HTL at FAST. This data provides a dry and wet assessment under controlled conditions.

3.1 Test Overview

As partial fulfilment of this contract with FRA, TTCI utilized the site visit of the DOTX218/220 consist on September 7, 2016, to provide calibration information for the newly installed GPR system on the T-20 car. GPR data was acquired at the FAST HTL at the TTC in Pueblo, CO. Since the entire FAST HTL was not serviceable at that time, the test plan was to complete several forward and backward passes of the consist around approximately 2 miles of the 2.9-mile loop. No data was acquired between HTL Section 3 and Section 8. A dry pass was logged first, then water was released at marked locations around the loop. Each location has different subgrade conditions, as shown in Table 9. Repeat time-metered surveys were undertaken on both the main and bypass sections of the FAST loop, prior to and after the release of approximately 1,000 gallons of water in each of the 10-tie wetted sections. These locations are indicated in Figure 24.

Table 9. HTL Subgrade Conditions of the Water Release Locations

Section No.	Tie No.	Bottom Layer
Section 29 (A)	Tie 124	Native Soil
Section 29 (B)	Tie 139	Vicksburg Clay
Section 29 (B)	Tie 200	Hot Mix Asphalt (HMA)
Section 40	Ties 500 and 520	HMA, Slab
Section 36	Tie 170	Native Soil

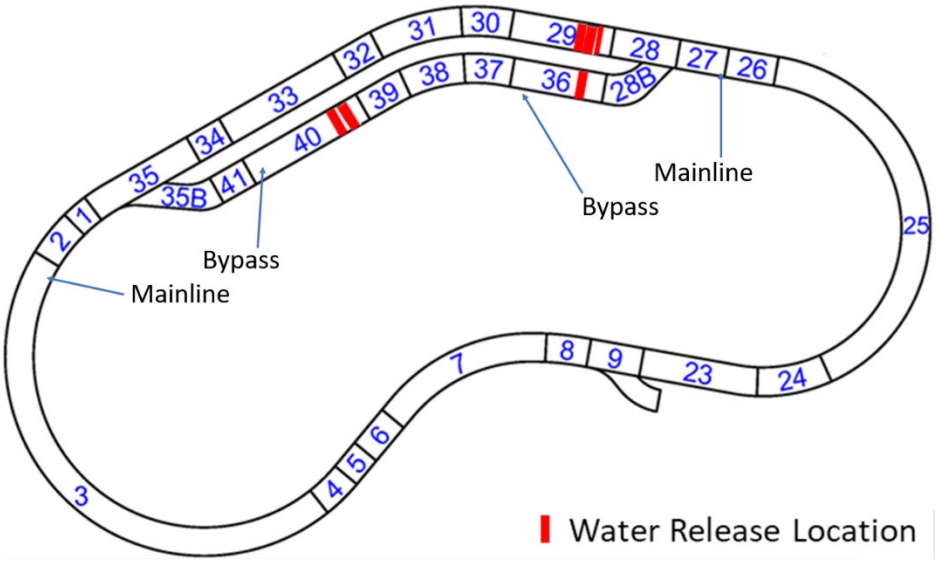

Figure 24. Designated Water Release Locations on the HTL at FAST

BBRI and Zetica analyzed the results of GPR data acquired by the T-20 car at the FAST HTL. Four test runs were performed for each watering location:

- Forward and backward pre-watering runs scanned the ballast in in-situ moisture conditions on four GPR channels. Data was checked for signal integrity before the water release was initiated. A minimum of 1,000 gallons of water was released at each site marked in red on the drawing in Figure 24.
- An initial run was performed immediately after the water release to observe moisture detection in upper sections of fouled ballast. Higher moisture should be detectable in upper ballast zone.
- A second run was performed after 1 hour to observe higher moisture in upper and mid-zone ballast areas.
- A third run was performed after 3 hours of the water release. Expect to see distributed moisture in the entire ballast zone, possibly with water ponding on top of the HMA and the open clay areas.

The following efforts were also made to investigate subsurface gradations, penetration resistance, and moisture:

- A variable energy dynamic cone penetration test using an instrumented rod to collect strength profile with depth (PANDA®) and insertion of camera into the same hole (geo-endoscopy) to video record ballast and soil layers for different sites.
- TTCI supplied photographs and observations from the different test locations at the FAST HTL.

Note that gradation tests were performed at the FAST HTL to calibrate/validate the GPR results, but were not used because of GPR antenna issues encountered at that time.

3.1.1 GPR Test

The primary objective of this GPR survey was to assess the ability of GPR to detect moisture within ballast. Eight survey forward and reverse runs were made by the T-20 car. The start and end of each water dump area was delineated in the GPR data using 12-inch by 16-inch (305 mm by 406 mm) aluminum plates (ADLs). The following list describes the direction and location of each numbered run:

Run 3 – Pre-Watering: Forward run over Main Loop

Run 4 – Pre-Watering: Reverse run through Bypass

Run 5 – Post-Watering: Forward run over Main Loop immediately after water dump

Run 6 – Post-Watering: Reverse run through Bypass immediately after water dump

Run 7 – Post-Watering: Forward run over Main Loop approximately 1 hour after water dump

Run 8 – Post-Watering: Reverse run through Bypass approximately 1 hour after water dump

Run 9 – Post-Watering: Forward run over Main Loop approximately 3 hours after water dump

Run 10 – Post-Watering: Reverse run through Bypass approximately 3 hours after water dump

Figure 25 is a photograph of a typical water release at HTL Section 40.

Figure 25. Typical Water Release at HTL Section 40

The GPR system on the T-20 has three 2 GHz antennas and one 400 MHz antenna, as shown in Figure 26. Two 2 GHz antennas for shoulder scanning were installed parallel to the track, 46 inches (117 cm) away from the track centerline. Crib scanning was fulfilled by one 400 MHz antenna and one 2 GHz antenna, which were placed in the track lateral direction.

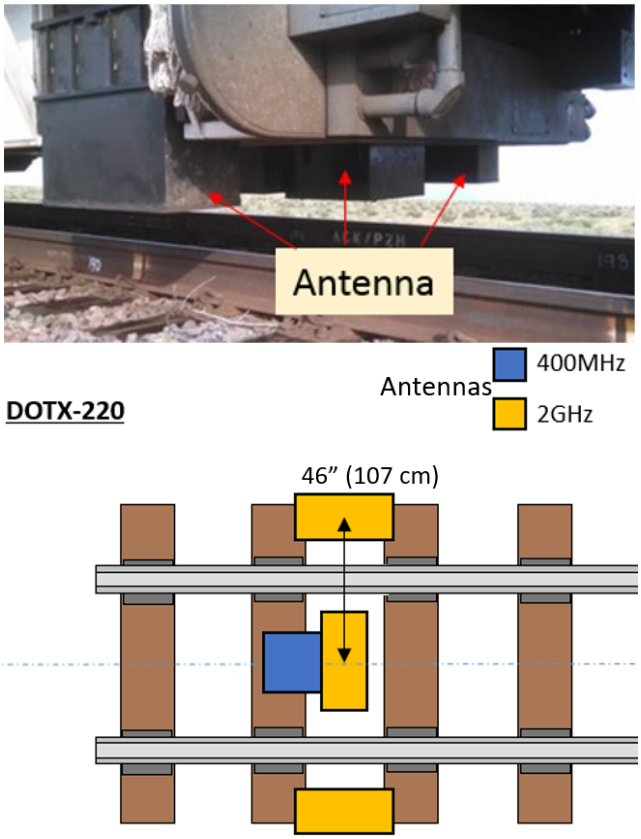

Figure 26. GPR System on T-20 Car; Diagram of Extended Shoulder Antenna Positions Relative to Rails

The GPR results for all four locations are discussed in the following sections. The positions of the ADL markers are indicated by yellow arrows. An analysis of the data has highlighted an issue with the shoulder 2 GHz antennas on the test car, which was subsequently addressed. As a result, data presented in this section are limited to those which were acquired with the center 2 GHz and 400 MHz antennas.

Section 29 – Location A

The processed radargram images in Figure 27 present the 400 MHz data acquired over the first of the two water release locations in Section 29. The positions of the ADL markers are indicated by yellow arrows. The most significant visible change in the data following release of the water is an increase in the reflectivity of a previously poorly defined interface at 8 nanoseconds of two-way travel time (TWTT). This increase is evident immediately following the water release. Approximately 3 hours after the water release, the amplitude of reflection at this interface has decreased, but remains above its pre-water release level.

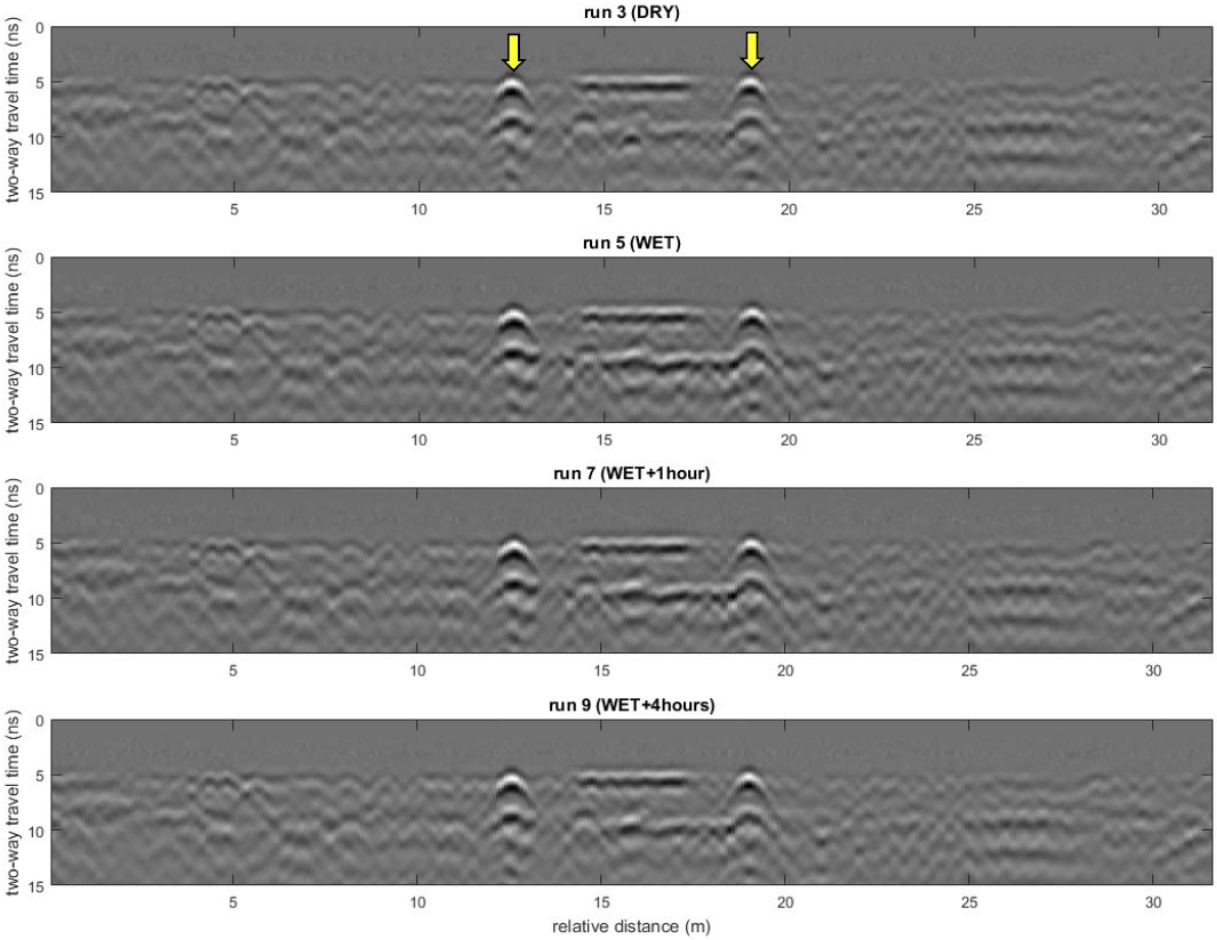

Figure 27. Section 29 Location A (Tie 124): GPR Radargrams from the 400 MHz Antenna

Figure 28 presents the 2 GHz data acquired prior to the water release (top) and immediately after the release (center), which also illustrates the change in reflectivity on the layer interface identified at 8 nanoseconds of TWTT, as seen in the 400 MHz data. The bottom image presents a

difference plot of signal amplitude derived from the upper two radargrams. The water release results in a well-defined change in signal amplitude throughout the measured time-depth range in the area between the two ADL markers, with the strongest increase observed at the primary interface. Outside the ADL markers, the difference plot shows no significant change below the surface.

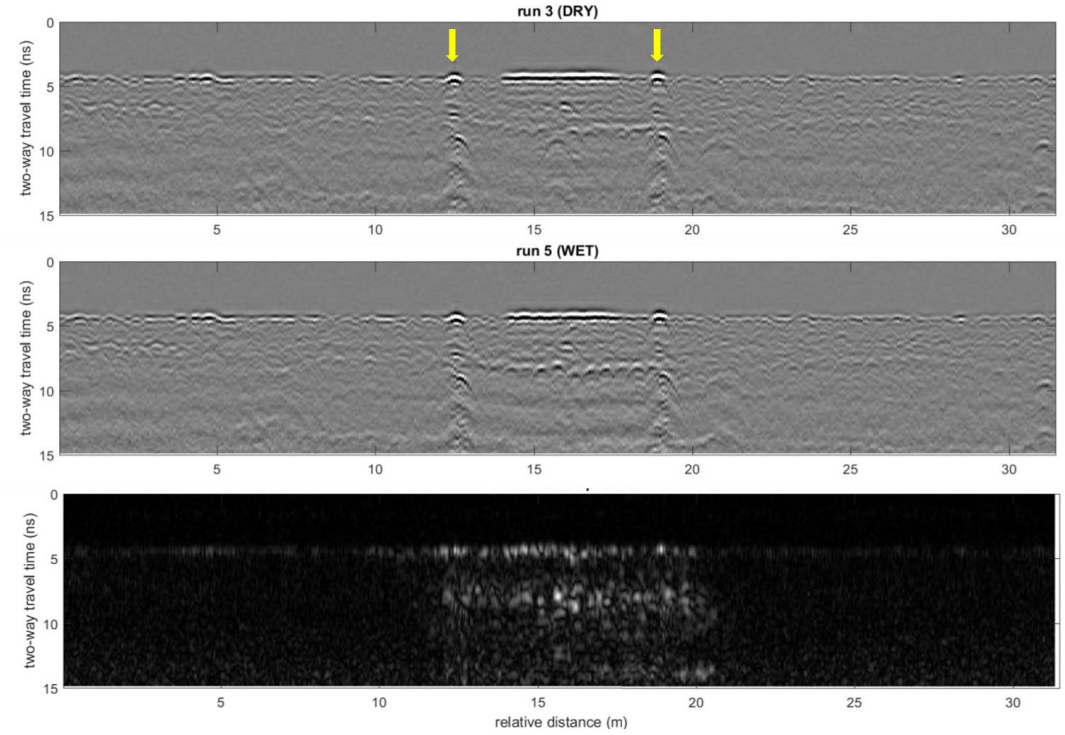

Figure 28. Section 29 Location A (Tie 124): GPR Radargrams from the 2 GHz Antenna

Figure 29 presents the modeled primary and secondary layer interface depths of Section 29 (at Location A and Location B) before and after watering. All depths were calculated using a signal velocity through the track bed of 5.5 in/ns (140 mm/ns). Two layer interfaces were identified within the data at modeled apparent depths of 9.8 to 13.8 inches (250 to 350 mm) and 23.6 to 29.5 inches (600 to 750 mm). These are interpreted as the base of clean ballast and the top of subgrade, respectively. The plot illustrates changes in the apparent depth of the two interfaces after the water release event. The primary interface exhibits minimal change, indicating that the water has resulted in no significant change in the dielectric signal of the overlying ballast. This implies that the ballast is free-draining and clean. An apparent increase in the depth of the secondary interface is observed immediately post-release, suggesting that water has been retained in the sub-ballast layer. This has resulted in an increase in the dielectric properties of the materials and a consequent decrease in GPR signal velocity. This could reveal a potential source of error in the modeled depth of the secondary layer interface, as an increase in dielectric signal variation is observed.

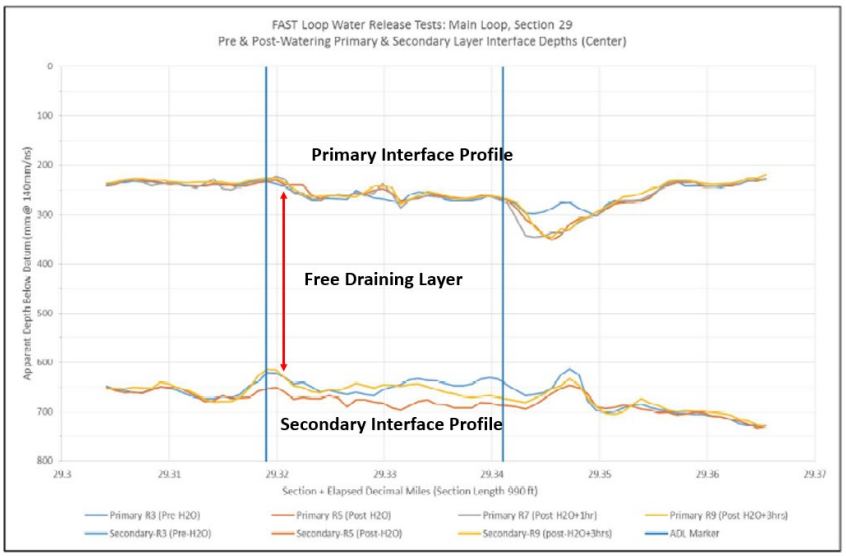

Figure 29. Section 29 Location A: Depth Calculation

Section 29 – Location B (Centered around Tie s139 and 200)

Unlike Location A, no clear layer interfaces were observed (see Table 9 for the location), implying that there is a gradational change in the dielectric from the ballast into the sub-ballast materials. The difference plot (Figure 30 bottom) shows small changes in response to wetting of the track bed. Outside the ADL markers, the difference plot shows no change below the surface. It would not be possible to identify the extent of moisture from a single survey in this location. Visually, the dry and wet survey results look almost identical. Only the difference plot shows subtle change. The 400 MHz data (Figure 31) shows a similar subtle change in reflection amplitude within the water release area immediately following the release event.

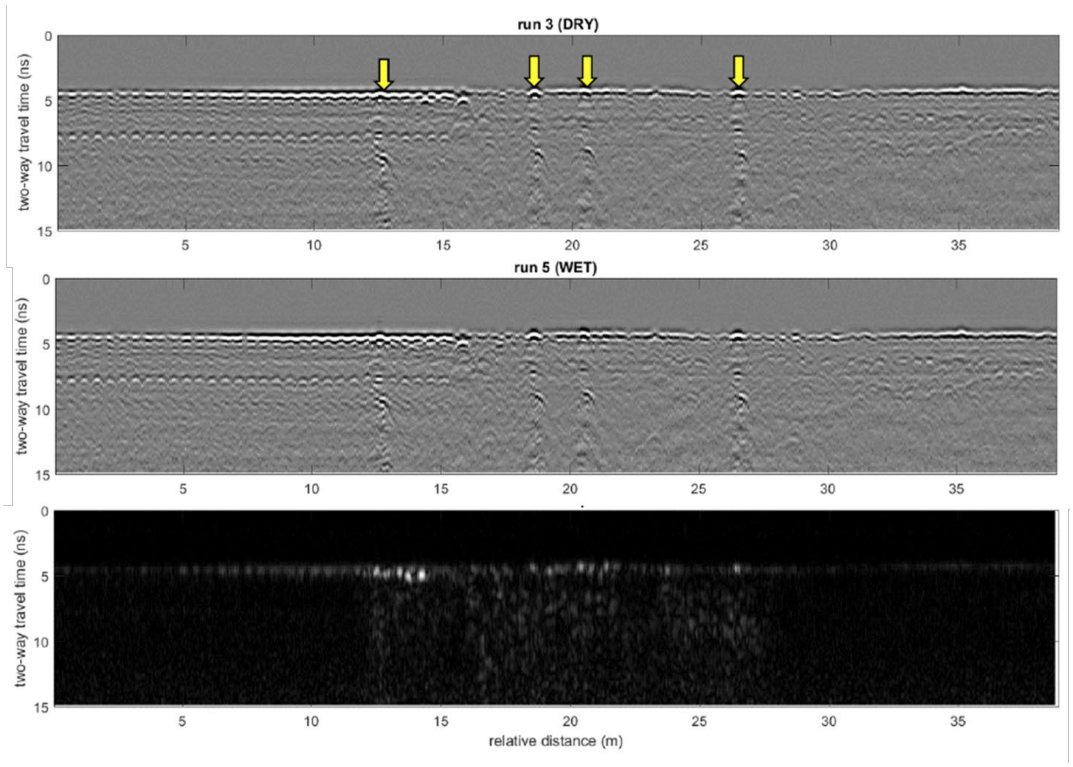

Figure 30. Section 29 Location B (Centered at Ties 139 and 200): GPR Radargrams from the 2 GHz Antenna

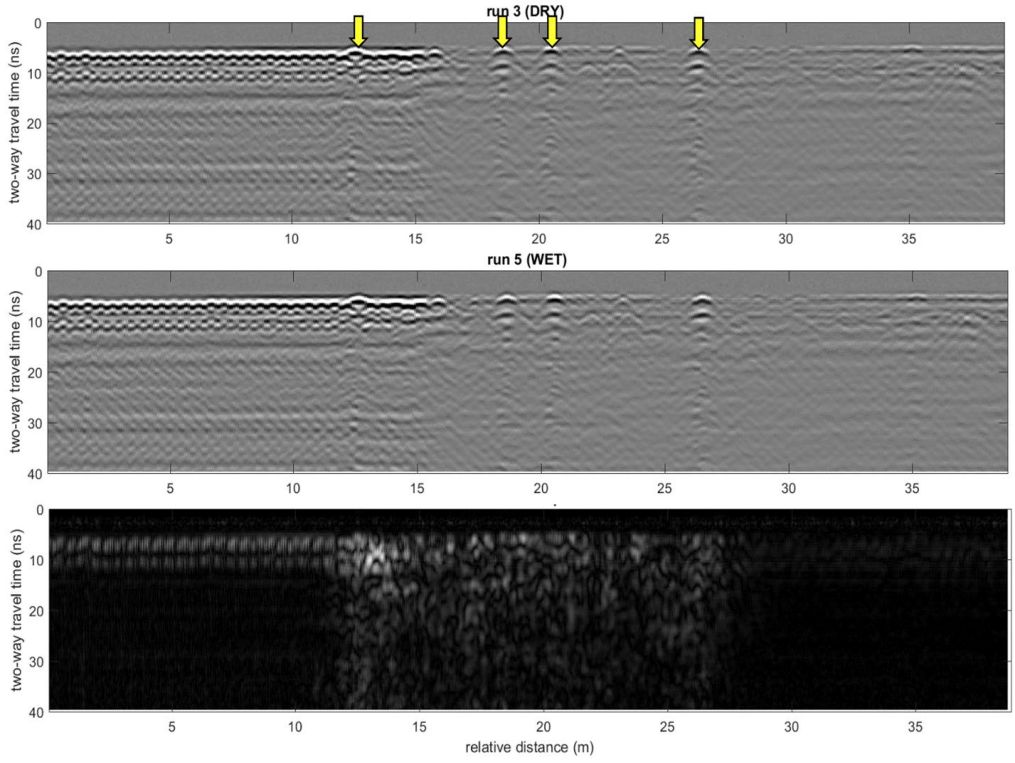

Figure 31. Section 29 Location B (Centered at Ties 139 and 200): GPR Radargrams from the 400 MHz Antenna

Section 36

In contrast to Section 29A, the reflection in the 2 GHz data (Figure 32) at the primary interface exhibits a visible decrease in amplitude subsequent to the release of the water. This is attributed to increased signal attenuation within the upper ballast layer associated with retention of water by relatively fouled ballast. The difference plot illustrates a pattern of well-defined changes in signal amplitude throughout the measured time-depth range in the area between the two ADL markers. Figure 33 shows GPR Radargrams from the 400 MHz antenna.

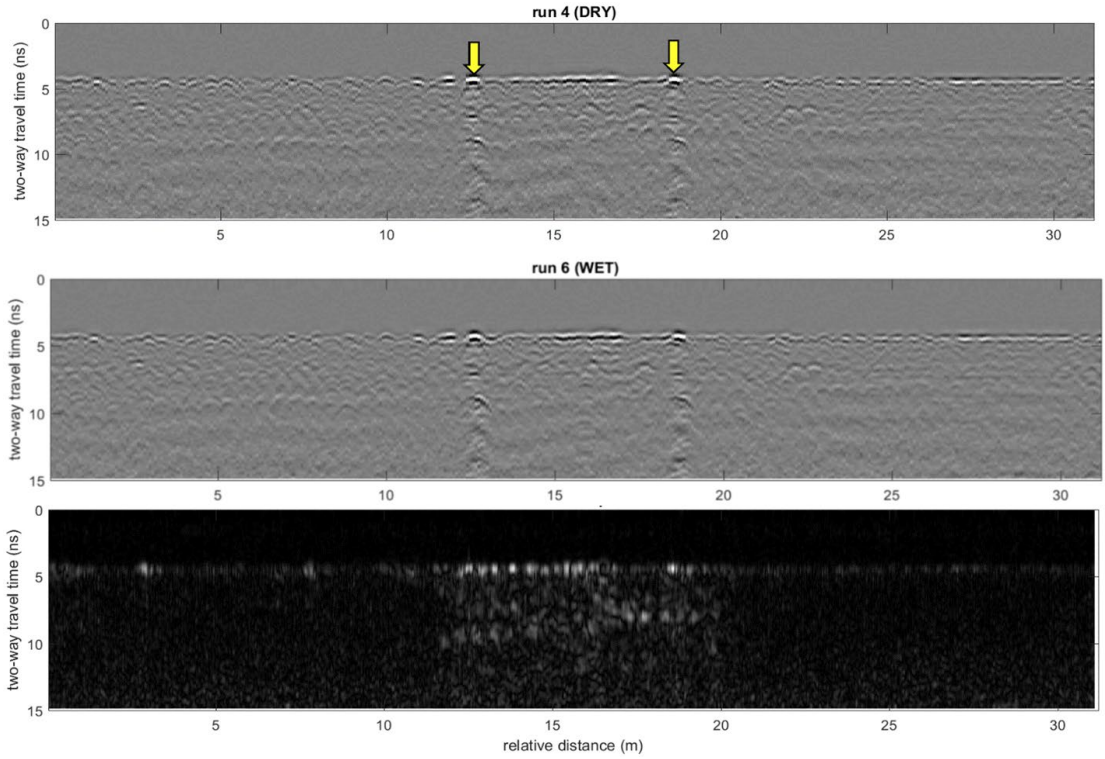

Figure 32. Section 36 (Centered at Tie 170): GPR Radargrams from the 2 GHz Antenna

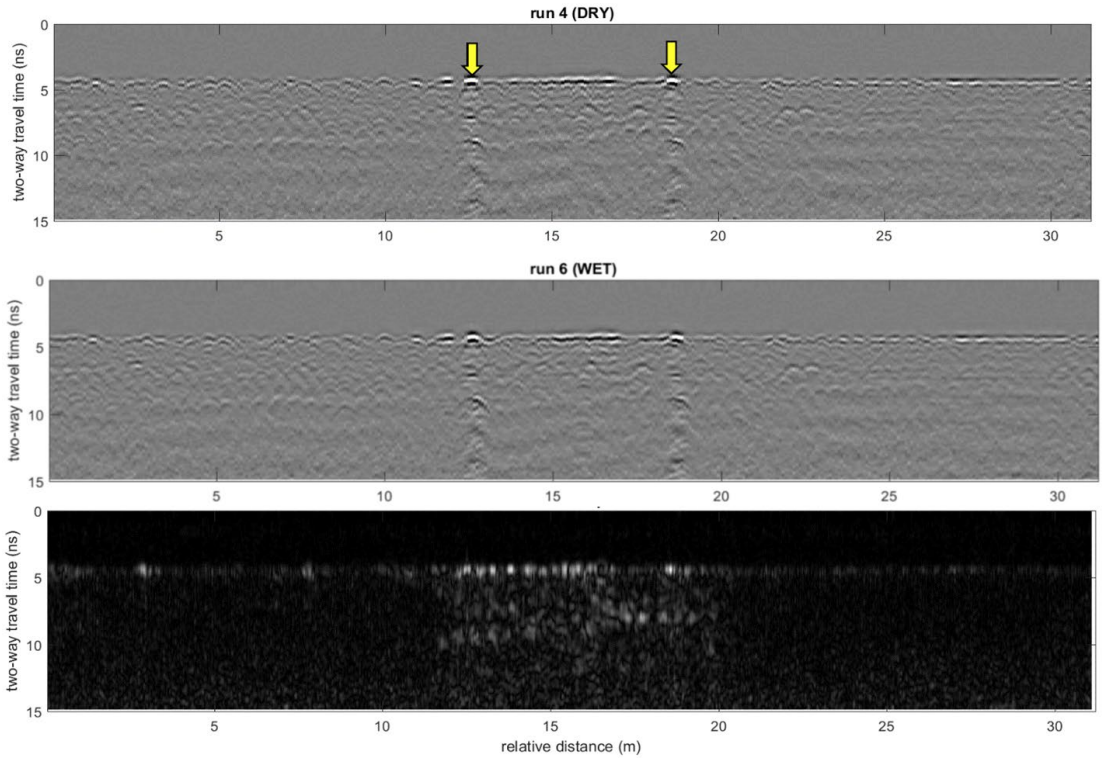

Figure 33. GPR Radargrams and Amplitude Difference Plot from the 400 MHz Antenna at Section 36

Section 40 (Centered at Ties 500 and 520)

An absence of identifiable layer interfaces within these two areas means that there is no visible indication of increased moisture within the track bed subsequent to the water release. The 2 GHz antenna difference plot (Figure 34) indicates that downward migration of water is being impeded with most of the variation confined to the top 15 nanoseconds. The apparent distribution of moisture suggests that either water was released over a wider area than planned, or water was able to flow down a relatively impermeable track bed layer towards Section 39. The 400 MHz data (Figure 35) shows similar changes in reflection amplitude within the water release area to that observed in the 2 GHz dataset.

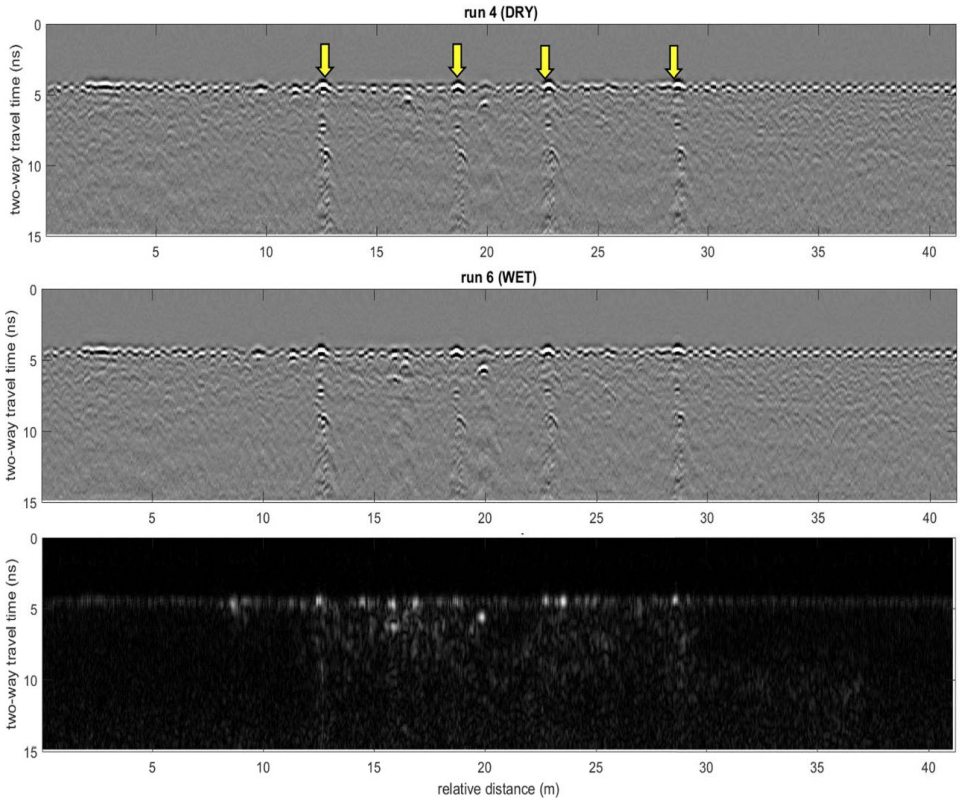

Figure 34. Section 40: GPR Radargrams from the 2 GHz Antenna

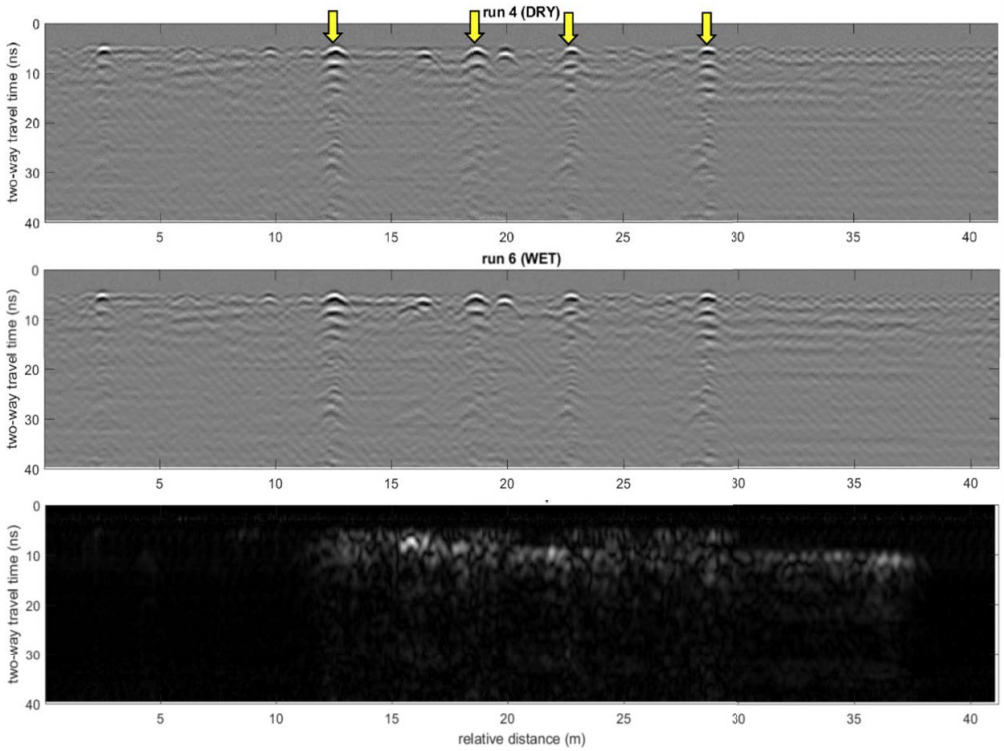

Figure 35. 400 MHz GPR Radargrams and Amplitude Difference Plot (bottom) From Section 40

3.1.2 Issue of Noise in Shoulder Antenna and Solution

Results from recent testing with the GPR system mounted on the T-20 car at the FAST HTL has highlighted an issue with data quality on both of the shoulder 2 GHz antennas.

The shoulder antennas were designed to meet the requirements of the Plate C clearance envelope (Figure 2), and consequently were mounted approximately 10.5 inches (267 mm) from the outside edge of each running rail when deployed (as measured to the centerline of the antenna). Antenna-rail proximity testing undertaken prior to the T-20 install indicated that this offset distance should not significantly degrade the GPR data quality. For practical reasons, testing had to be undertaken with the antennas outside of the shielded housings used on the T-20 car.

Existing railbound 2 GHz shoulder installations undertaken by Zetica on other platforms have not been affected. In these instances, the antenna-to-rail offset has been larger (+14 inches [+356 mm]). The increased offset (~21 inches) from the center 2 GHz antenna to the inside edge of the rails means that the center data on the DOTX220 installation is unaffected, with the antenna providing comparable results to data acquired using other acquisition platforms.

Although both shoulder antennas were functioning, the reduced quality data from the shoulder 2 GHz antennas has a similar appearance to data acquired over poor quality track bed, with rapid attenuation of the signal and a consequent dominance of multiple ("ringing") reflections. This ringing was addressed with subsequent design changes Figure 36 provides examples of 2 GHz data from the center and shoulder from runs undertaken at the TTC. The center data (upper plot) shows a clear layer reflection from 6,332 feet to 6,660 feet (1,930 m to 2,030 m). However, the shoulder signal (lower plot) was attenuated fast, making the layer reflection unclear. Note that the shoulder data shows the expected subsurface features in some areas (e.g., reflection at 6,529 feet [1,990 m]), but the signal-to-noise ratio is generally much lower than the center.

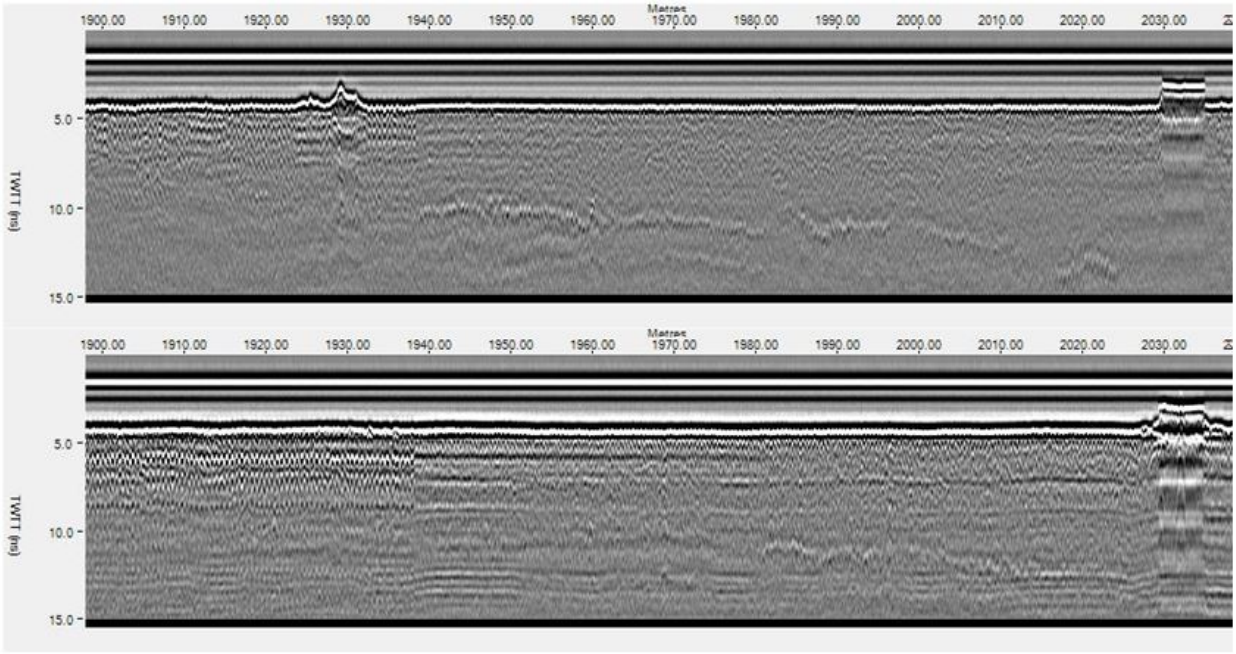

Figure 36. Example Data: TTCI HTL at the FAST
(Upper Plot is Center Data; Lower Plot is Shoulder Data)

It is suspected that the multipath reflections associated with rails and metallic antenna housing is the possible cause of this shoulder antenna issue. It is possible that there is an effective multiple pathway, which allows the GPR signal to bounce back and forth in the air gap between the rails and the antenna and overwhelm the (weaker) signals from the subsurface. These reverberations are high-amplitude and due to vehicle suspension movement, are not constant in time. This makes them difficult to remove in post-processing.

Based on the results of the testing, the following recommendations were made and implemented:

- The use of non-metallic housings has been shown to provide limited improvement in data quality compared to the current metallic housings. It was therefore recommended that the current housings be retained as they provide additional benefit in the form of EMI shielding.
- Move the shoulder antennas outboard and raise the antennas to ensure they remain within the Plate C envelope. The results of trolley-based tests suggest that an increase in the height and lateral offset of the shoulder antennas of 3.4 inches and 4 inches, respectively was required.

Add radar-absorbent material (RAM) shielding in the gap between the shoulder and center antennas to reduce the number of multiple reflection pathways caused by the close proximity of the shoulder antennas to the rail and the body of the test car (in particular within the locker space between the antennas). Figure 41 (blue hatching) shows proposed foam RAM placement locations.

Based on the results of the recent testing, the following recommendations are made:

- The use of nonmetallic housings has been shown to provide limited improvement in data quality compared to the current metallic housings. Therefore, it is recommended that the current housings be retained, as they provide additional benefit in the form of EMI (electro-magnetic induction) shielding.
- Move the shoulder antennas outboard and raise the antennas to ensure they remain within the Plate C envelope. The results of trolley-based tests suggest that an increase in the height and lateral offset of the shoulder antennas of 3.4 inches (86 mm) and 4 inches (102 mm), respectively, is required.
- A 10-degree rotation produces some improvement, but not as significant as increasing the lateral and vertical offset.
- Radar-absorbent plugs were mounted below the vehicle in the space between the shoulder and center antennas to prevent ringing in the data associated with reflected radiation from the locker cavity.
- Add foam RAM shielding to the areas around the antenna housing, to reduce the number of multiple reflection pathways caused by the close proximity of the antenna to the rail and the body of the test car (see Figure 37).

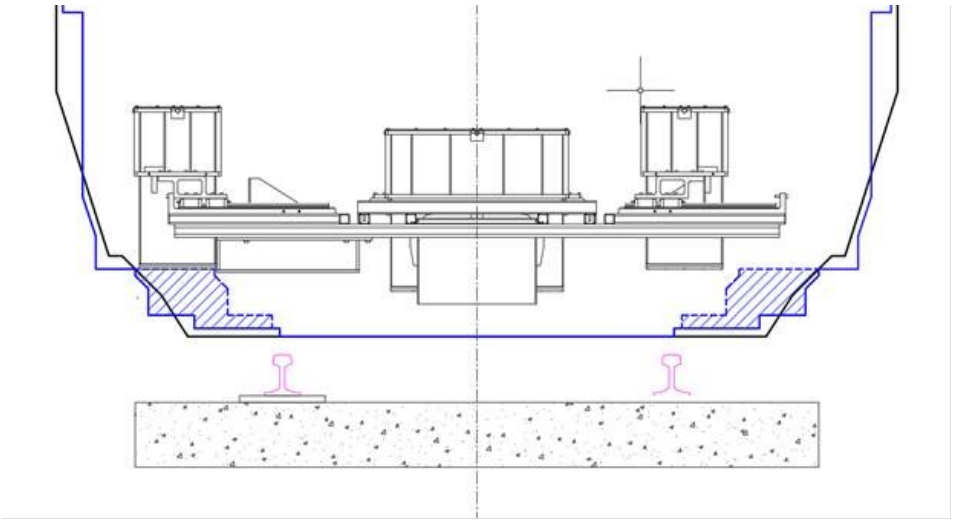

Figure 37. Shielding between the Shoulder and Center Antennas (Blue Hatching Shows Shielding Locations)

3.1.3 Dynamic Cone Penetrometer (DCP) Test and Geo-Endoscopy Test

The DCP test consists of driving a set of steel rods equipped with a conical tip into the soil by hammering (standardized hammer). At each hammer blow, the energy is measured in the anvil with energy gages. Other sensors simultaneously measure the settlement or vertical displacement of the cone. All the data is transmitted to the acquisition unit equipped with customized software. The results are given as penetrograms, graphs that show the California Bearing Ratio (CBR) according to depth.

Geo-endoscopy tests consist of introducing a small diameter (0.3 inch [8 mm]) endoscopic probe into a hole previously made by DCP tests or by any other boring method. A video is then continuously recorded to characterize the different soil layers. Images extracted from this video are then computed using automatic image analysis programs to provide information for each layer, such as thickness, nature, humidity, etc. Endoscopic images (Table 10) and DCP data are processed at the same time to define and characterize the different substructure layers (Figure 38 to Figure 41). Appendix F contains more information regarding these tests.

There are three levels of moisture determined using endoscopic images:

- Dry
- Wet
- Saturated

Table 10. Visual Criteria for the Endoscopic Images

Layer	Visual Criteria
Ballast	Voids between ballast grains are filled with air
Fouled Ballast	Voids are partially or completely filled with fine grained material
Interlayer	Mix of the upper layer ballasted and lower layer
Sub-ballast Layer	Backfill material that is present only in new lines
Subgrade	Usually natural soil, but may be artificial fill in embankment and approaches

Section 29 Location A

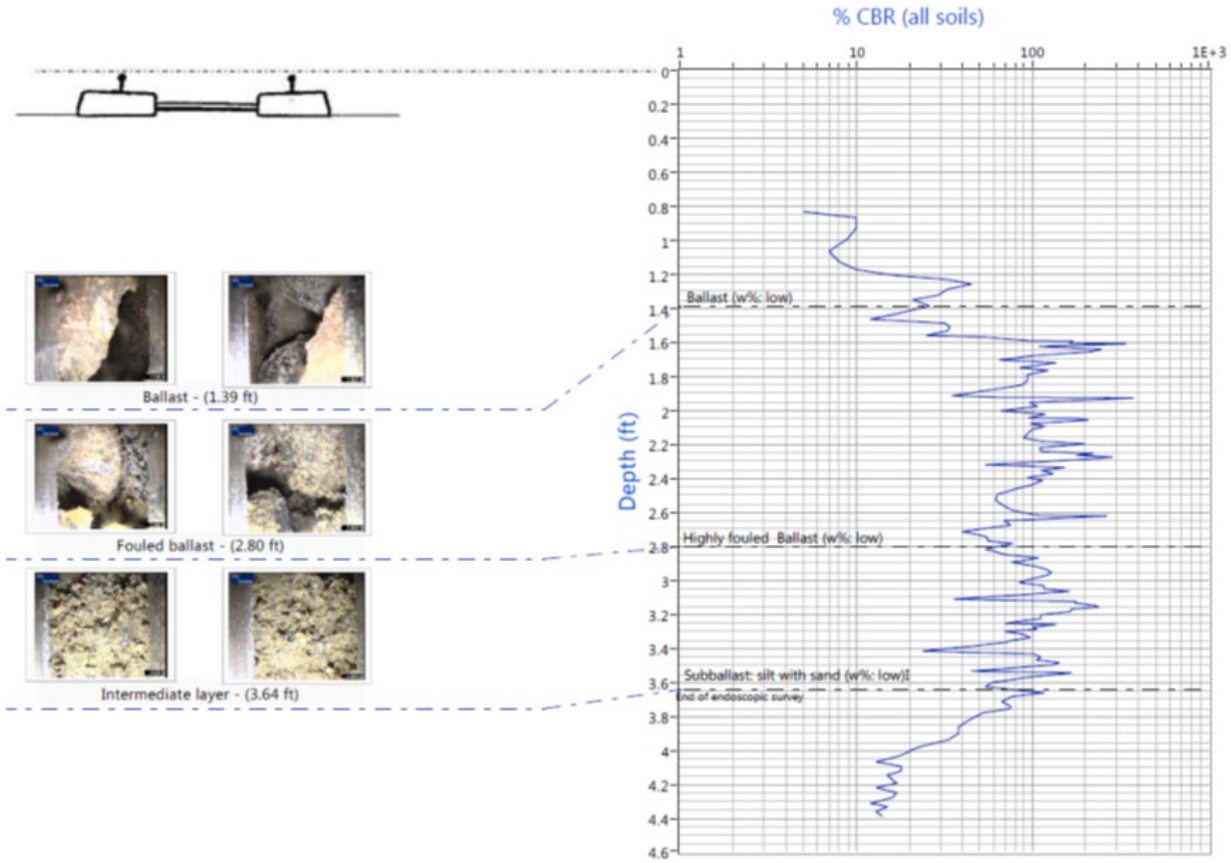

Figure 38. Section 29 Location A Endoscopic Images and DCP Data

Section 29 Location B

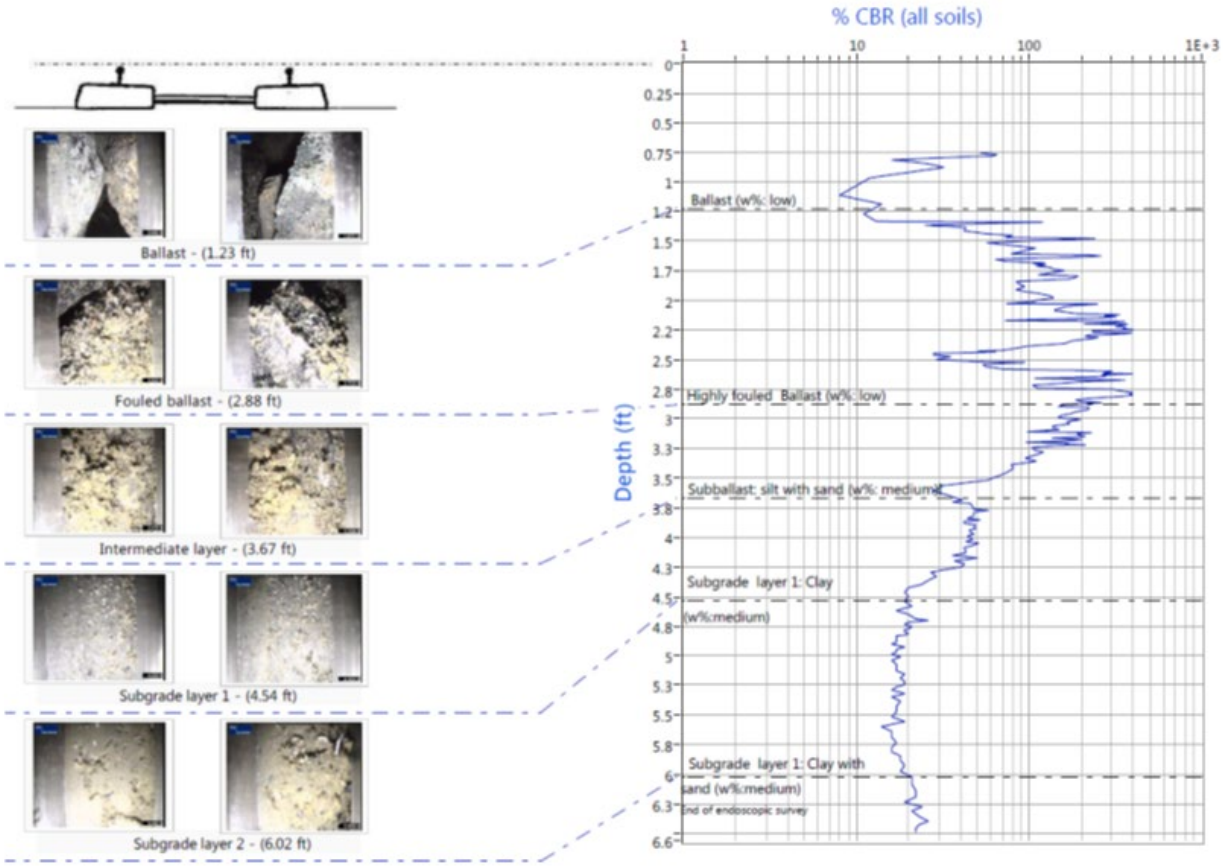

Figure 39. Section 29 Location B Endoscopic Images and DCP Data

Section 36

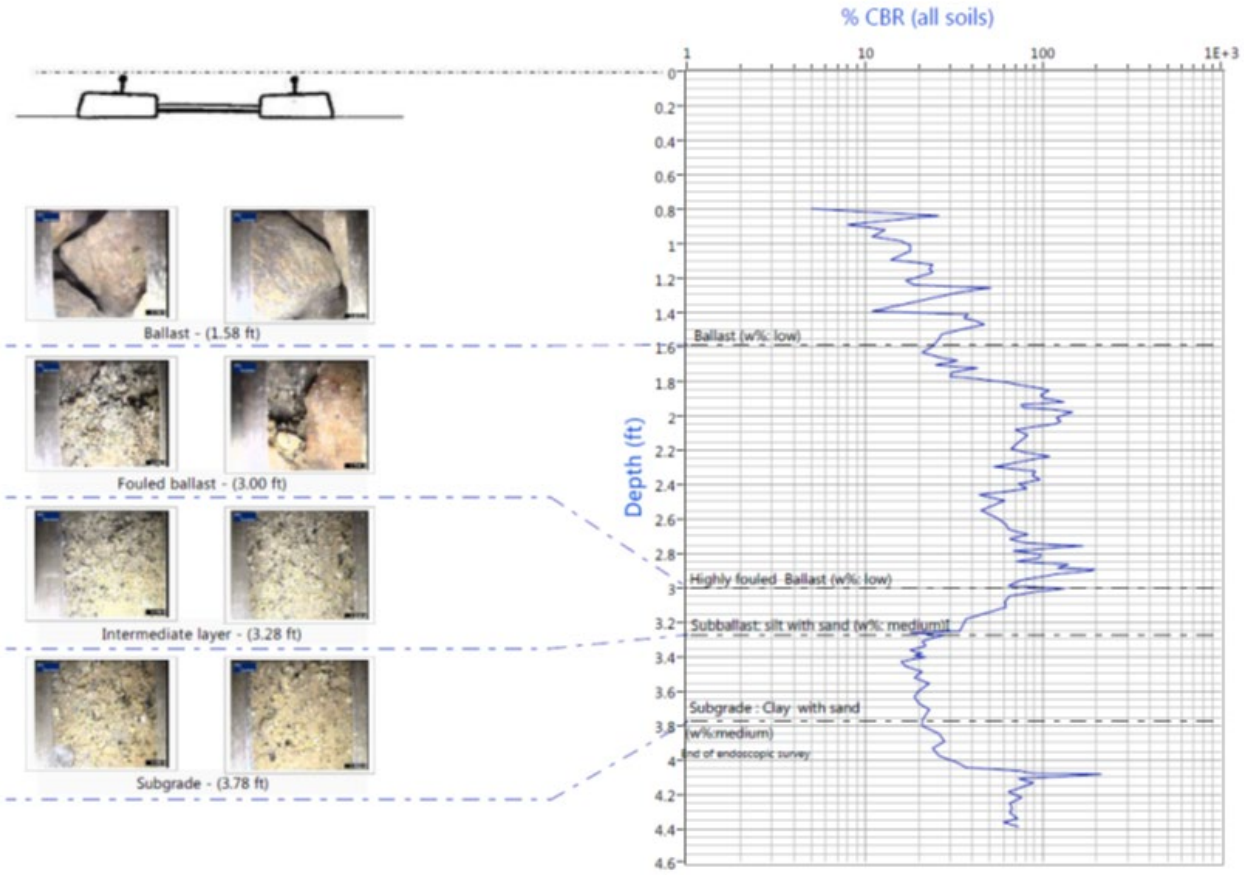

Figure 40. Section 36 Endoscopic Images and DCP Data

Section 40

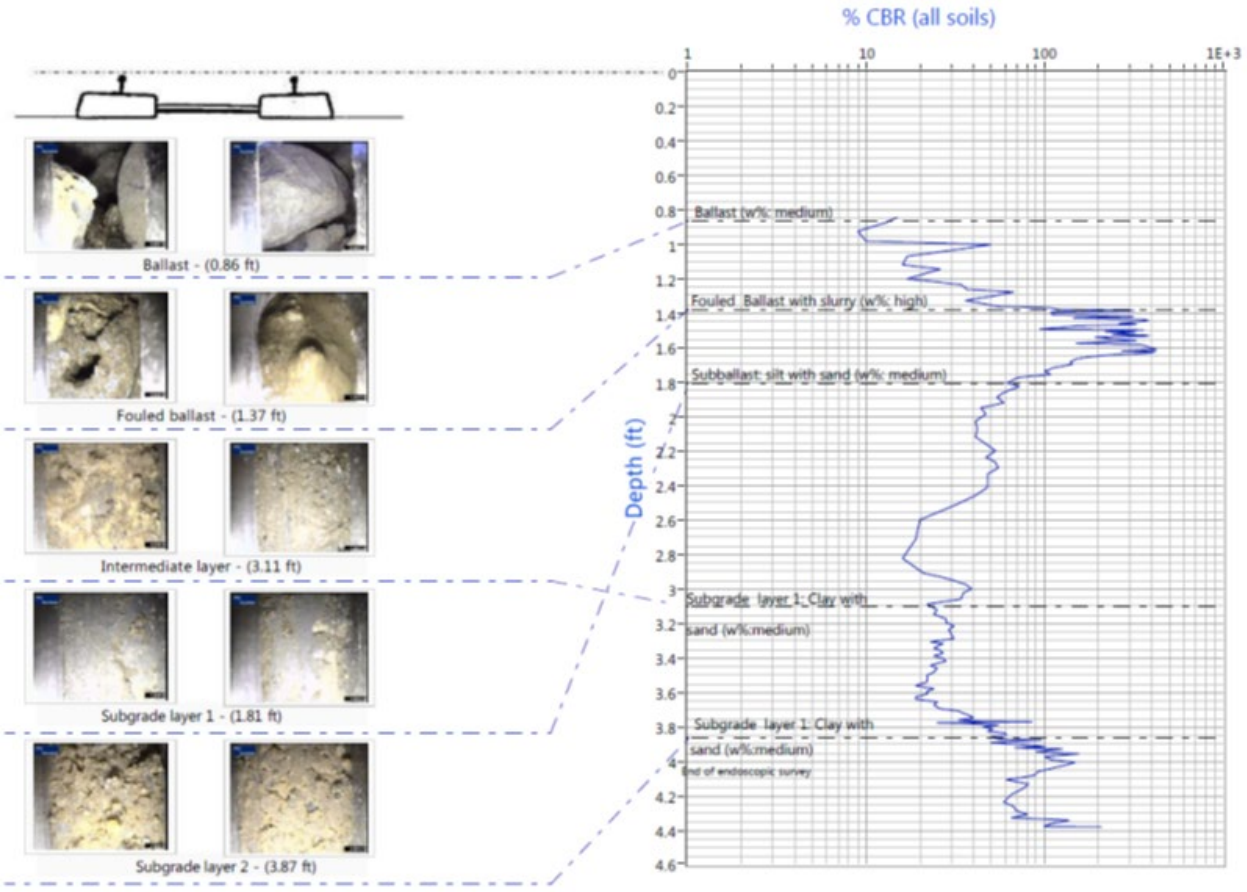

Figure 41. Section 40 Endoscopic Images and DCP Data

3.1.4 Summary and Conclusions

Table 11 presents a summary of the FAST GPR tests.

Table 11. Summary of the FAST GPR Tests

Section	Observations	Interpretation	Comments
Section 29A	Minimal change seen in data before ~8 ns. Significant brightening seen of layer at ~8 ns. Change seen in apparent depth of deeper layers.	This is likely to be clean ballast with good drainage with moisture being retained by the layer below.	After wetting, the data shows an anomalously bright layer at the base of clean ballast. This is due to the increased dielectric contrast at the boundary between the well-drained ballast and wet/fouled material below. This is a systematic change that can provide evidence of moisture content without a repeat survey. With repeat data, an increase in the apparent depth of deeper

Section	Observations	Interpretation	Comments
			layers is seen. This is due to a reduced speed of wave propagation in the wet layer.
Section 29B	No clear layers seen in this area. Difference plot shows change in response to wetting.	The difference plot shows the lateral extent of the water release area.	The difference plot (at least two separate surveys) shows where subtle changes in arrival time and amplitude have occurred, but, as there is no pattern to these changes, it would not have been possible to identify moisture from a single survey of this area.
Section 36	Layer at ~9 ns becomes weaker and its apparent depth increases.	In this case, water is being retained above the primary layer, relating to relatively fouled ballast. This results in increased attenuation and a slower propagation velocity in the upper layer, causing the primary to reduce in amplitude and arrive later.	The change in amplitude is subtle and does not stand out as anomalous in either the dry or wet data. As such, the moisture would be difficult to detect with a single survey. With repeat data, it is possible to identify the run with higher moisture content and where that moisture is distributed.
Section 40	Layers are generally not very clear in this area. Difference plot shows lateral extent of moisture extending ~33 feet (10 m) beyond surface plates (towards Section 39). The change in moisture content appears to increase in depth towards Section 39.	The apparent distribution of moisture suggests that either water was released over a wider area than planned, or water was able to flow down a gradient towards Section 39.	After wetting, there is an extra layer, which is most visible at ~8 ns from 98.4–114.8 feet (30–35 m) of the plotted distance. This might be interpreted as evidence of moisture in a single survey but could be easily confused with a change in material type. The repeat data allows us to identify that the moisture level has increased and estimate its lateral and vertical distribution.

The results of the tests highlighted the challenges in determining the moisture content from GPR track bed surveys.

For the available spots that repeat survey information:

- Difference plots can be used to highlight subtle changes in arrival time and amplitude that result from changes in percent moisture content. These provide an effective map of the lateral and vertical changes in percent moisture that have occurred.
- Where moisture is retained within the material above a layer boundary (i.e., in fouled ballast), the associated increase in the dielectric of the material will result in an apparent increase in layer thickness (Figure 29). Comparison of the modelled depths derived from the individual surveys may be utilized to determine relative changes in percent moisture content.

In the case of a single survey:

- Analysis of the relative amplitude of reflections at layer boundaries within the track bed can be used to infer relative moisture levels at the interface, but this method is ambiguous due to the following:
  - Localized changes in material type (such as subgrade or fouling changes or moisture changes) above or below the interface may also result in changes in amplitude
  - In cases where the ballast is relatively fouled, increased signal attenuation as a result of the elevated moisture levels that can result in a decrease rather than increase in layer amplitude (e.g., Section 36)

Although both the 2 GHz and 400 MHz antennas can be used to map the amplitude differences between repeat runs, the 2 GHz offers the following important advantages:

- A more detailed difference plot compared with the 400 MHz antenna, showing areas of the track bed most affected by moisture ingress and egress
- An accurate measure of the subtle changes in layer thickness required for analysis of relative changes in layer dielectric and, thus, moisture
- Normalization of the signal required for reflection amplitude analysis. The longer wavelength of the 400 MHz antenna means that the breakthrough (direct coupling arrival) and surface reflections cannot be separated, preventing accurate amplitude normalization.

Additionally, the 2 GHz is utilized for modeling of the BFI. The BFI can be considered to provide a measure of "moisture potential" within the ballast, as fouling is directly related to the free-draining capability of the ballast. Where the BFI is high, the potential for elevated moisture levels within the ballast is higher (irrespective of environmental factors). As shown in Section 29A, where the ballast is free-draining (i.e., modeled BFI = Moderately Clean), moisture levels will remain low even after a wetting event.

4. Third 30-Mile Data Gathering and Processing Field Trip—Ravenna Subdivision, Nebraska

During the week of August 28, 2017, TTCI, Sol Solution, BBRI, Zetica, and BNSF performed a joint study to demonstrate and calibrate the new GPR system mounted on FRA's T-20 research car on revenue service track.

The test objectives were the following:

- Physically sample and test multiple track locations with diverse ballast conditions and obtain the layer depths, gradation, and moisture of each location
- Compare the sampling results with the GPR measurements to assess the capability of GPR to detect and model the presence of ballast fines and moist substructure conditions
- Comparison of the modeled BFI determined from the T-20 and hi-rail datasets with the calculated FI obtained from gradation of bulk ballast samples
- Comparison of the modeled FDL determined from the T-20 and hi-rail datasets with measured depths to fouling observed in the sampling tubes

4.1 Site Background

The BNSF Ravenna Subdivision from MP 10 to MP 40 was selected for this study and is shown in Figure 42. This line is a double mainline track, with Track 1 primarily concrete ties and Track 2 primarily timber ties. The line supports about 45 million gross tons (MGT) annually of dominantly coal train traffic.

Figure 42. Ravenna Subdivision Sampling and Test Section

4.1.1 Work Description

Multiple methods were used to characterize the ballast. Truck-mounted GPR and T-20's GPR mount were used to estimate the FDL and ballast fouling. Dynamic penetrometer methods and

geo-endoscopy methods were used to aid in determining layer depths, moisture, and track stiffness by cone resistance. TTCI physically sampled the ballast using BNSF's vibrometer to measure gradation and moisture content. Shelby tubes and baggie samples were also taken at select locations for analysis of fines index properties. All these methods are discussed in the report.

BBRI arrived onsite during the week of August 21, 2017, to perform preliminary work on GPR characterization of the Ravenna Line test section using a standard hi-rail truck. The purpose of this work was to test the present condition of the track using a standard method and equipment, and to provide a comparison of the GPR baseline for the upcoming T-20 GPR system analysis. The results of this work are presented in this section.

Sample locations were recommended based on previous truck hi-rail runs on this line in 2015 and 2016. The goal was to identify a variety of fouling types and GPR signatures that would be beneficial to the current calibration work for the T-20 GPR system. The sampling sites recommended are identified in Table 12. Appendix D contains additional information.

Table 12. Recommended Sites for 2017 Ballast Sampling on Ravenna Line, 2015–2016 Data

BFI Key		
Category	BFI	Description
1	>=40	Highly Fouled
2	20 - < 40	Fouled
3	10 - < 20	Moderately Fouled
4	1 - < 10	Moderately Clean
5	>1	Clean

Location	Track ID	Milepost	Tie Type	BFI Left	BFI Center	BFI Right
01	1	11.047	Concrete	2	1	4
02	1	11.058	Concrete	3	2	4
03	1	11.151	Concrete	4	4	4
04	1	13.563	Concrete	4	5	5
05	1	22.700	Concrete	5	4	4
06	1	22.717	Concrete	4	2	4
07	1	22.734	Concrete	3	1	3
08	1	22.772	Concrete	4	2	4
09	1	23.811	Concrete	5	4	4
10	1	24.037	Concrete	4	3	4
11	1	25.788	Concrete	5	4	4
12	1	26.737	Concrete	4	2	4
13	1	26.763	Concrete	4	3	4
14	1	27.729	Wood	5	3	4
15	1	27.754	Wood	4	1	4
16	1	35.578	Wood	5	2	3
17	2	11.027	Wood	3	2	2
18	2	11.084	Wood	3	1	3
19	2	13.854	Wood	3	1	3
20	2	14.237	Wood	3	1	3

Location	Track ID	Milepost	Tie Type	BFI Left	BFI Center	BFI Right
21	2	22.780	Wood	4	3	5
22	2	25.791	Wood	4	3	4
23	2	26.766	Wood	3	1	4
24	2	27.178	Wood	4	3	4
25	2	27.243	Wood	4	2	4
26	2	35.558	Concrete	4	1	4
27	2	37.771	Wood	4	3	4
28	2	26.732	Wood	3	2	4
29	2	39.871	Wood	2	2	2
30	2	39.990	Wood	3	1	3

4.1.2 Physical Sampling Plan

TTCI sampled nine track locations with 2 to 6 samples per location for a total of 39 samples. The sampling locations were collaboratively selected prior to sampling, with the goal of selecting locations with diverse conditions. These locations were generally between Seward, NE, and Milford, NE, with a single site (No. 1, ID 29) located about 10 miles west of Seward, NE. Table 13 shows general information from the nine sites and Table 14 lists the Global Positioning System (GPS) coordinates. Figure 43 displays the locations.

Table 13. General Information of the Nine Sampled Site Locations

Number	Sample ID*	Milepost	Date	Track	Tie	Number of Samples
1	29	39.871	8/28/2017	2	Timber	6
2	23	26.767	8/29/2017	2	Timber	4
3	28	26.732	8/29/2017	2	Timber	6
4	22	25.791	8/29/2017	2	Timber	6
5	11	25.788	8/30/2017	1	Concrete	4
6	13	26.763	8/30/2017	1	Concrete	4
7	14	27.729	8/30/2017	1, Switch	Timber	3
8	8	22.772	9/1/2017	1	Concrete	4
9	6	22.717	9/1/2017	1	Concrete	2

*Track 1 is primarily concrete ties and Track 2 is primarily wood ties.

Table 14. GPS Coordinates of the Nine Sampled Locations

Number	Sample ID*	Milepost	Date	Lateral	Longitudinal
1	29	39.871	8/28/2017	40.894447	-97.296814
2	23	26.767	8/29/2017	40.871158	-97.089321
3	28	26.732	8/29/2017	40.870723	-97.089179
4	22	25.791	8/29/2017	40.858169	-97.085078
5	11	25.788	8/30/2017	40.858116	-97.085000
6	13	26.763	8/30/2017	40.872000	-97.089532
7	14	27.729	8/30/2017	40.884424	-97.093596
8	8	22.772	9/1/2017	40.814565	-97.070758
9	6	22.717	9/1/2017	40.813809	-97.070512

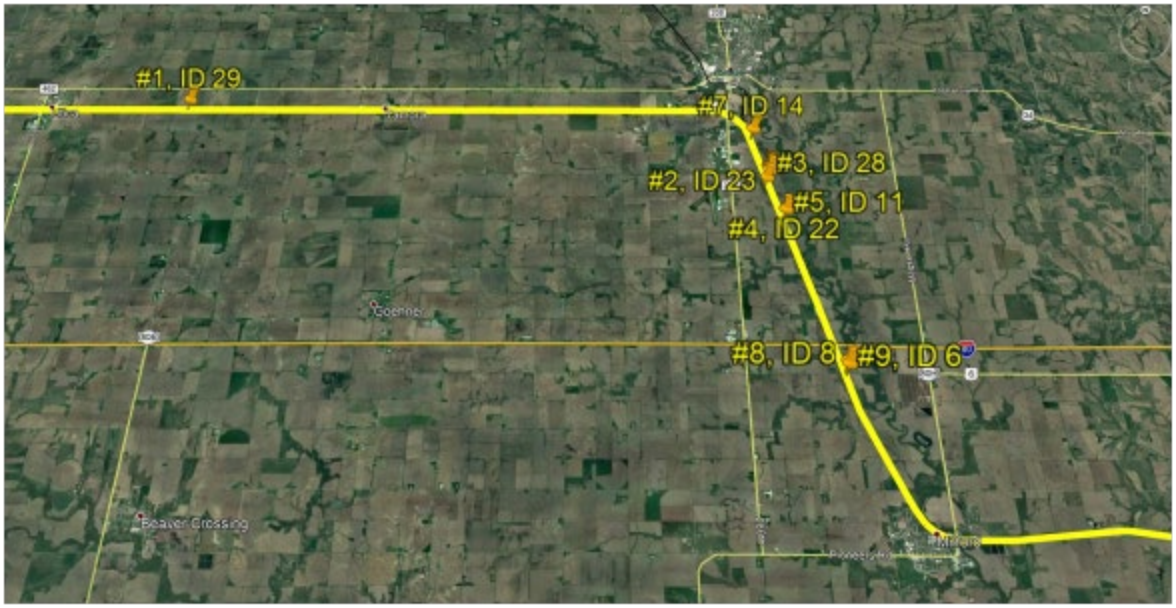

Figure 43. Ravenna Subdivision Sampling Locations

The vibrosampling involved advancing an 8-inch (203 mm) square tube 16 inches (406 mm) deep into the ballast using a hydraulic head that secured the tube, and it produced an axial vibratory oscillation to advance the tube as it was attached and driven by a backhoe. Figure 44 is a photograph of the installation process. Once the tube was driven, the team hand excavated the sampled ballast into 5-gallon buckets down to the 16-inch (406 mm) sample base depth. The samples were then marked, weighed, and transported back to the TTC for gradation testing.

Figure 44. BNSF Vibrosampler at Work

Sample locations typically involved sampling the center of track in the crib (C+0), left shoulder (L+0), and right shoulder (R+0). Additionally, the sample locations were taken two cribs away, in the direction of a higher MP and are referred to as L+2, C+2, and R+2 in this report.

Photographs of a typical site location (Site 4 MP 25.791) is displayed in Figure 45a, and the switch at (Site 7 MP 27.729) is displayed in Figure 45b.

The rail was 136-RE with concrete ties and elastic fasteners on Track 1, and timber ties with cut spikes on Track 2. The ballast surface at all locations were clean and most of the fine particles appeared to be coal. This is notable for the gradation analyses because the specific gravity of coal is about half that of most earth materials. Therefore, a higher percentage of coal per volume will result in a reduced mass, and, therefore, reduced fine weights.

(a)

(b)

Figure 45. Photographs of (a) Site No. 4 (MP 25.791) and (b) the Switch at Site No. 7 (MP 27.729)

Descriptions of each of the nine sites are listed below, along with moisture and gradation results compared against BFI from the GPR measurements.

Site 1: MP 39.871 (ID 29)

The first site was sampled on August 28, 2017. Site 1 was located at MP 39.871 on Track 2, had timber ties, and no other obvious features. Six samples were taken at Locations L+0, L+2, C+0, C+2, R+0, and R+2.

Fine particles were observed immediately underneath the ballast, about 1-inch (25 mm), which were moist and appeared to be primarily coal particles. At C+0, clay was observed near the bottom few inches of the excavation, and the R+0 and R+2 locations had standing water about 10 inches (254 mm) below the surface (see Figure 46). For this reason, the R+0 and R+2 sampling had to stop at 10 inches (254 mm), and the fines gradation results are not believed to be representative of in-situ conditions. The standing water is believed to occur because the clay in the center of the track prevented drainage. Three Shelby tube samples were taken at L+0, C+0, and C+2.

Table 15 displays the moisture and gradation results from Site 1 and compares them with the modeled results of the T-20 BFI. Percent passing is the percentage of fines that passes the No. 4 sieve. FI is an index that sums the percentage of fines passing the No.4 sieve and the percentage of mass passing the No. 200 sieve as determined by laboratory sieve tests. It should be noted that the samples analyzed by TTCI were processed using a dry-sieving process to capture and retain fines for future processing (e.g., plasticity, fines type) if needed, answer questions anticipated during discussions, and to retain sample mass integrity for the record. Dry sieving typically produces fines results that are lower than that obtained by the wet-sieving process, but the wet-sieved fines are lost and unavailable for any future questions or work. BNSF provided additional data by obtaining independent samples and wet sieving the ballast, which is presented along with the TTCI dry-sieve data. BNSF results are provided in Appendix E.

Table 16 displays the fine analysis results from the Shelby tube samples. Note, Atterberg Limits were performed on soil passing the No. 40 sieve (fine sand and fines) so larger particles were disregarded. Liquid limit, plastic limit, and plasticity index are three common indices in geotechnical engineering that give insight into the size and type of fine particles and how plastic, (i.e., malleable when wet) the fine particles are. Plasticity index is calculated by subtracting the plastic limit from the liquid limit. The classification group names used are the following: CL is clay of low plasticity, OL is organic silt or organic clay, and ML is silt.

Table 15. Ballast Sampling Results from Site 1, MP 39.871 (ID 29)

Location	Moisture	% Passing	FI	BFI
L+0	4.5%	18.6	20.6	2
L+2	5.3%	25.2	27.3	2
C+0	6.1%	22.7	25.0	2
C+2	6.9%	24.9	27.1	2
R+0	1.5%	2.6	3.0	2
R+2	1.2%	1.4	1.7	2

Table 16. Shelby Tube Sample Results from Site 1, MP 39.871 (ID 29)

Location	Liquid Limit	Plastic Limit	Plasticity Index	Classification
L+0	36	18	18	CL* or OL**
C+0	39	17	22	CL or OL
C+2	42	17	25	CL or OL

*CL = clay of low plasticity **OL = organic silt or organic clay

Figure 46. Photograph of the Standing Water in R+2 Sampling Location

Site 2: MP 26.767 (ID 23)

The second site was sampled on August 29, 2017. Samples were taken at Locations C+0, C+2, R+0, and R+2.

During the driving process, the vibrosampler encountered a hard layer. During sampling, fine particles were observed near the surface, were generally wet and plastic like, and appeared to be coal. The subgrade varied, depending on the location with the right side (R+2) encountering sand, whereas the rest appeared to be sand with coal. Figure 47 (a) and Figure 47 (b) show the sandy subgrade, and Figure 48 (a) and Figure 48 (b) show the coal particles contaminating the ballast to the bottom of the tube. It should be noted that small amounts of coal can make the material look very dark and cause coal percentage to be overestimated. Two Shelby tube samples were taken at C+0 and R+2. Table 17 displays the moisture and gradation results, and Table 18 displays the Shelby tube results from Site 2.

Table 17. Sampling Results from Site 2, MP 26.767 (ID 23) (see Table 12 for BFI Key)

Location	Moisture	% Passing	Lab FI	Modeled BFI
C+0	6.8%	17.0	18.1	1
C+2	6.0%	16.3	17.3	1
R+0	8.9%	25.5	27.1	4
R+2	4.0%	19.4	19.5	4

Table 18. Shelby Tube Sample Results from Site 2, MP 26.767 (ID 23)

Location	Liquid Limit	Plastic Limit	Plasticity Index	Classification
C+0	-	-	NP*	ML** or OL***
R+2	25	15	10	CL**** or OL

* NP = non-plastic ** ML = silt ***OL = organic silt or organic clay ****CL = organic silt or organic clay

Figure 47. Photographs of the Sand at the Bottom of the R+2 Location (a) Bottom of Tube (b) Bucket

Figure 48. Photographs of the Coal Particles at the Bottom of the C+0 Location (a) Bottom of Tub (b) Bucket

Site 3: MP 26.732 (ID 28)

The third site was sampled on August 29, 2017. Six samples were taken at this site at Locations L+0, L+2, C+0, C+2, R+0, and R+2.

The vibrosampler process was fairly easy to drive with some possible hardpan in the center of the track. Fines were encountered about 3 to 5 inches (76 to 127 mm) from the surface and the subgrade started at about 12 inches (305 mm). On the left shoulder, the subbase was a sandy clay consistency, the right side was more of clayey sand that began at about 15 inches (381 mm) in depth, and the center remained a highly plastic coal fouling with no noticeable base.

Two Shelby tube samples were taken at L+0 and C+0. The L+0 subgrade was a silty clay with sand, medium brown, moist with coal particles. The C+0 subgrade consisted of black fine gravel,

moist, and gravely sand. Table 19 displays the moisture and gradation results and Table 20 displays the Shelby tube results from Site 2.

Table 19. Sampling Results from Site 3, MP 26.732 (ID 28)

Location	Moisture	% Passing	FI	BFI
L+0	6.6%	13.1	14.1	3
L+2	5.0%	11.5	12.4	3
C+0	7.3%	15.8	17.3	2
C+2	8.3%	11.5	12.4	2
R+0	9.3%	19.2	20.6	4
R+2	6.7%	22.2	24.0	4

Table 20. Shelby Tube Sample Results from Site 3, MP 26.732 (ID 28)

Location	Liquid Limit	Plastic Limit	Plasticity Index	Classification
L+0	-	-	NP*	ML** or OL***
C+0	28	14	14	CL**** or OL

*NP = ??? **ML = silt ***OL = organic silt or organic clay ****CL = clay of low plasticity

Site 4: MP 25.791 (ID 22)

The fourth site was sampled on August 30, 2017. All six samples were taken at L+0, L+2, C+0, C+2, R+0, and R+2.

The vibrosampler process had some difficulties driving about 7 to 8 inches (178 to 203 mm) in depth because of the highly compacted ballast present, but the shoulders were relatively easy to drive. The ballast appeared to be new and the track was likely recently undercut or experienced shoulder cleaning. The first 10 inches (254 mm) in depth consisted of fairly new ballast and then transitioned to a fouled gravel and sand mixture with coal at 12 inches (305 mm) in depth. The right and left shoulders were fairly dry with the center was moist. No subgrade was observed and the coal was plastic.

No Shelby tube samples were taken due to the hard base. Table 21 displays the moisture and gradation results of Site 4.

Table 21. Sampling Results from Site 4, MP 25.791 (ID 22)

Location	Moisture	% Passing	FI	BFI
L+0	2.3%	3.7	4.2	4
L+2	1.0%	3.8	4.5	4
C+0	3.3%	9.9	10.5	3
C+2	2.5%	10.1	10.7	3
R+0	2.1%	5.7	6.5	4
R+2	1.0%	5.4	6.6	4

Site 5: MP 25.788 (ID 11)

The fifth site was sampled on August 31, 2017. Four samples were taken at Locations L+0, C+0, C+2, and R+0.

The vibrosampler had some difficulties driving tubes in the center because of the highly compacted ballast present, but was easier to drive in the shoulders. The site has ballast down to 16 inches (406 mm) and some sand at the bottom. No Shelby tube samples were taken. Table 22 displays the moisture and gradation results of Site 5. Since this site had very little fines and was located in a dry section, the apparent moisture fell into the margin of error for the methods and instrumentation; thus, the negative calculated moisture percentage.

Table 22. Sampling Results from Site 5, MP 25.788 (ID 11)

Location	Moisture	% Passing	FI	BFI
L+0	-0.5%	0.3	0.4	5
C+0	-0.3%	1.0	1.3	4
C+2	-0.2%	0.4	0.7	4
R+0	-0.6%	0.2	0.3	4

Site 6: MP 26.763 (ID 13)

The sixth site was sampled on August 31, 2017. Four samples were taken at Locations L+0, C+0, C+2, and R+0.

The vibrosampler had some difficulties driving tubes in the center, but was easier to drive in the shoulders. The shoulders had about 11 to 12 inches (279 to 305 mm) of ballast and transitioned to sandy sub-ballast underneath. The C+0 sample was very hard about 2 to 3 inches (51 to 76 mm) below the surface. No Shelby tube samples were taken. Table 23 displays the moisture and gradation results of Site 6.

Table 23. Sampling Results from Site 6, MP 26.763 (ID 13)

Location	Moisture	% Passing	FI	BFI
L+0	1.2%	6.8	7.4	4
C+0	4.6%	10.5	11.5	3
C+2	2.0%	7.5	8.2	3
R+0	1.2%	3.9	4.3	4

Site 7: MP 27.729 (ID 14)

The seventh site was sampled on August 31, 2017. The site was located at a switch, and three samples were taken at Locations L+0, C+0, and C+2.

The locations had coal particles immediately underneath the top of the ballast and the particles were drier. No Shelby tube samples were taken. Table 24 displays the moisture and gradation results of Site 7.

Table 24. Sampling Results from Site 7, MP 27.729 (ID 14)

Location	Moisture	% Passing	FI	BFI
L+0	3.7%	12.8	13.4	5
C+0	3.7%	23.6	30.3	3
C+2	2.8%	19.6	20.8	3

Site 8: MP 22.772 (ID 8)

The eighth site was sampled on September 1, 2017. Four samples were taken at Locations L+0, C+0, C+2, and R+0.

The vibrosampler had difficulties driving in the center because of the highly compacted ballast present at about 12 inches (305 mm) in depth while the shoulders were easy to drive. The shoulders consisted of relatively clean ballast down to 8 inches (203 mm) and then was completed in fine-contaminated ballast at 12 inches (305 mm). The fine particles were a gravely sand that was very dry. The center had fine particles at about 8 inches (203 mm) in depth and was moist, likely clayey silt. No Shelby tube samples were taken. Table 25 displays the moisture and gradation results of Site 8.

Table 25. Sampling Results from Site 8, MP 22.772 (ID 28)

Location	Moisture	% Passing	FI	BFI
L+0	0.4%	5.7	7.8	4
C+0	2.8%	13.1	14.7	2
C+2	2.8%	12.7	14.4	2
R+0	0.9%	1.5	1.9	4

Site 9: MP 22.717 (ID 6)

The ninth site was sampled on September 1, 2017. The site had a high ballast shoulder of about 33 inches (838 mm) on the right side of the track. Two samples were taken at Locations L+0 and C+0.

The vibrosampler had difficulties driving in the center, but was easier to drive in the shoulder. The left shoulder was initially clean, but eventually experienced fine-contamination from ballast degradation. The fine particles were dry and gravely sand sized. The center was clean to 8 inches (203 mm) deep. At that depth, there was dry coal and some clay at the bottom with increasing moisture and depth. No Shelby tube samples were taken. Table 26 displays the moisture and gradation results of Site 9.

Table 26. Sampling Results from Site 9, MP 22.717 (ID 6)

Location	Moisture	% Passing	FI	BFI
L+0	-0.2%	1.6	1.9	4
C+0	3.8%	11.0	12.2	2

4.1.3 Sampling Results and Discussion

Physical ballast sampling is a tedious process, and multiple factors can produce inconsistencies in the data. First, the track substructure can experience natural spatial variations that can make obtaining a representative gradation difficult. While the GPR is typically averaged over 30 feet (9.1 m), the physical sampling only selects one or two specific locations over that 30-foot (9.1-m) section. If there is much variability in the fine content, the selected location may have more or less fines than the surrounding regions.

Second, the vibrosampler only collects enough ballast for a single 5-gallon bucket of material. According to ASTM D6913/D6913M-17, the ballast volume should be about five, 5-gallon

buckets worth of material if the maximum ballast size is 2.5 inches (64 mm) [12]. This may additionally play a role in variability.

Third, the fine content can influence the results. As mentioned earlier, coal has a specific gravity about half of most fine materials, so this means ballast with 20 percent coal fines can perform similarly to ballast with 40 percent of ballast degraded fines. The influence of moisture on volume also plays an undefined role, as does the GPR response signature to coal.

TTCI used a dry-sieving process to retain fines for additional analysis, and for closer examination of fines characteristics if needed, since the fine material was expected to consist mostly of non-cohesive or low-cohesive particles. BNSF performed independent sampling at the sites and used a wet-sieving process, which produces a more representative analysis despite the loss of fine material (see Section 4.1.5 and Appendix E). The fines percentage was significantly larger using the wet-sieving process, indicating that some cohesive fines were present.

Table 27 provides a summary of the results. The track locations with two samples (from Locations C+0 and C+2) are averaged and the difference is calculated. Unsurprisingly, the greater variations occurred at locations with higher levels of fine-contamination. The consistency at most locations suggest that the variations are likely due to spatial variation in properties and that some locations do experience spatial variations of FI up to about 10.

The sampling results from locations 2 feet (610 mm) apart can be compared to get insight into consistency and variability in response. Out of the 15 locations that have samples 2 feet (610 mm) apart, four of them have FI values that vary by more than 4. These locations are: (1) ID 14 – Center with 9.5, (2) ID 23 – Right with 7.6, (3) ID 29 – Left with 6.7, and (4) ID 28 – Center with 4.9.

Figure 49 presents the relationship between FI and moisture content and is presented by (a) track location (left shoulder, center, right shoulder) and (b) site ID location. The results show a strong relationship between FI and moisture content. This was anticipated, as clean ballast will not absorb significant moisture, so greater degree of fines will likely have greater moisture. A few sites appeared to have high amounts of moisture, including Site IDs 22, 23, and 28.

Table 27. Summary of Sampling Results

Sampling Site Location ID	Location	Average Moisture	Moisture Difference	Average FI	FI Difference
6	Left	-0.2	n/a	1.9	n/a
	Center	3.8	n/a	12.2	n/a
8	Left	0.4	n/a	7.8	n/a
	Center	2.8	0.0	14.6	0.3
	Right	0.9	n/a	1.9	n/a
11	Left	-0.5	n/a	0.4	n/a
	Center	-0.3	0.1	1.0	0.6
	Right	-0.6	n/a	0.3	n/a
13	Left	1.2	n/a	7.4	n/a
	Center	3.3	2.6	9.9	3.3
	Right	1.2	n/a	4.3	n/a
14	Left	3.7	n/a	13.4	n/a
	Center	3.3	0.9	25.6	9.5
22	Left	1.7	1.3	4.4	0.3
	Center	2.9	0.8	10.6	0.2
	Right	1.6	1.1	6.6	0.1
23	Center	6.4	0.8	17.7	0.8
	Right	6.5	4.9	23.3	7.6
28	Left	5.8	1.6	13.3	1.7
	Center	7.8	1.0	14.9	4.9
	Right	8.0	2.6	22.3	3.4
29	Left	4.9	0.8	24.0	6.7
	Center	6.5	0.8	26.1	2.1
	Right	1.4	0.3	2.4	1.3

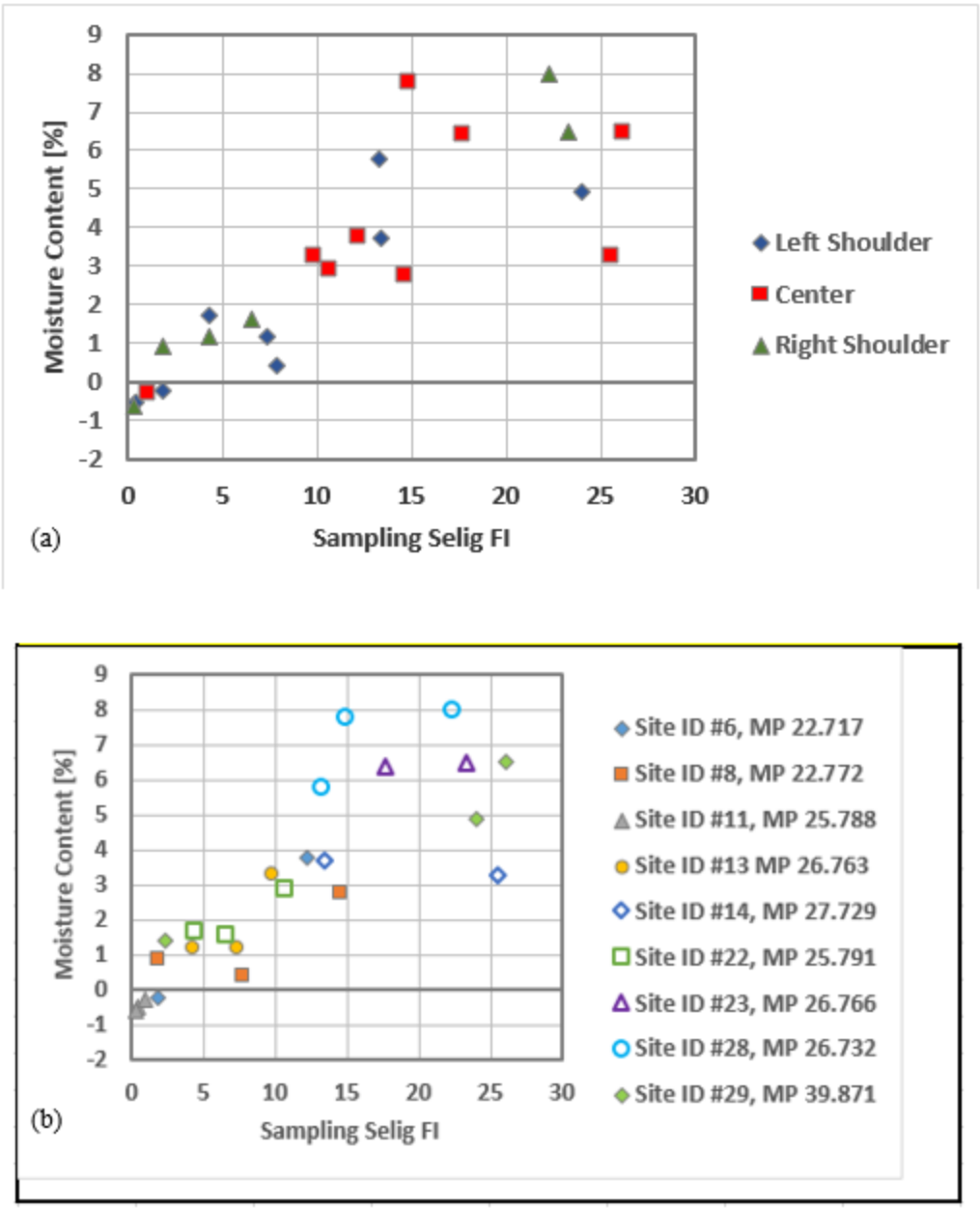

Figure 49. (a) and (b) Relationship Between FI and Moisture Content from Sampling

There is a notable correlation between moisture content and the FI. However, the dry-sieving process used by TTCI lowers the FI by 3 to 6 below what it would be if a wet-sieving process was used (as in the comparable BNSF data Section 4.1.5), so the line would appear "flatter" with a wet-sieving comparison.

4.1.4 DCP and Geo-Endoscopy Results

DCP and geo-endoscopy tests provided additional results, including: (a) depth of ballast, fouled ballast, and subgrade layers, and (b) cone resistance with depth. The cone resistance is presented as a CBR, in which higher values indicate stiffer material. The ballast layer is typically

underestimated because the cone will prefer penetration through the ballast voids; however, it should give a better estimate of fine-contaminated ballast and subgrade material. Since the focus of the study is ballast, the cone resistance values are presented but not used.

Table 28 presents the depths of each layer and Table 29 presents the average CBR value of each layer and a representative value for the first 16 inches (406 mm). In both tables, the four layers are: ballast (clean), fouled (ballast), inter (intermediate layer), and subgrade.

Table 28. Layer Depths from DCP Tests (All Values in Inches)

Sampling Site Location ID	Location	Ballast	Fouled	Intermediate	Subgrade	Inter*
6	Left	11.04	14.64	18.72	-	1.36
	Center	6.48	13.56	17.04	-	2.44
8	Left	11.04	15.36	22.20	28.32	0.64
	Center	6.96	10.08	16.68	-	5.92
11	Left	12.48	23.28	27.12	-	3.52
	Center	9.84	20.16	30.96	34.44	6.16
13	Center	6.36	13.20	15.12	-	2.80
14	Left	7.32	15.72	25.44	29.76	0.28
	Center	0.96	8.88	20.40	-	7.12
	Right	6.36	13.44	24.84	-	2.56
22	Left	10.44	11.64	26.76	32.04	4.36
	Center	6.48	12.60	25.44	30.60	3.40
	Right	7.92	13.56	30.12	35.28	2.44
23	Left	7.32	11.40	31.08	36.00	4.60
	Center	3.72	6.96	26.64	29.16	9.04
28	Left	3.00	8.88	23.16	30.12	7.12
	Center	3.72	13.20	27.72	30.60	2.80
	Right	2.64	3.72	21.48	28.92	12.28
29	Left	7.56	9.84	20.64	24.60	6.16
	Center	4.32	11.28	20.16	23.88	4.72

* The term inter* represents the depth of the intermediate layer until 16 inches (406.4 mm) is reached

Table 29. California Bearing Ratio Values from DCP Tests

Sample Site ID	Location	Ballast	Fouled	Intermediate	Subgrade	Representative
6	Left	23.02	63.39	98.48	-	38.52
	Center	21.63	60.61	117.30	-	53.47
8	Left	14.07	79.48	85.78	60.23	34.60
	Center	17.59	22.57	92.23	-	46.18
11	Left	15.08	42.20	69.40	-	21.05
	Center	25.63	39.24	53.74	14.77	30.87
13	Center	35.92	73.51	114.20	-	65.69
14	Left	29.00	37.49	60.71	61.89	34.01
	Center	3.65	16.58	58.50	-	34.46
	Right	4.50	43.61	103.10	-	37.58
22	Left	17.55	23.58	39.12	8.79	23.88
	Center	20.52	36.82	60.81	25.06	35.32
	Right	17.01	10.46	40.09	6.56	18.22
23	Left	8.33	18.14	23.91	3.40	15.31
	Center	6.48	45.07	28.88	3.06	26.95
28	Left	16.69	42.07	12.15	4.25	24.00
	Center	13.74	42.98	39.99	2.71	35.66
	Right	13.51	10.67	18.96	6.98	17.50
29	Left	15.77	44.87	39.07	7.55	28.89
	Center	8.36	19.11	60.36	5.92	28.38

4.1.5 Ballast Sampling and Discussion

Pre-sampling conducted by TTCI indicated that most of the survey area consisted of soils that were of low cohesiveness. For example, at Location 29 (MP 39.871) in Figure 50 most of soils consisted of Fillmore silt loam, followed by Butler silt loam. Silt loam has variable minor sand and clay, but is mostly silt with low cohesiveness. Therefore, a dry-sieving analysis format was chosen for processing the ballast samples, especially since there was not enough sample material collected for duplicates. The dry-sieving process also retained fines for further analysis.

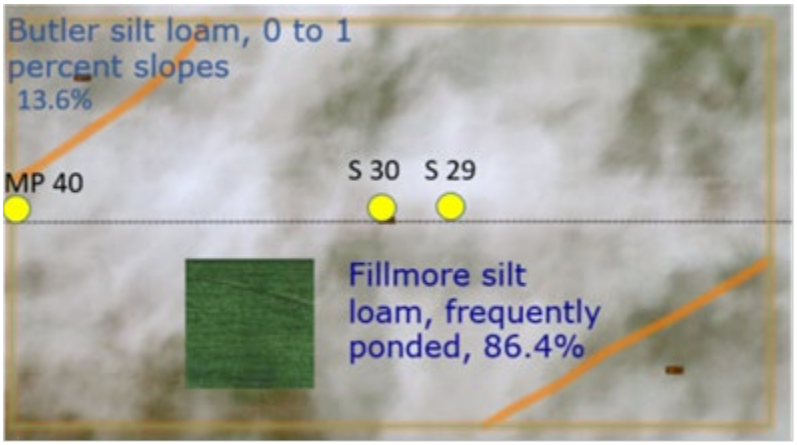

Figure 50. Native Soil Types at the Ravenna Site Generally Consisted of Silty Soils with Anticipated Low Cohesion (from the United States Department of Agriculture [USDA] Web Soil Survey)

BNSF performed independent sampling and analysis of several of the locations that were previously sampled by TTCI. During analysis of the ballast samples, BNSF used a wet-sieving process to determine fines content of the material. The results are shown in Figure 51 through Figure 53, as well as in Appendix C.

Location 8

Sample	Passing #200 Sieve (%)	
	Unwashed (TTCI)	Washed (BNSF)
8L+0	2.1	4.0
8C-2		9.0
8C+0	1.6	7.9
8C+2	1.7	
8R+0	0.3	5.1
8R-2		3.9
Average	**1.4**	**6.0**

Figure 51. Washed Samples Showed About 4 Times the Average Ballast No. 200 Fines than Dry-Sieve Results Showed at this Location

Location 13

Sample	Passing #200 Sieve (%)	
	Unwashed (TTCI)	Washed (BNSF)
13L-2		6.4
13L+0	0.6	
13C-2		13.4
13C+0	1.0	
13C+2	0.7	
13R-2		3.3
13R+0	0.4	
Average	**0.7**	**7.7**

Figure 52. Washed Samples Indicated No. 200 Minus Washed Fines Content Averaged about 10 Times the Dry Sample Results

Location 29

Sample	Passing #200 Sieve (%)	
	Unwashed (TTCI)	Washed (BNSF)
29L-5		7.7
29L-7		4.5
29L+0	1.9	
29L+2	2.1	
29C-5		7.0
29C-7		5.2
29C+0	2.3	
29C+2	2.2	
29R-5		9.7
29R-7		8.3
29R+0	0.4	
29R+2	0.3	
Average	**1.5**	**7.1**

Figure 53. Significant Differences in Dry vs. Wet-Sieve Results for the No. 200 Minus Fines Content of the Sampled Ballast

Wet and Dry Sieving Discussion

The wet-sieving process showed that the No. 200 minus fines portion of the ballast had unanticipated cohesive properties which affected the sieving results during the laboratory dry-sieving process. The effect that this fines percentage has on moisture retention and ballast mass behavior also needs to be recognized during analysis of the data dependent on this quantitative metric, such as GPR-derived BFI.

The dry-sieving process resulted in an average of 1.3 percent fines passing the No. 200 sieve for these samples. The wet-sieving process resulted in a calculated average of 6.8 percent fines passing the No. 200 sieve. However, because of the low percentage of the fines relative to the ballast mass volume at these sites, the overall effect is minimal, and the conclusions are the same (Figure 54 and Figure 55).

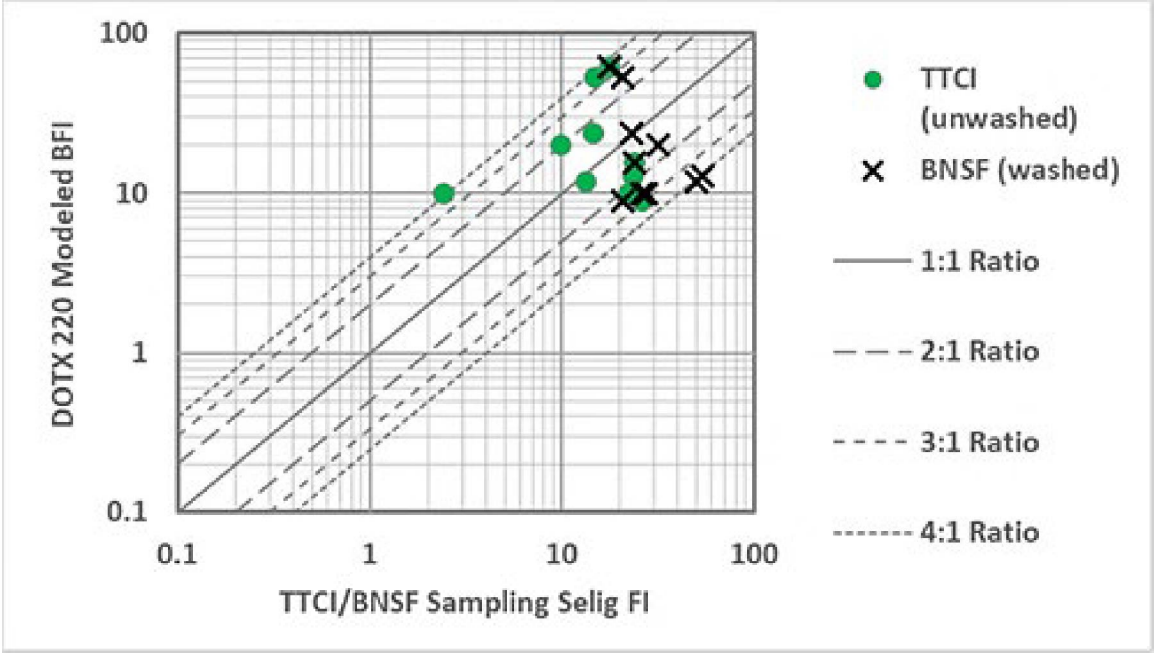

Figure 54. A Comparison of the T-20 Modelled BFI vs. the Wet and Dry-Sieving Results

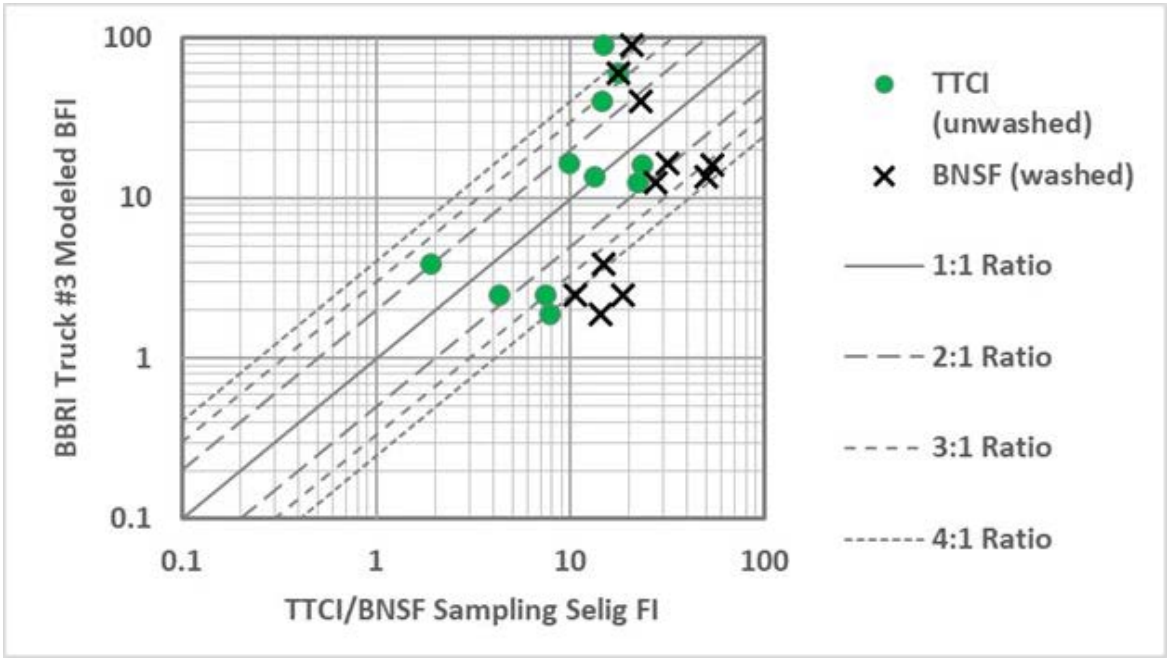

Figure 55. A Comparison of a Hi-Rail GPR Truck Modelled BFI vs. the Wet and Dry-Sieving Results

T-20 GPR Comparison with Hi-Rail GPR Data

Hi-rail GPR data has been collected for several years in the railroad industry; consequently, a comparison of the hi-rail GPR data with the new T-20 GPR system is a reasonable and necessary

metric to consider during system calibration. This subsection presents a comparison of select hi-rail and T-20 data to recognize and address any discrepancies between the two. Detailed comparisons between the T-20 and typical Hi-Rail vehicle are presented in Appendix E.

The layout of the GPR antennas on the T-20 car is presented in Figure 56. It involves three 2 GHz antennas a single 400 MHz antenna. Comparing against the ballast sampling locations (see Figure 57), the shoulder GPR antennas are over the edge of the tie, whereas the sampling occurred about 1 foot (305 mm) away from the tie. This may cause discrepancies in the data from natural spatial variations. It is generally observed that the track center has more fines than the shoulders, and that fouling increases towards the rail seat due to the effects of repeat loading-unloading cycles on ballast attrition.

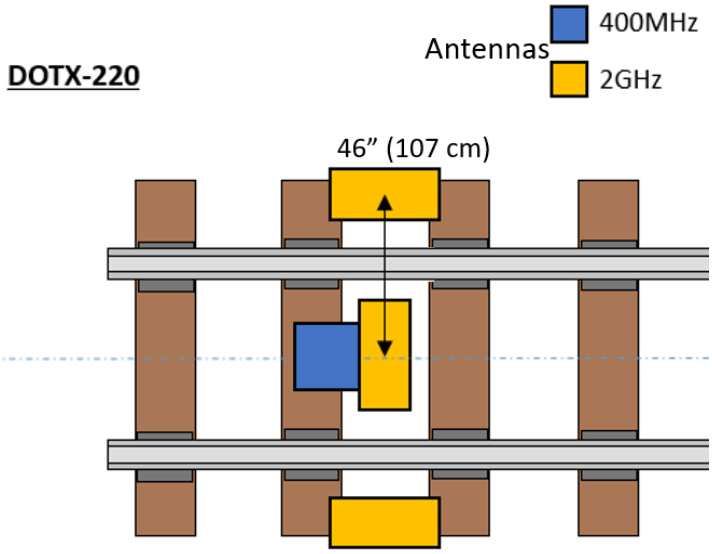

Figure 56. Layout of GPR Antennas
(Photo Courtesy of BBRI)

Figure 57. Sample Locations at Site ID 22, MP 25.7907
(Photo Courtesy of BBRI)

Comparison of the modeled BFI results determined using data from the hi-rail truck with that from the T-20 car revealed a consistent discrepancy in the shoulder BFI values for sites with concrete ties, with the T-20 shoulder results representing significant outliers. This difference is not observed over wooden ties.

In the raw 2 GHz dataset of the shoulder data at locations with concrete ties, residual near-surface hyperbolic artifacts were observed, believed to be caused by reflections from clips and reinforcing bars within these ties. These were not observed at the center of the concrete ties, possibly caused by different orientation of the antenna that is optimized to avoid electromagnet coupling with the reinforcing bars. Figure 58 shows the comparison of shoulder and center data.

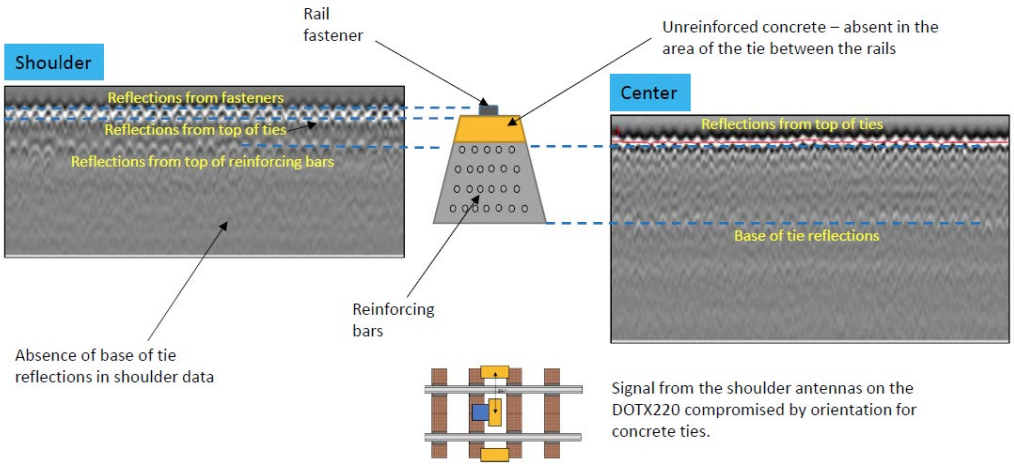

Figure 58. Diagram Explaining Residual Noise
(Photo Courtesy of BBRI)

The effects of the interference on the modeled shoulder BFI are highlighted by comparison of the center and shoulder results from the T-20 car and the hi-rail acquired over a transition from wood to concrete ties. Figure 59 shows the left shoulder, center, and right shoulder BFI with distance. The orange is the results of the hi-rail truck while the blue is the results of the T-20 car. The transition of wood to concrete occurs at MP 14.6. A clear difference is observed for the shoulder BFI values because of differences in antenna positioning, whereas the T-20 center results remain similar to the hi-rail.

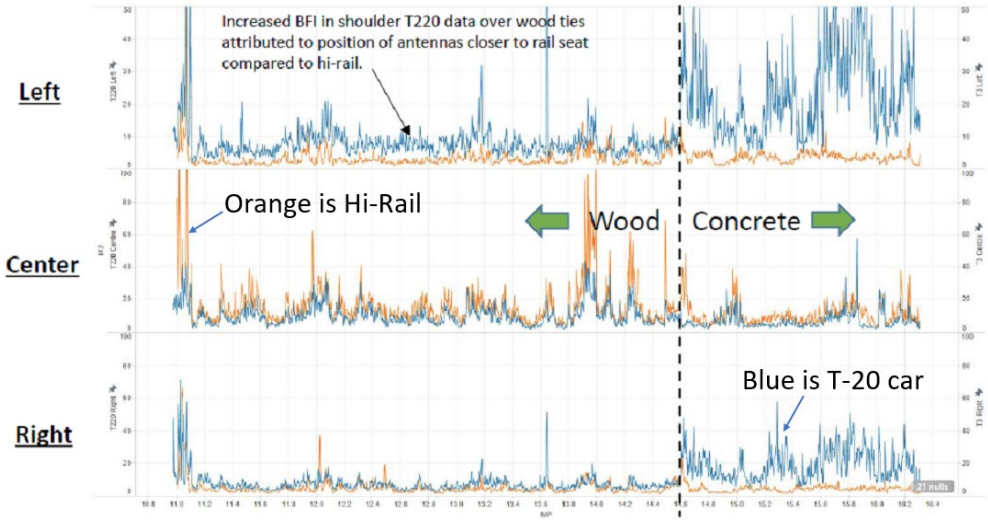

Figure 59. Diagram Showing BFI During Transition from Wood Ties to Concrete Ties (Photo Courtesy of BBRI)

To further check the influence of reinforcing bars in concrete ties, other locations measured by the T-20 car with concrete ties were re-analyzed. The results show the interference was less apparent than at the Ravenna Subdivision. This suggests that properties of the concrete ties may play a role along with antenna orientation.

Due to the interference, the shoulder data from concrete tie locations are excluded from the analysis. This removal is shown in the results and discussion in subsequent sections.

Future testing is proposed to better understand the exact nature and cause of the interference and mitigate this effect.

4.1.6 General Comparison: FDL

In this report, the T-20 GPR is compared with the hi-rail GPR data additional estimates and comparisons located in Appendix E.

The figures below provide a comparison of the modeled T-20 and hi-rail FDL with the measured depth to fouling observed in the ballast sampling tubes as measured by BBRI-Zetica. The FDL represents the depth of clean ballast that allows for the drainage of water.

Plots of the T-20 and hi-rail comparisons are displayed in Figure 60 and Figure 61, respectively. Both show data labeled by sample location and track position (left (l), center (c) and right (r)). Results acquired over the shoulders at sample locations with concrete ties have been removed from the T-20 plot (as discussed in Section 4.1.6).

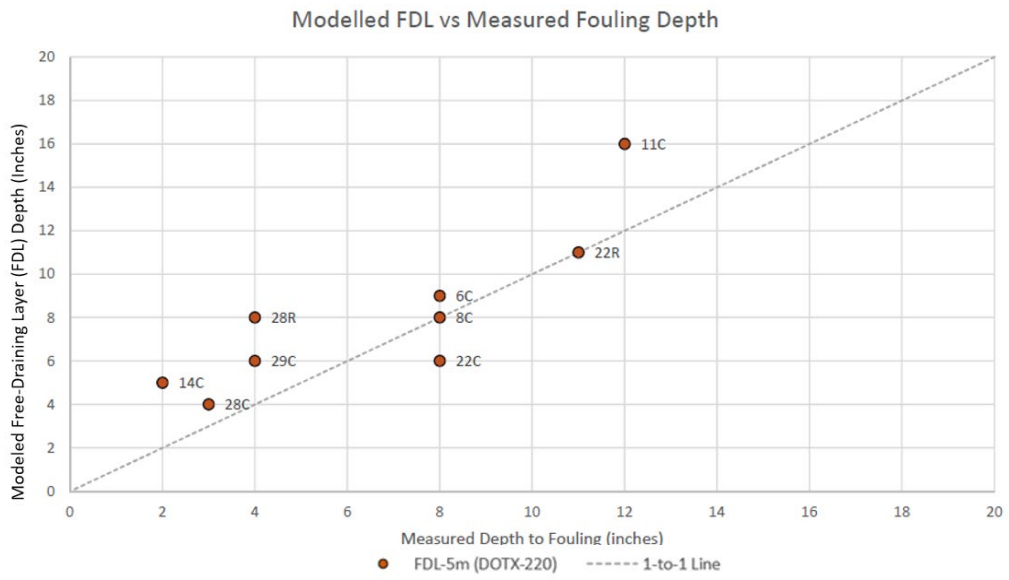

Figure 60. Relationship Between Modeled T-20 FDL and Measured Depth to Fouling in Sampling Tubes
(Courtesy of BB/Zetica)

The results show good correlation between the modeled FDL and the measured depth to fouling. There are no other consistent outliers.

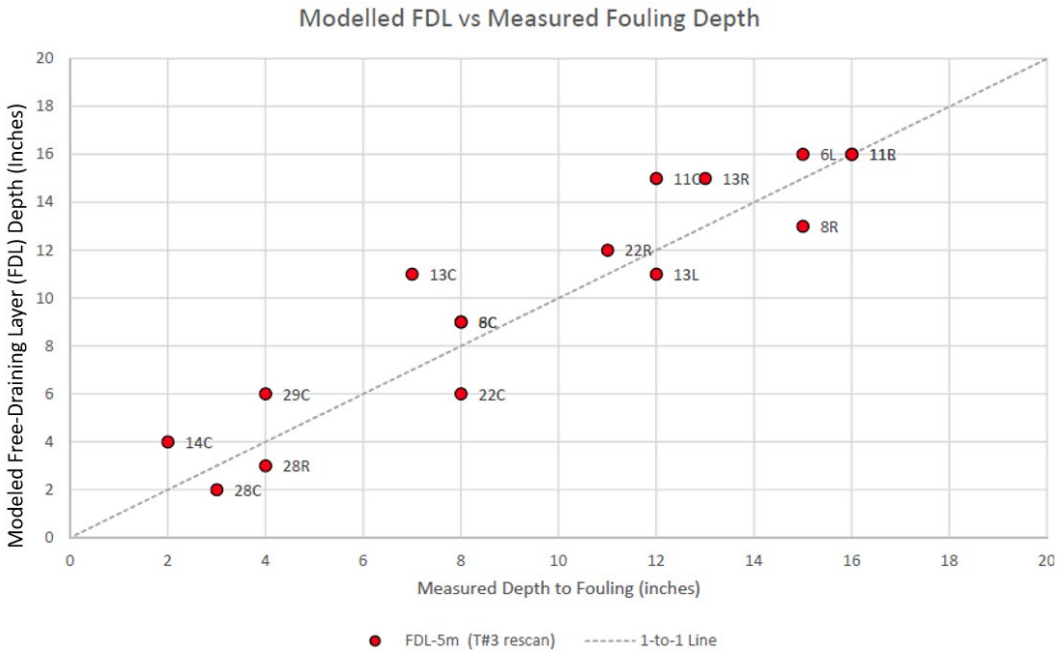

Figure 61. Relationship Between Modeled Hi-Rail FDL and Measured Depth to Fouling in Sampling Tubes

FDL-Fouling Index Relationship

The FDL and FI are anticipated to be related because the greater the depth of clean ballast (greater FDL), the less fines will be present in the ballast (lower FI). Figure 63 compares the modeled FDL derived from the T-20 GPR data and the hi-rail data with the TTCI sampling FI for all center samples. Figure 64 compares the modeled FDL derived from the hi-rail GPR data with the TTCI sampling FI for all samples and sample positions.

The results in both Figure 62 and Figure 63 illustrate a strong relationship between the FDL and sample FI. Both plots indicate that at FI values greater than ~25, the FDL thickness can be expected to be close to zero. This potentially has important implications for the planning of track maintenance, particularly undercutting and track surfacing.

Figure 62 highlights the consistency between the hi-rail derived FDL and the T-20 results. In most cases the difference in modeled FDL is less than 2 inches.

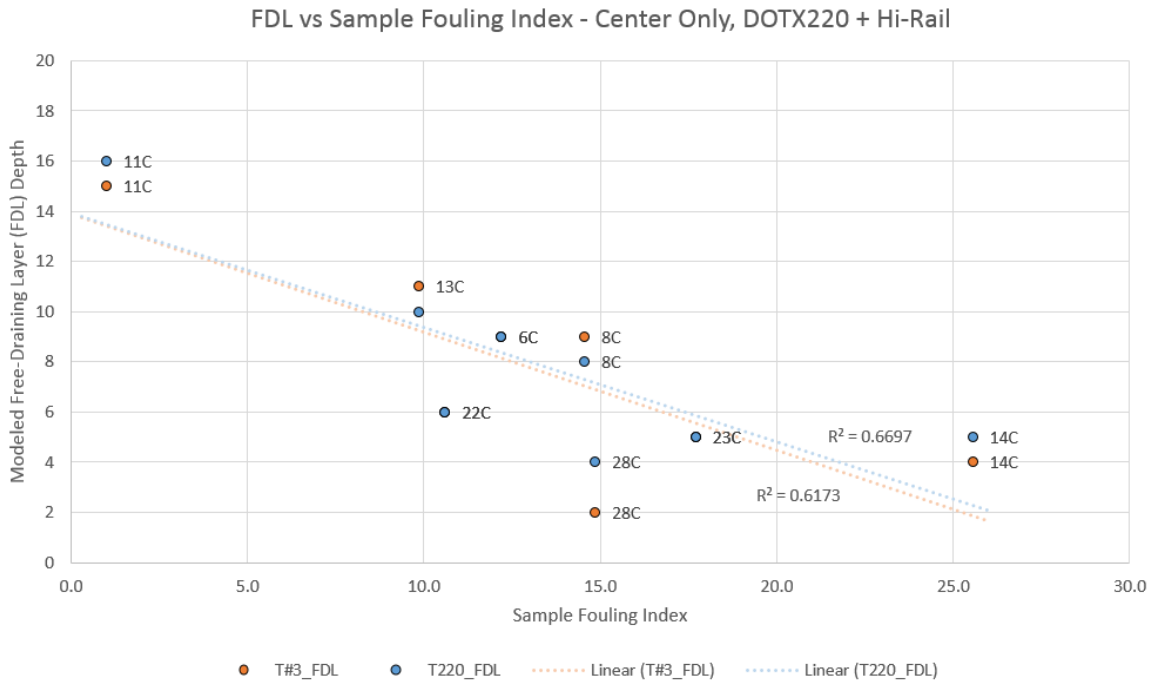

Figure 62. Relationship Between Modeled T-20 FDL and Sample FI for all Center Samples

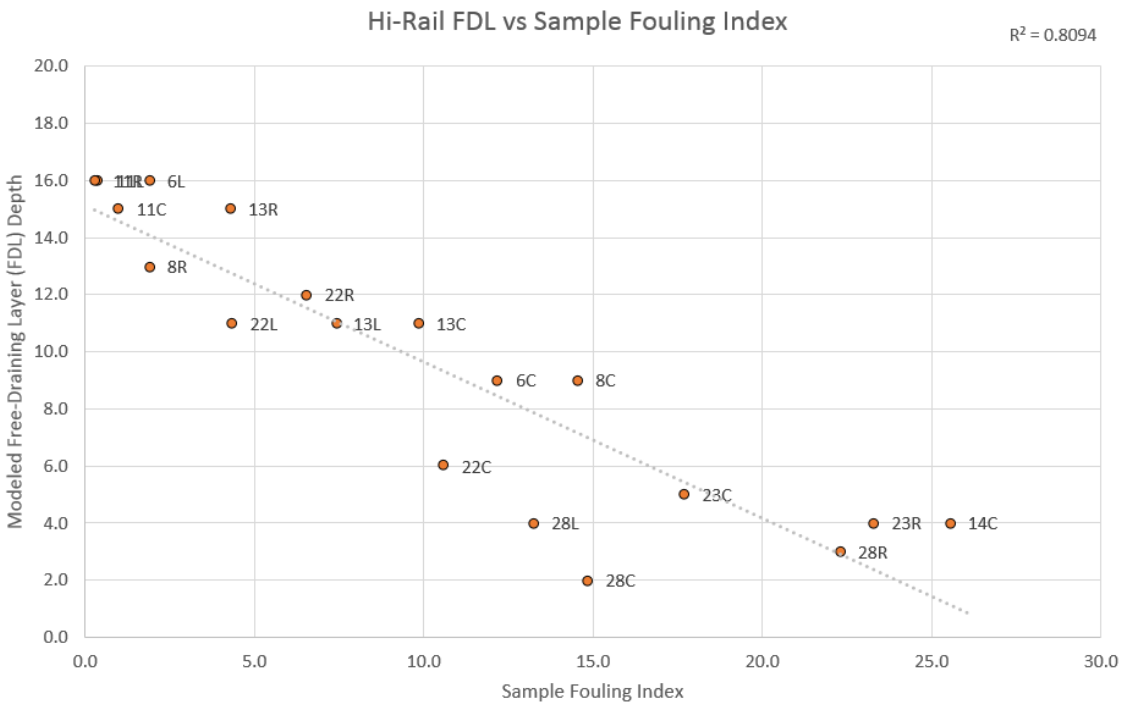

Figure 63. Relationship Between Modeled BB-Zetica Hi-Rail FDL and Sample FI for all Results (Center and Shoulders)

4.1.7 General Comparison of BFI

A second objective of the site visit was to compare the BFI derived from the T-20 GPR data with the measured FI results obtained from the ballast samples. FI is an index that measures the amount fines present in the ballast and is the mass percentage of particles passing the No. 4 sieve (P_4) plus the mass percentage of fines passing the No. 200 sieve (P_{200}).

$$FI = P_4 + P_{200}$$

While the behavior of fine-contaminated ballast is not fully understood, laboratory testing and field observations generally show that ballast with a higher FI, when significant moisture is present, have reduced stiffness, increased settlement rates, and decreased drainage capabilities. The influence of silt- and clay-sized fines (P_{200}) is doubled in the FI index, because it is believed to have a greater negative influence than sand-sized fines.

The BFI is calculated with three methods: (a) truck GPR data, (b) T-20 GPR, and (c) physical sampling. Discussions of the T-20 and physical samplings are discussed in previous sections. For this report, only (b) T-20 GPR, and (c) physical sampling are compared, but comparisons of BFI with the Truck data can be referenced in E

To determine the correlation between the physical sampling and T-20 GPR measurements of BFI, the data is plotted in Figure 64 in (a) logarithmic scale and (b) linear scale. Presenting the data in both scales is helpful for analysis and understanding because they emphasize different aspects of the data. In the logarithmic scale, the lower BFI values are emphasized and it is easier to determine the distance from the ideal 1:1 ratio line, which would represent a perfect match. Essentially, if the physical sampling produced an FI of 10 and the T-20 GPR produced a BFI of

30, the data point would fall on the 3:1 ratio line (mid-sized dashed line). This 3:1 line is at an equal distance to the 1:1 ratio line for all FI values. In the linear scale, the higher values of BFI are emphasized, because higher BFI values are undesirable in track.

The results from Figure 64 (a) shows most of the data is within the 4:1 ratio line, but with a few outliers. These outliers are shoulder data over concrete ties (Figure 65), which are believed to be problematic because of reasons discussed in the previous section. The results from Figure 64 (b) show discrepancies for high FI values in the center track. This is discussed in more detail later in the section.

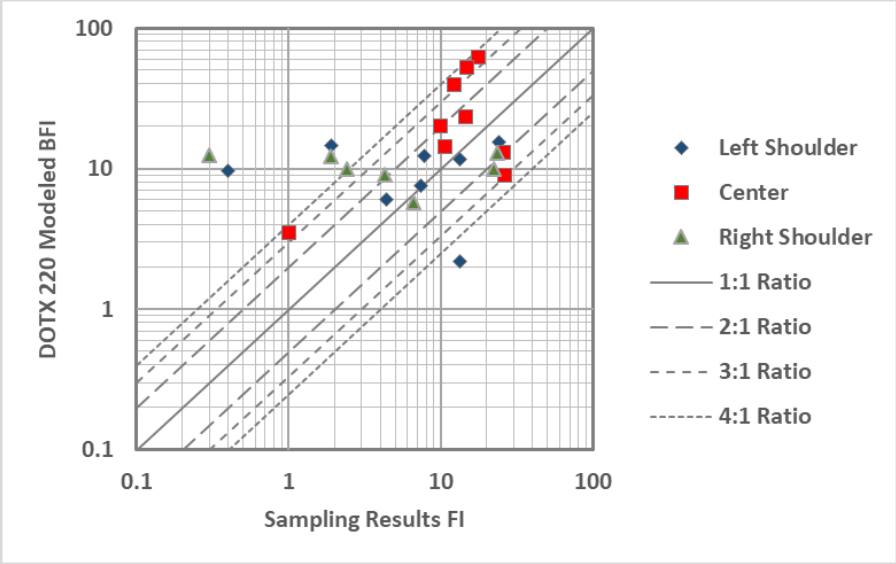

(a)

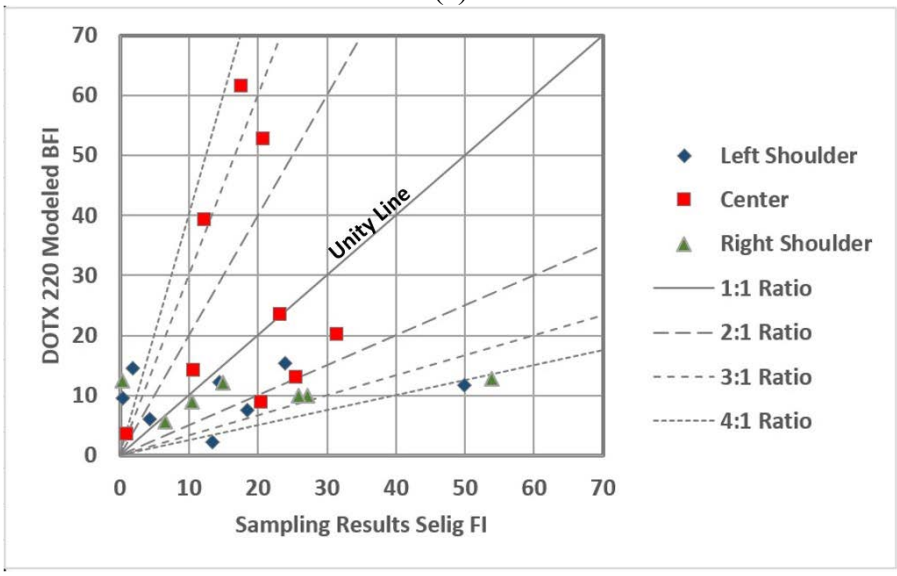

(b)

Figure 64. Relationship between Sampling FI and T-20 BFI Relative to Shoulder and Center Sampling Locations

Figure 65 isolates and highlights the shoulder GPR locations on concrete ties and the fully saturated sample in Site ID 29. Concrete shoulder locations showed more deviation from the unity line. Concrete shoulder values are removed from all subsequent BFI data comparisons.

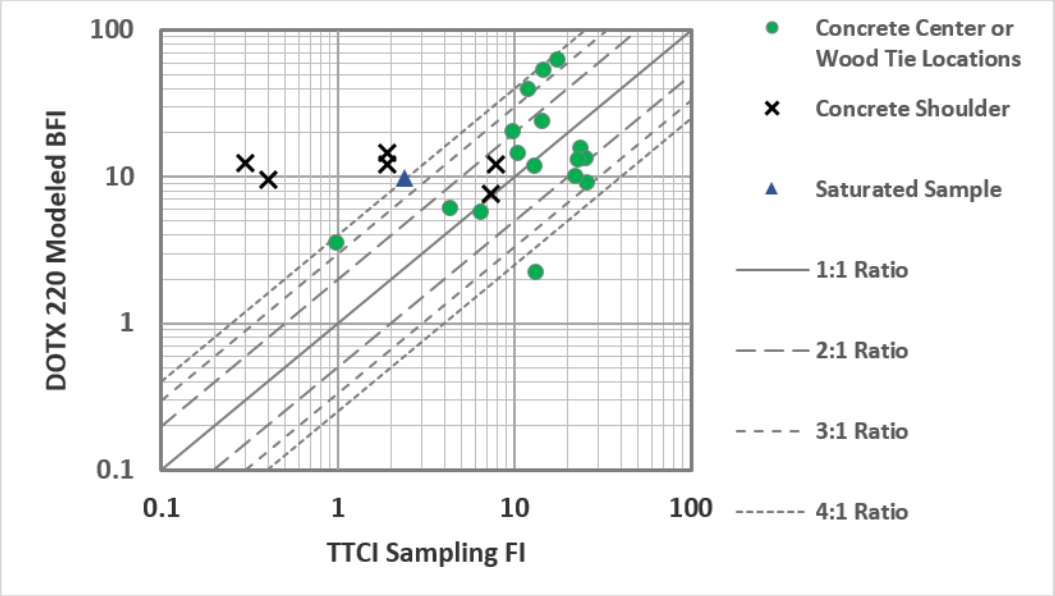

Figure 65. Relationship Between Sampling FI and T-20 BFI, Highlighting the Concrete Tie Shoulder Locations

Figure 66 displays the same data as Figure 67, but with the shoulder results from concrete ties removed. Figure 67 shows identical data, but separated by Site ID location instead of track location. To summarize the observations during sampling, Site IDs 23, 28, and 29 had significant coal fines that appeared near the surface, Site ID 14 had significant fines near the surface, but the composition was unclear, and the remaining Sites IDs appeared to have a distinct ballast layer with coal fines and subgrade material underneath.

The results show the estimated BFI values were generally larger in the track center than the measured FI from physical sampling and lower in the shoulders. It is unclear what causes this, but a few possible remarks are listed as follows:

- The low specific gravity of coal fines could produce FI values that are lower than anticipated, whereas the plasticity of coal fines and its ability to retain moisture may cause an overestimation with the GPR-derived BFI. To support this, the center of the track was noticeably wetter than the shoulders and BFI values of 60 are generally very high. In addition, the Truck 3 values had BFI values over 90, which is much greater than the anticipated BFI of 30 to 50. The center of Sites 23 and 28 was contaminated with primarily wet coal fouling. Site 6 did not appear to have significant coal fines so the explanation for that site is unknown. Site 29 also had significant amounts of moist coal fines but also had clay and other subgrade materials. Since the fines that retain moisture will absorb the GPR waves and coal fines absorb more moisture than other fines such as silt or sand, this may explain some of the high BFI values.

- For the shoulders, the T-20 shoulder locations are closer to the track than the sample locations. Higher BFI values are anticipated closer to track so this may have influenced the results.
- The single sampling locations and low ballast amounts during sampling compared to the averaging of the BFI over 15 feet may result in the samples being unrepresentative of the true FI.

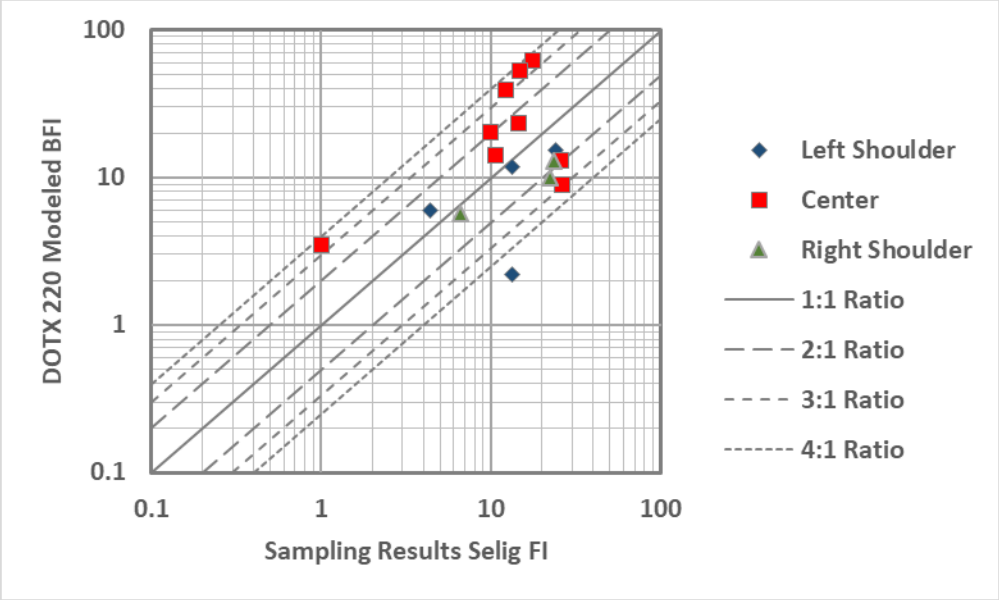

(a)

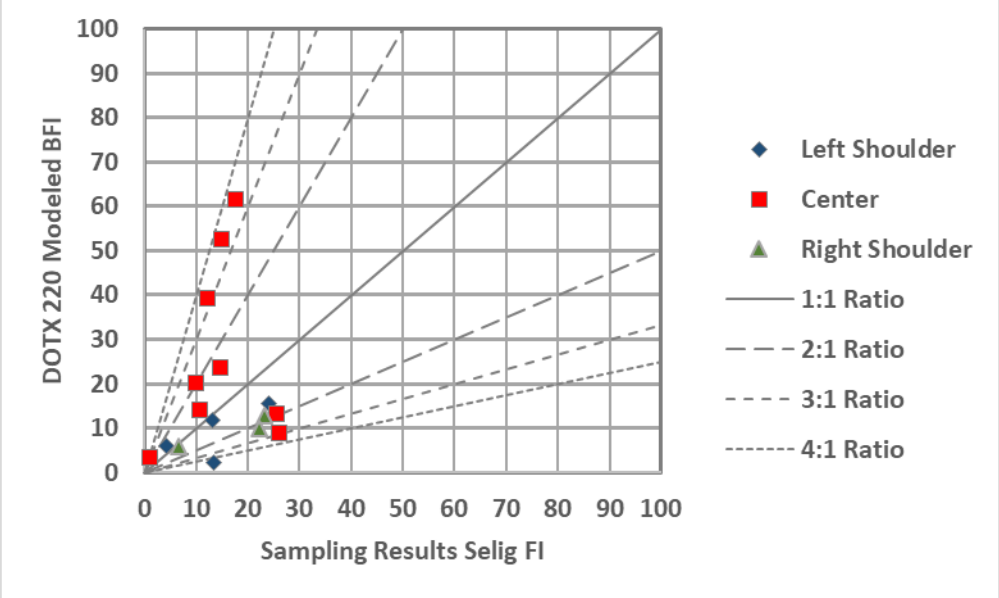

(b)

Figure 66. Relationship Between Sampling FI and T-20 BFI Separated by Track Location with Concrete Shoulder and Saturated Data Removed

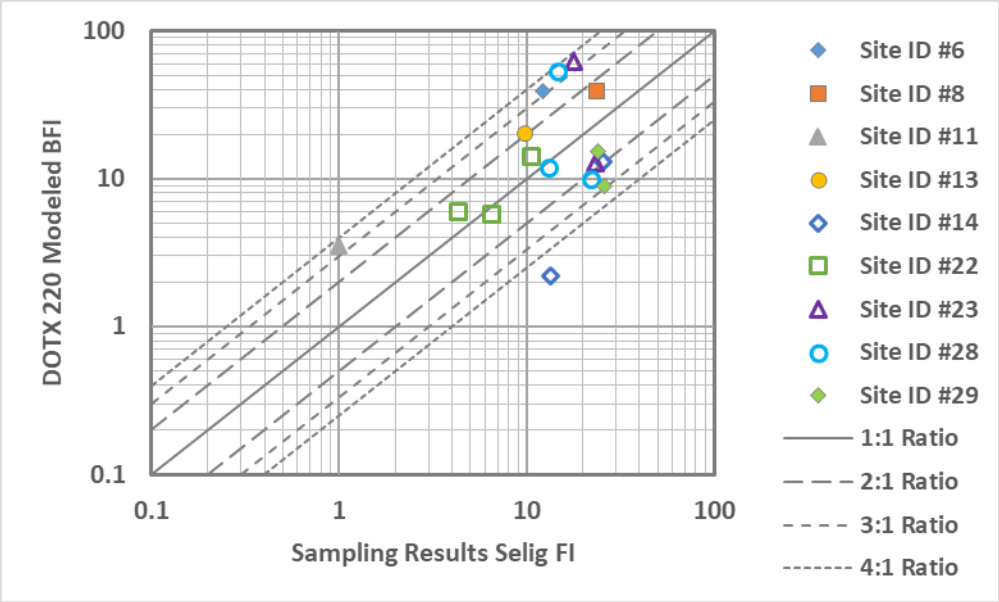

(a)

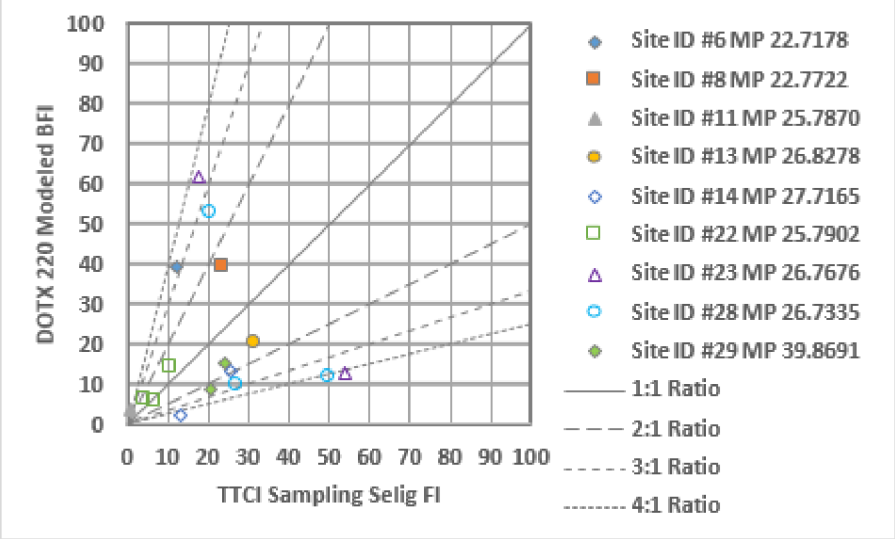

(b)

Figure 67. Relationship between Sampling FI and T-20 BFI Separated by Track Location with Concrete Shoulder and Saturated Data Removed

4.1.8 FDL-BFI Relationship

The FDL and BFI are anticipated to be related, because the greater the thickness of clean ballast (greater FDL), the lower amount of fines that will also be present in the ballast (less BFI). Figure 68 compares the FDL and BFI calculated from the T-20 GPR. Both the track location and site ID location are displayed with the shoulder data from the concrete ties excluded from Figure 68.

The results from Figure 68 show a strong relationship, but with multiple outliers from the center of the track. The primary outliers are Site IDs 23, 28, and 6, which are the same outliers as in Figure 67. Site IDs 8 and 13 are also outliers but to a lesser extent.

Assuming a linear relation between FDL and BFI is anticipated, this suggests that the BFI values from GPR are higher than the estimation from other metrics. A potential reason is how the GPR reacts to wet coal fouling, but further investigation is required before any strong conclusion can be made. A second explanation is that a parabolic relation is anticipated and the FI values from sampling are lower because of the lower specific gravity of coal. Consequently, best fit lines and R^2 error correlations are not offered until further study is done.

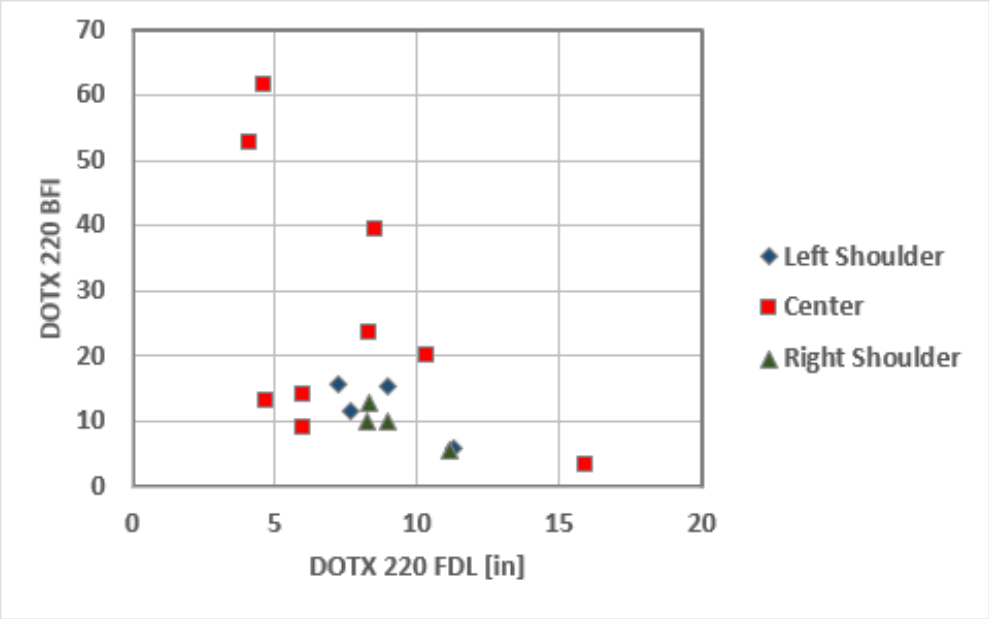

a)

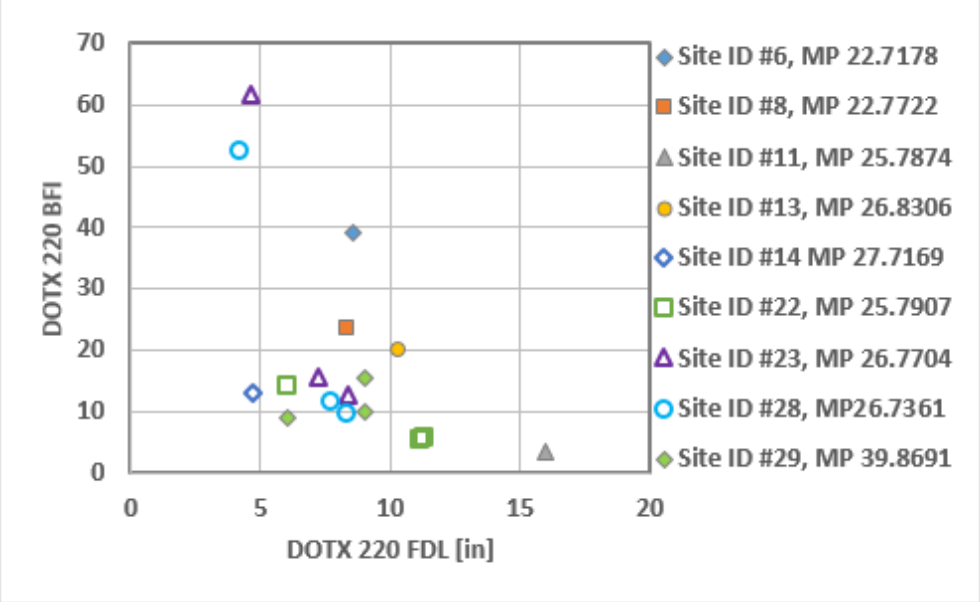

(b)

Figure 68. Relationship between T-20 FDL and BFI Separated by (a) Track Location and (b) Site ID

4.1.9 Data Comparisons Discussion

The percent passing the No. 4 sieve from the physical sampling by TTCI is plotted against the BFI modeled from the GPR to compare these metrics. The results are displayed in Figure 69. As anticipated, there was a general correlation with the BFI decreasing (increased fouling) with increasing percent passing.

Other methods for assessing the depth of the free draining layer include driving a DCP and measuring layer stiffness, or by cone penetrometer (CPT) push methods. These methods can measure layer stiffness by blow counts needed to penetrate a certain depth through the material, or by system pressure needed to push the CPT the same distance through the measured layer.

For this work, an instrumented DCP was used to measure layer stiffness blow by blow, using standard wave theory correlations. In addition, a videoscope (endoscope) was utilized after the DCP was finished to photograph and record a video of the penetrated section. This provided information for correlation of the DCP results, especially with respect to soil and ballast grain size changes and changes to relative moisture content of the material.

Two examples of these correlations are provided below, and additional information may be obtained from Appendix D.

In Figure 69 (a), the primary locations were the right shoulder samples at Locations 23 and 28 and samples at Location 14 and 29. DCP information (MP 26.766) was chosen for comparison with Location #23 (MP 26.767), since a rough correlation may be valid. Of course, it must be recognized that subsurface conditions can change very quickly, even at this scale, but over a large area, general trends may be expected.

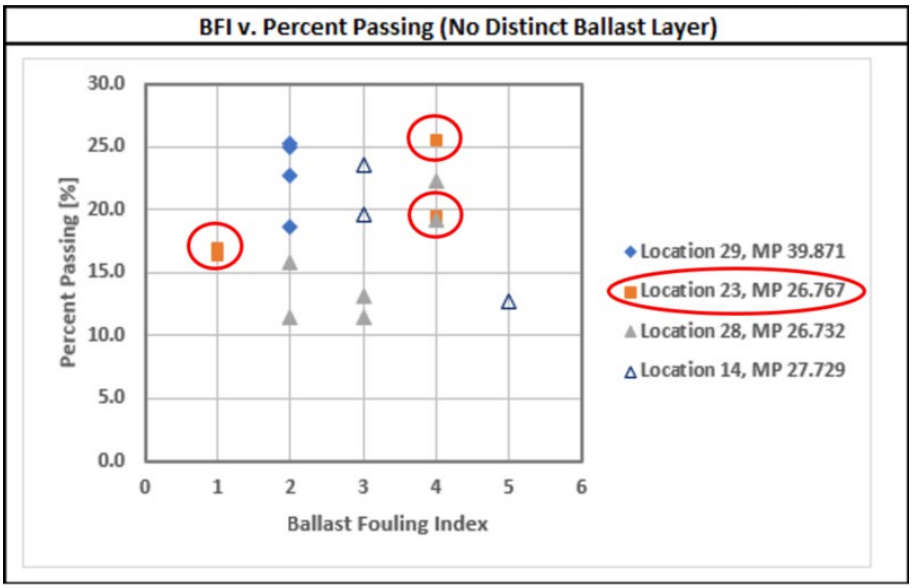

(a)

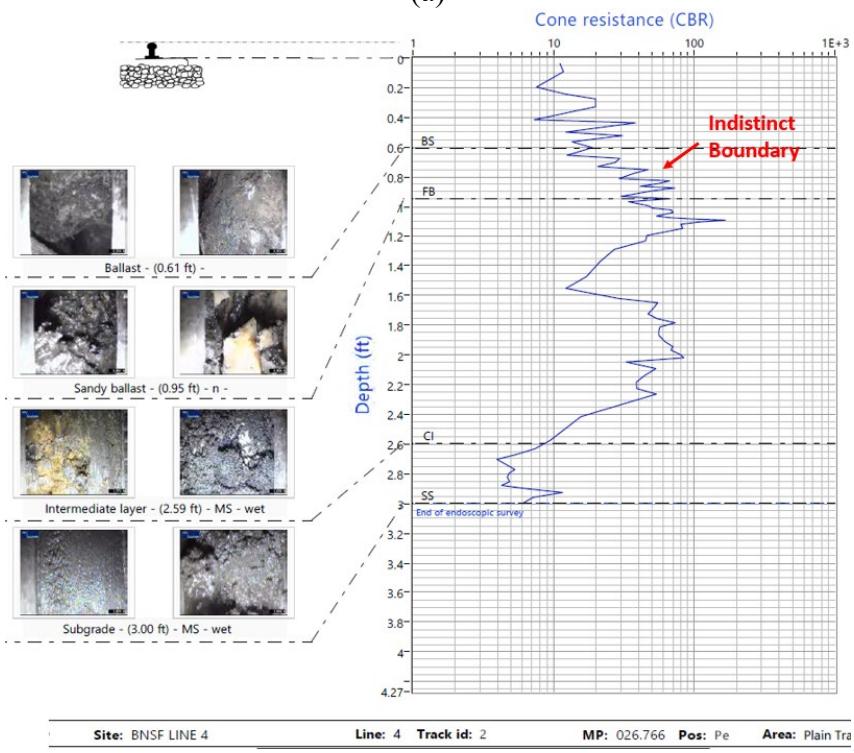

(b)

Figure 69. Comparison of Chart Scatter (a) Noted at a Site Where Gradational Boundary is Using DCP and (b) Endoscope Observations Methods

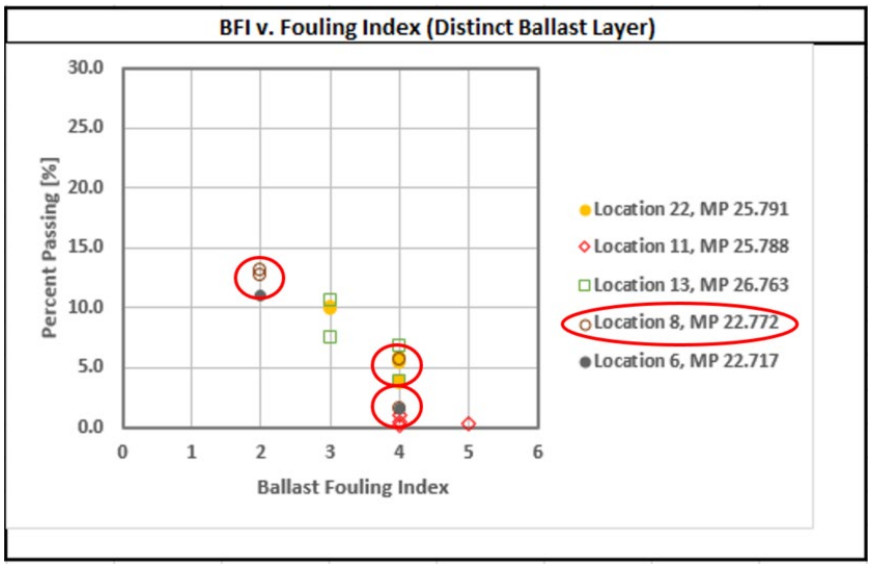

(a)

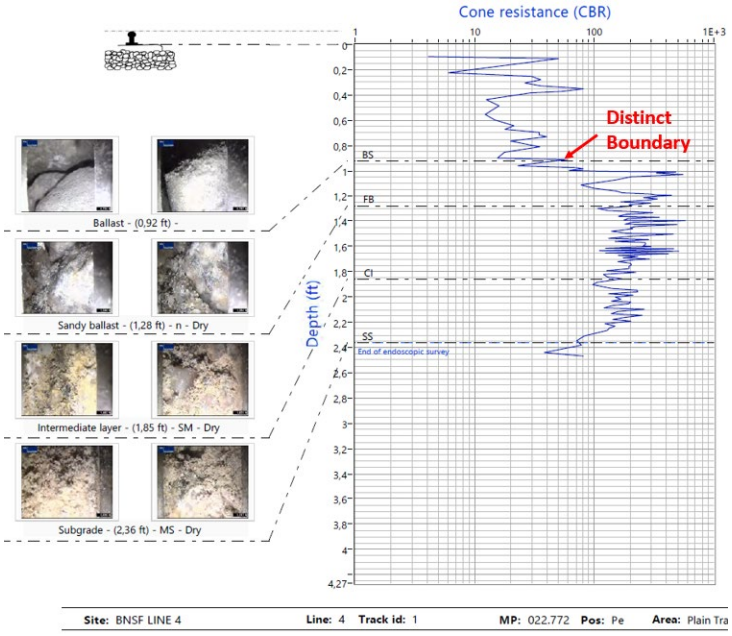

(b)

Figure 70. Comparison of Chart Scatter (a) Noted at a Site Where a Distinct Boundary is Using DCP and Endoscope Observations Methods (b). Note That the Correlation is Stronger Where a Distinct Boundary is Noted

Figure 69 and Figure 70 use the same observation and analysis methods, but provide a comparison between sites that had no distinct clean ballast layer where fine-contamination began just below the surface (Locations 14, 23, 28, and 29), and the sites that had a distinct clean ballast layer from potential undercutting or shoulder cleaning (Locations 6, 8, 11, 13, and 22). This was determined by noting the depth of clean ballast during physical sampling and is also apparent by the geo-endoscope results. As shown in Figure 69, the sites with no distinct clean ballast layer consists of all the outliers from Figure 68 and shows little relation between BFI and Percent Passing the No. 4 sieve. However, a strong correlation exists for Figure 70, which only

shows the sites that had a distinct clean ballast layer. This suggests a distinct ballast layer may play a role in favorable GPR results correlations, and that effective modeling using GPR returns may be negatively affected by a gradual gradational boundary, rather than a distinct boundary.

To help validate this observation, a best-fit trend line was fitted through the data in Figure 68 and the difference between the predicted percent passing from BFI calculations (best-fit line) and the percent passing measured from physical sampling was calculated. This deviation was then plotted against the depth observed by the geo-endoscope observation method and general depth measurements taken during physical sampling.

The results in Figure 71 and Figure 72 show a general agreement that ballast depth influences the ability of BFI to predict percent passing. There are differences between the two ballast depth determination methods, but the general trend still appears to hold.

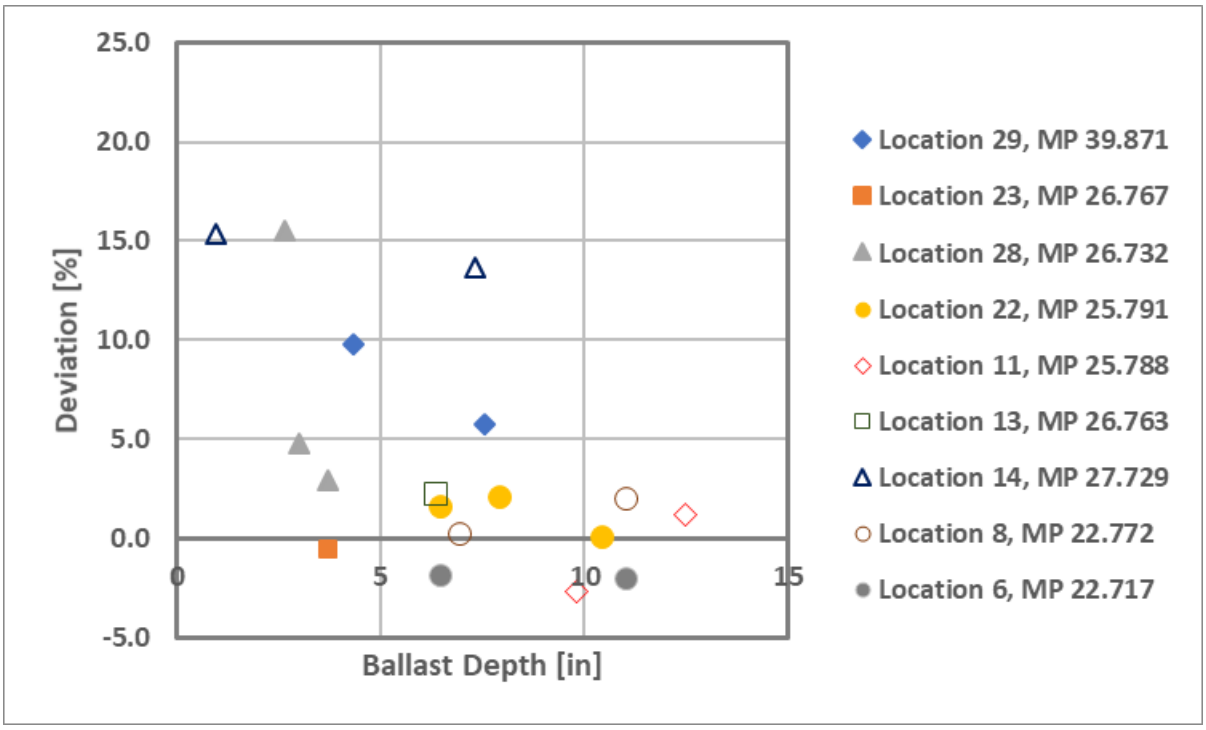

Figure 71. Difference Between Predicted and Measured Percent Passing the No. 4 Sieve vs. Ballast Depth Measured by DCP

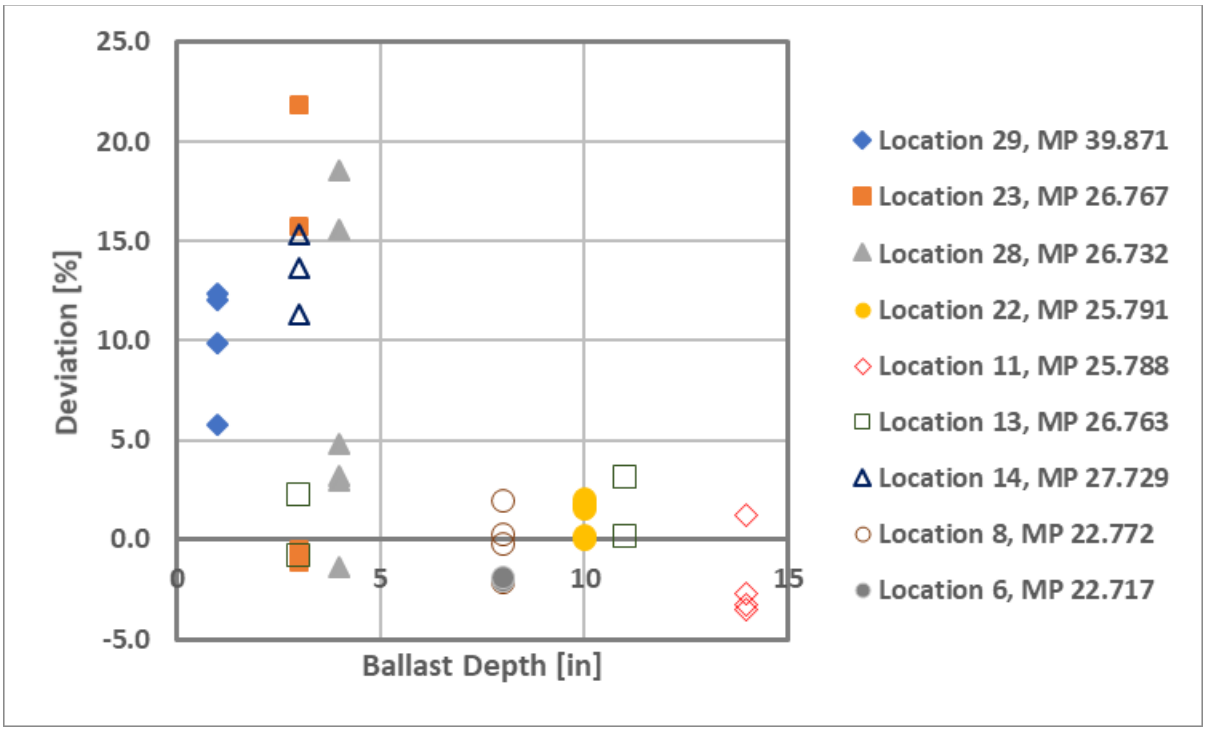

Figure 72. Difference Between Predicted and Measured Percent Passing the No. 4 Sieve vs. Ballast Depth Measured During Physical Sampling

Other explanations for the outliers are a higher non-coal fine content, which would increase the percent passing by mass because of the higher specific gravity of non-coal fines. However, this cannot be verified and would not be believed to have a significant impact on the results.

Other potential correlations, such as cone resistance, were attempted, but no correlations were obtained. For example, BFI was plotted against the average cone resistance for a depth of 16 inches (406 mm) in Figure 73, but no obvious trends were observed.

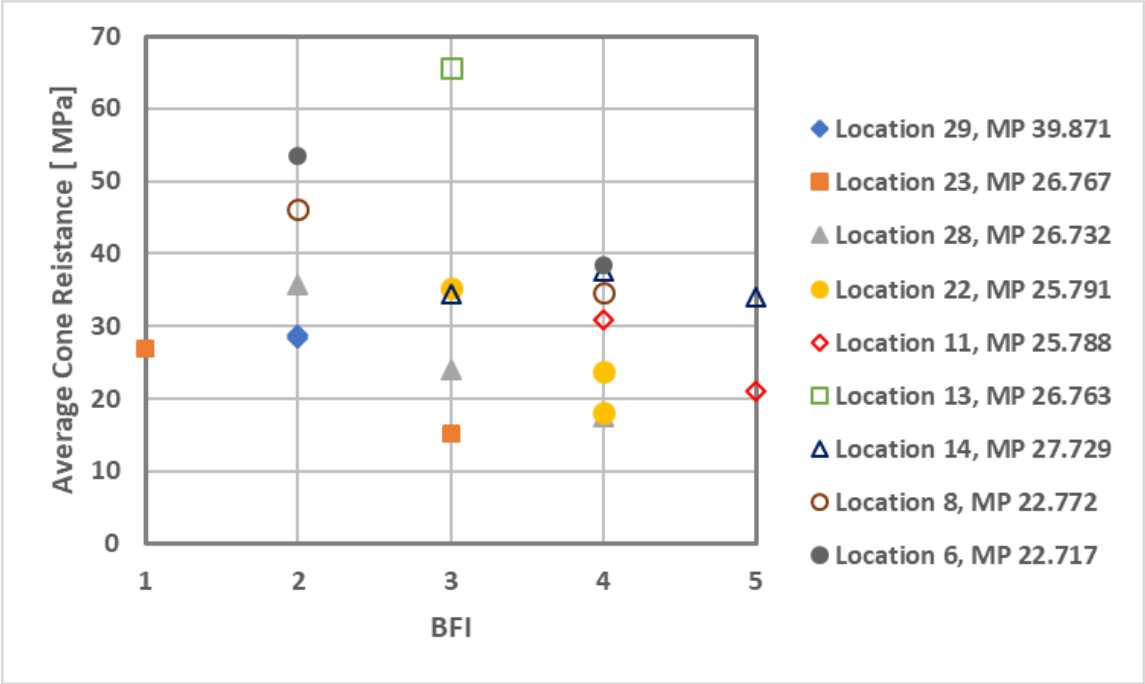

(a)

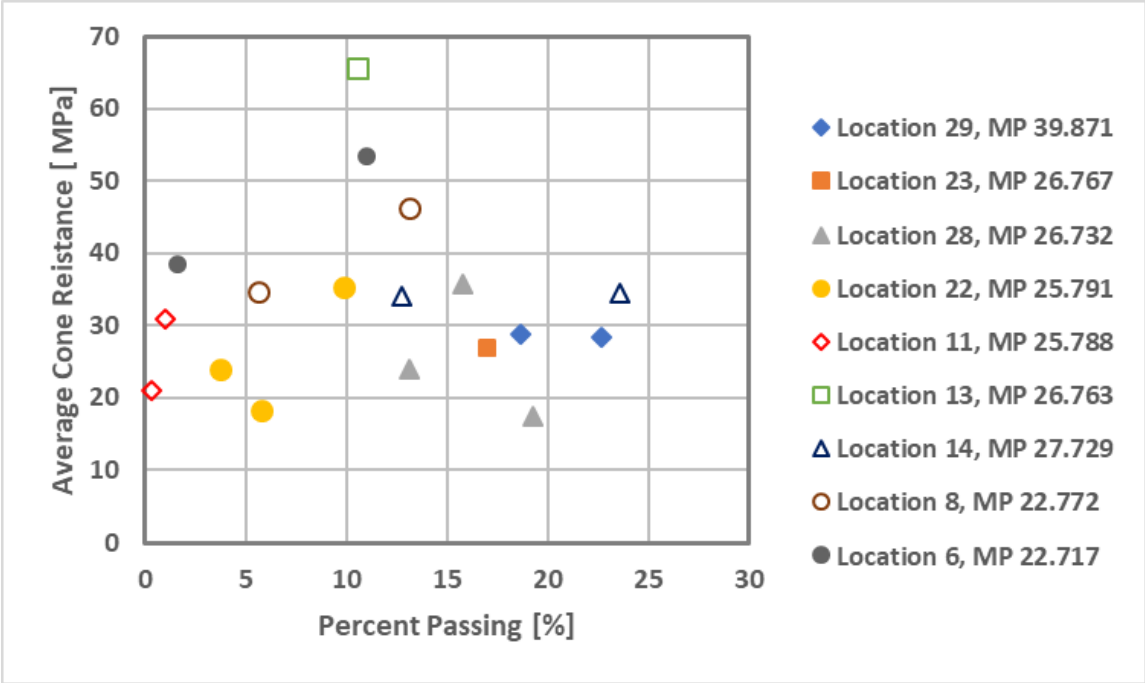

(b)

Figure 73. Average Cone Resistance vs. (a) BFI and (b) Percent Passing the No. 4 Sieve

4.1.10 Summary and Remarks

The study has resulted in the successful implementation of a multi-channel GPR system on the T-20 inspection car. Train-borne GPR surveys potentially provide railroads with a means of

remotely surveying and analyzing the track bed to better understand the nature and extent of track bed degradation and better plan track bed maintenance or remediation.

The study identified several deployment issues specific to a train-mounted GPR system associated with the restrictions imposed by the Association of American Railroads' Plate C clearance envelope. Modifications to the system were identified and implemented during the study to improve system performance.

Comparisons of the performance of the T-20 GPR system against conventional hi-rail based GPR survey data have indicated that the system can produce comparable ballast fouling, FDL, and layer depth interpretation results in the track center under all track conditions.

The following are specific evaluation details:

- TTCI, Sol Solution, BBRI, and BSNF conducted sampling and field testing at a total of nine site locations along BNSF's Ravenna Subdivision. TTCI obtained 39 samples, whereas Sol Solution performed 20 tests. BBRI/Zetica processed a total of ~28 miles of T-20 GPR data on each of the two mains between approximately MP 11 and MP 39.
- Moisture correlates well to BFI (Figure 73), since clean ballast will not absorb or retain moisture well. This is especially apparent at the lower FI values, since higher FI values have a numerically higher potential range of moisture content than lower FI. The BFI appeared to strongly correlate with percent passing the No. 4 sieve in track regions with a distinct clean ballast layer. There was no correlation in regions in which there was no such layer.
- While the BFI is observed to be less well correlated, the overall correlation is observed to fall within the error limits identified from previous, more extensive sampling programs undertaken on Class I railroads in North America. Results from the T-20 GPR system present a good match in the center with those of the hi-rail truck. Shoulder antenna positioning is still being researched and calibrated.
- The FDL presents a robust method of determining the degree of ballast fouling within the track bed because the analysis is restricted to the clean ballast layer. Unlike the BFI, which averages fouling over the full track bed depth range (typically 16 inches), the FDL directly models the depth to the base of the clean ballast layer. The thickness of clean ballast is a key parameter affecting the stability of the ballast layer and an important metric is planning ballast maintenance.
- The modeled T-20 FDL shows good correlation with the measured fouling depth for all samples with the exception of the shoulder data acquired over concrete ties and the Sol Solution results.
- The modeled FDL was consistently 2 inches (51 mm) greater than the clean ballast depth measured by DCP and geo-endoscope methods. This suggests that the same layer interface is measured but have systematic differences of the exact depth due to different methods.
- A strong relationship was observed between the ballast depth and FI from the physical measurements. The GPR shows a similar relation between FDL and BFI, but with more outliers. These may be due to the influence of higher moisture retention of coal fines, but more study is required before strong conclusions can be made.

- A strong correlation is also observed between ballast depth as measured by the DCP and geo-endoscope methods and the T-20 GPR system, although there was an apparent offset of approximately 2 inches (51 mm) evident also. The T-20 data shows approximately an addition of 2 inches (51 mm) of clean ballast compared to the DCP and geo-endoscope observations.
- Coal fines were observed during physical sampling with the center locations having increased moisture and fines than the shoulder locations. The coal fines were plastic when moist and retained significant moisture. This is important because coal fines have a specific gravity half of typical fine material, possibly leading to a reduced FI from sampling. Additionally, the high moisture retention of the coal fines will attenuate the GPR waves to a greater extent than fines with lower moisture retention, producing a higher BFI value.
- TTCI sampling showed spatial variation in the sampling results with differences of FI of high as nine between locations 2 feet (610 mm) away. This has implications in the results, because the GPR results average over a distance of 30 feet (9.1 m), whereas the sampling takes samples at one or two specific locations and may not be representative of the average of the 30-foot (9.1-m) length.
- The BFI showed a general relation with the FI from physical samples but often showed differences of up to +/- 4 times. Deeper analyses show the BFI in the center of the track is consistently greater than the FI while the shoulders show a lower value. This is related to sample size discrepancy (BFI is modelled over 15 feet), and may also be due to the effect of moisture and different locations of the shoulder antennas and shoulder samples.
- While the BFI is observed to be less well correlated, the overall correlation is observed to fall within the error limits identified from previous, more extensive sampling programs undertaken on Class I railroads in North America. Results from the T-20 GPR system present a good match in the center with those of the hi-rail truck.
- The positions of the shoulder antennas on the T-20 car are laterally offset from the positions of the ballast samples, with the antennas located inboard of the ends of the ties while the samples were taken approximately 1-foot away from the tie edge (consistent with the shoulder antenna positions on the BBRI hi-rail trucks). This is believed to be partly responsible for observed discrepancies between the shoulder BFI results and the measured FI due to spatial variability in fouling across the track bed.
- Comparisons between the T-20 shoulder data and the hi-rail shoulder data suggest interference of the T-20 shoulder data with concrete ties. This is likely due to the orientation of the shoulder antennas and further investigation is required. That data is omitted from the analyses.

5. Conclusion and Recommendations

The BFI and the gradations analysis both estimated the amount of fines based on Selig's FI, but there appeared to be a weak correlation. Additional work needs to be done to find out why this is so: whether the type of fines present may have a significant role in influencing the modeled BFI, or natural fines variations, etc.

In comparing the antenna positioning from the T-20 versus hi-rail truck, and TTCI sampling locations, the shoulder GPR antennas are over the edge of the tie while the sampling occurred about 1 foot (305 mm) away from the tie. This may cause discrepancies in the data from natural spatial variations. In addition, antenna orientation differences between the T-20 versus hi-rail truck is also different, which affects the signal penetration and reflection characteristics. This should be explored for consistency unless an algorithm can be modified for this purpose.

As was noted in the comparisons of the wet- versus dry-sieve tests and discussion, the hi-rail truck and T-20 GPR modeling results may be underestimating the BFI by some degree. This may be best addressed in the analysis algorithm or by additional research and refinement.

Reduced antenna performance and a correspondingly lower correlation from the shoulder antennas over concrete ties is believed to be associated with the proximity of the antennas to the tie ends and rails, both of which are restrictions imposed by Plate C. Additional studies have been recommended to mitigate these effects.

Table 30. GPR T-20 Research Summary Table

Data Collection	Tests	Conclusions	Further Work
1st CSX	System and Antenna Tests	Fitment on T-20 functioning System Components generally functioned as designed Good design for overlays and TBIRs	Right shoulder antenna repaired in 2017
2nd FAST	Wet/Dry Water Release	Primary interface profile unchanged by water release Difference plots show relative M% changes	Shoulder issues on antenna, subsequently addressed Secondary interface profile—more scatter with increased M% Additional research and analysis needed
3rd Ravenna	T-20 Data Gathering Hi-Rail Truck Vibratory Sampling and Gradations DCP/Endoscope	Good correlations: Moisture – BFI BFI for T-20 and hi-rail Fouling Depth: FDL – measured depth FDL – BFI Ballast depth – FI Good alternative to backhoe samples Good comparison tool	Address BFI – Gradations Issues Concrete tie-antenna issues FDL – Shoulder data over concrete ties FDL – Endoscope discrepancies BFI – Coal fouling correlations Larger sample size Deeper sampling depth Additional work needed for GPR correlations to be reliable

6. References

1. Li, D., Hyslip, J., Sussman, T., and Chrismer, S. (2016). *Railway Geotechnics.* CRC Press, Boca Raton, FL.
2. Eriksen, A., Gascoyne, J., Mangan, C., and Fraser, R. (2010). "Practical Applications of GPR Surveys for Trackbed Characterisation in the UK, Ireland, USA and Australia." *RTSA Conference on Railway Engineering*, Wellington, New Zealand.
3. Hyslip, J. P., Olhoeft, G. R., Smith, S. S., and Selig, E. T. (2005). "Ground Penetrating Radar for Railroad Track Substructure Evaluation." Report No. FRA/ORD-05/04, Federal Railroad Administration: U.S. Department of Transportation, Washington, DC.
4. Selig, E. T. and Cantrell, D. (2001). "Track Substructure Maintenance – From Theory to Practice." *American Railway Engineering and Maintenance-of-Way Association Annual Conference*, Chicago, IL.
5. Milsom, J., Eriksen, A. (2011). *Field Geophysics.* 4th edition. John Wiley and Sons, Chichester, West Sussex, UK.
6. Federal Railroad Administration. (2017). Ground Penetrating Radar Technology Evaluation on the High Tonnage Loop: Phase 2. Technical Report No DOT/FRA/ORD-17/19. Washington, DC: US Department of Transportation.
7. Federal Railroad Administration. (2017). Ground Penetrating Radar Technology Evaluation on the High Tonnage Loop: Phase 1. Technical Report No DOT/FRA/ORD-17/18. Washington, DC: US Department of Transportation.
8. Hyslip, J., Trosino, M., and Faircloth, J. (2011). "Railway Embankment Assessment and Case Studies." *Proceedings of International Heavy Haul Association Specialty Conference*, Calgary, Canada.
9. Selig, E. T. and Waters, J. M. (1994). *Track Geotechnology and Substructure Management*. Thomas Telford, London, UK.
10. Selig, E. T. (2014). "Railway Substructure Engineering."
11. Code of Federal Regulations. (2017). Title 49 Transportation. 49 CFR. Chapter II. Federal Railroad Administration, Department of Transportation. Part 213 Track Safety Standards. Washington, DC.
12. ASTM International. (2017). ASTM D6913/ASTMD6913M-17 "Standard Test Methods for Particle-Size Distribution (Gradation) of Soils Using Sieve Analysis." ASTM International, West Conshohocken, PA.

Appendix

Federal Railroad Administration. (2020). Ground Penetrating Radar (GPR) Technology Evaluation and Implementation: Appendices A Through F. Report No. DOT/FRA/ORD-20/18. Washington, DC: U.S. Department of Transportation.

Abbreviations and Acronyms

ACRONYM	EXPLANATION
ADLs	Aluminum Plates
BBRI	Balfour Beatty Rail, Inc.
BDI	Ballast Depth Index
BFI	Ballast Fouling Index
BNSF	Burlington Northern Santa Fe Railway
BTI	Ballast Thickness Index
CBR	California Bearing Ratio
CSX	CSX Transportation
DCP	Dynamic Cone Penetration
FAST	Facility for Accelerated Service Testing
FDL	Fouling Depth Layer
FI	Fouling Index
FRA	Federal Railroad Administration
GRMS	Gage Restraint Measurement System
GHz	Gigahertz
GPS	Global Positioning System
GPR	Ground Penetrating Radar
HMA	Hot Mix Asphalt
HTL	High Tonnage Loop
LAE	Layer Amplitude Exceedance
LRI	Layer Roughness Index
MHz	Megahertz
MP	Milepost
MGT	Million Gross Tons
MLI	Moisture Likelihood Index
RAM	Radar Absorbent Material
TBIR	Trackbed Inspection Report
TSQI	Track Substructure Quality Index
TTC	Transportation Technology Center (the site)

ACRONYM	EXPLANATION
TTCI	Transportation Technology Center, Inc. (the company)
TWTT	Two-way Travel Time
USDA	United States Department of Agriculture
Zetica	Zetica Rail